Doctoral Thesis

A Novel Sample Preparation Technology

for Sepsis Diagnosis

Cell-Specific Electric Field Induced Lysis in a Microfluidic

Flow-Through System

Carried out for the purpose of obtaining the degree Doctor technicae (Dr. techn.),
submitted at Vienna University of Technology, Faculty of Electrical Engineering and
Information Technology, by

Klemens Johannes Wassermann

Mat.Nr.: 0206718

Under the supervision of

Ao.Univ.Prof. Dipl.-Ing. Dr. Franz Keplinger

Institute of Sensor and Actuator Systems

reviewed by

Univ.Prof. Dr. Eva-Kathrin Ehmoser	Univ.Prof. Dipl.-Ing. Dr. Peter Ertl
Institute for Synthetic Bioarchitectures	Institute of Applied Synthetic Chemistry
University of Natural Resources and Life Science. Vienna	Vienna University of Technology

I confirm, that going to press of this thesis needs the confirmation of the examination committee.

Affidavit

I declare in lieu of oath, that I wrote this thesis and performed the associated research myself, using only literature cited in this volume. If text passages from sources are used literally, they are marked as such.

I confirm that this work is original and has not been submitted elsewhere for any examination, nor is it currently under consideration for a thesis elsewhere.

Vienna, March, 2019   *Klemens Wassermann*

Kurzfassung

Eine der größten Herausforderungen, die sich unsere Gesellschaft heute und in Zukunft stellen muss, ist die Eindämmung des Aufkommens multiresistenter Keime und die damit einhergehende erhöhte Mortalitäts- und Morbiditätsrate durch Sepsis. Auch politisch, von Seiten der Obama Administration, der Europäischen Kommission und der G7, wurde diese Herausforderung erkannt und Aktionspläne sowie Strategiepapiere entwickelt.[1–3] Eine Voraussetzung im Kampf gegen multiresistente Keime ist eine schnelle und sensitive Detektion und Charakterisierung von Pathogenen, um eine frühe, zielgerichtete Therapie zu initiieren. Allerdings scheitern moderne Entwicklungen aus Forschung und Industrie immer noch bei der Ablöse der langwierigen Blutkultur als Gold-Standard. Die größte Hürde hierbei, die hohe Komplexität der Blutprobe und die marginale Anzahl an Analyten, wurde zwar bereits von Unternehmen und Forschungsgruppen identifiziert, aber noch nicht befriedigend bewältigt. Als Antwort auf diese Notwendigkeit konzentriert sich die in dieser Dissertationsschrift vorgestellte Arbeit auf die Entwicklung einer innovativen Technologie, die ein großes Potenzial für eine neue Art der Probenvorbereitung bietet und hier an Hand eines Labor-Demonstrators gezeigt wird. Durch die Verwendung von elektrischen Feldern wird der Unterschied in der Anfälligkeit von menschlichen Zellen und prokaryotischen Zellen verwendet, um menschliche Blutzellen in einer schnellen, spezifischen, kostengünstigen und vollautomatischen Weise in einem mikrofluidischen Durchfluss-Chip effizient zu lysieren, um eventuelle, im Blut befindliche Pathogene aufreinigen und aufkonzentrieren zu können. Um die theoretische Zelltyp-Spezifität von elektrischen Feldern in einer mikrofluidischen Konstruktion zu realisieren, werden die elektrochemischen Effekte an der Elektroden/Elektrolyt-Grenzfläche durch die Entwicklung einer neuartigen und vielversprechenden Passivierungsstrategie der Elektroden deutlich reduziert. Für das Erreichen dieses Ziels wurden die elektrischen Eigenschaften verschiedener Passivierungsstrategien in analytischer Weise untersucht, optimiert und führten zur Anwendung von dielektrischen Dünnfilmen mit hoher Permittivität. In Bezug auf die klassischen und weit verbreiteten Ansätze, die noch von nicht passivierten Elektroden

Gebrauch machen, ist die Einführung von Passivierungsschichten mit hoher Permittivität für zukünftige Elektrochemie-freie elektrische Feldanwendungen in der Biotechnologie von potenziell großer Bedeutung.

Abstract

The fight against antimicrobial resistance together with sepsis associated mortality, morbidity and health care costs is one of the biggest global challenges society is facing today and in future. Efforts to develop action plans, concepts and strategies to combat this challenge have therefore been major focus points for the Obama administration, the European Commission's Directorate for Health Research and the G7 summit in 2015.[1-3] A fundamental prerequisite for the urgently needed targeted therapy is fast and sensitive pathogen detection and characterization. Modern technologies, however, struggle to sufficiently meet the requirements to replace blood culture, today's tedious gold standard. The biggest hurdle, which is the complexity of the sample blood and the marginal amount of analyte, has already been identified by companies and academia, but is not yet addressed in a satisfying manner. In answer to this need, the work presented in this thesis focusses on the development of an innovative technology bearing a huge potential as a new sample preparation strategy and is demonstrated in a lab-scale demonstrator. By using electric fields, the difference in the susceptibility of human cells and prokaryotic cells is used to efficiently lyse human blood cells in a fast, specific, cost efficient and fully automated manner in a microfluidic flow-through chip. Thus, blood-borne pathogens can be purified and concentrated for highly sensitive and specific detection. To gain cell-type specificity of electric fields in a microfluidic design, superimposing electrochemical effects at the electrode/electrolyte interface are significantly reduced by the development of a novel and promising electrode passivation design. Thus the electrical characteristics of different passivation strategies were investigated and resulted in the application of high-k dielectric thin films. In respect to the classical approaches which still make use of bare metal electrodes, the introduction of high-k dielectric passivation strategies is of utmost importance for future electrochemistry-liberated electric field applications in biotechnology.

Nachher ist sogar ein Narr klug.

Homer

Acknowledgments

First, I would like to thank my supervisor Professor Franz Keplinger for his patients in sharing his knowledge and for the valued support. I am very grateful for his guidance and input. Thank you very much.

This work was supported by the n[f+b] Life Science Call and the AIT Austrian Institute of Technology. I am indeed grateful for the financial support that I have received.

I am indebted to all the people who have made this work a success, especially my supervisor at AIT Dr. Johannes Peham for his immense commitment to the project. I am very grateful for your patience and your guidance in electrical engineering to which I was a novice at the start of the thesis. Also I would like to thank you for your guidance as a leading example for an applied researcher. I would also like to say a big thank you to the project leader Dr. Christa Nöhammer for giving me the freedom to develop ideas and her patience in times of unexpected challenges.

I would also like to thank our Head of Business Unit, Dr. Martin Weber and our Department Head Dr. Michaela Fritz for supporting the development of my idea. My sincere gratitude

This work would not have been a success if not for the moral support of some wonderful people that I met at AIT. This list is long, but I would like to specially mention Ciril Rozman, Drago Sticker, Mario Rothbauer, Helene Zirath, Thomas Maier, Walter Pulverer, Matthias Wielscher and Silvia Schönthaler. Thank you for being such great colleagues.

Also, I would like to acknowledge Dr. Sven Barth from the Institute of Materials Chemistry at TU Wien for his uncomplicated and kind support during my first thermal oxidation experiments.

I would like to specially thank my wonderful wife Jasmin Weingartner. Thank you for your love, care and endless support including lab visits at 3 am with sandwiches and Red Bull. Hugs and kisses to my awesome cool kids Victoria and Katharina, you are the reason I strive to the father you deserve. To my parents Johann and Marta and to my sister Esther: I would not be where I am today without your great support, mentorship and trust. Especially I would like to thank my father for your support and our long, inspiring discussions when technical difficulties are on the horizon. I am eternally grateful for having such a wonderful family!

Table of Content

List of Abbreviations

AC	Alternating current
ACCP	American college of chest physicians
APTES	3-Aminopropyltriethoxysilane
AST	Antimicrobial susceptibility testing
BSI	Blood stream infection
CAD	Computer-aided design
CCD	Charge-coupled device
CDC	Centers for disease control and prevention
CFU	Colony forming units
cpTi	Commercially pure titanium
CRE	Carbapenem-resistant *Enterobacteriaceae*
DC	Direct current
div	Division
DMEM	Dulbecco's modified eagle medium
DNA	Deoxyribonucleic acid
DSOF	Duration of SIRS before organ failure
ECLU	Electric cell lysis unit
EDTA	Ethylenediaminetetraacetic acid
FBS	Fetal bovine serum
FISH	Fluorescenct *in-situ* hybridization
ID	Rapid identification
IST	internal transcribed spacer region
ITO	Indium tin oxide
KPC	Klebsiella pneumoniae Carbapenemase

LB	Luria-Bertani
LOC	Lab on a chip
LOD	Limit of detection
MALDI-TOF	Matrix-associated laser desorption ionization-time of flight
MOF	Multiple organ failure
MPTES	3-Mercaptopropyltriethoxysilane
MRSA	Methicillin resistant *Staphylococcus aureus*
MS	Mass spectroscopy
µTAS	Micro total analysis system
NAT	Nucleic acid tests
NGS	Next generation sequencing
PBMC	Peripheral blood mononuclear cells
PBS	Phosphate buffered saline
PCB	Printed circuit board
PCR	Polymerase chain reaction
PEEK	Polyether ether ketone
Pen/Strep	Penicillin/Streptomycin
POC	Point of care
PTFE	Polytetrafluoroethylene
RNA	Ribonucleic acid
SA	Staphylococcus aureus
SCCM	Society of critical care medicine
SEM	Scanning electron microscopy
SIRS	Systemic Inflammatory Response Syndrome
sqAC	Square wave alternating current
TMP	Trans membrane potential
VRE	Vancomycin-resistant Enterococcus

Chapter 1

Introduction

1.1 Sepsis

Sepsis is still a major killer, being the third most common cause of death in Germany.[4] Sepsis is the clinical syndrome resulting from a host's systemic inflammatory response to an infection and is a major international health care problem.[5] Most commonly, a primary bacterial infection of the lungs, brain, urinary tract, skin, or abdominal organs is the starting point of a systemic blood stream infection (BSI). According to the Centers for Disease Control and Prevention (CDC), BSI can be defined as the presence of viable bacteria or fungi in the blood (i.e. bacteremia or fungemia, respectively).[6] Studies have shown clinically significant bacteremia in adults is characterized by low pathogen numbers, for example, 10 colony forming units (CFU)/ml in 73% of adults with Gram-negative bacteremia and 1–30 CFU/ml in more than half of adult patients with staphylococcal and streptococcal endocarditis.[7] More than 50% of sepsis cases are caused by Gram-positive staphylococci.[8] Other commonly implicated bacteria include *Streptococcus pyogenes*, *Escherichia coli*, *Pseudomonas aeruginosa*, and *Klebsiella* species. Fungal sepsis accounts for approximately 5% of severe sepsis and septic shock cases; the most common cause of fungal sepsis is infection by *Candida* species of yeast, a nosocomial infection frequently acquired in hospitals.[9]

In 1992, four different progressive stages of sepsis were defined by the American College of Chest Physicians (ACCP) and the Society of Critical Care Medicine (SCCM).[10,11]

i.   **Systemic Inflammatory Response Syndrome (SIRS)**, which is defined as the presence of at least two of the following: Body temperature greater than 38.3°C or lower than 36°C; heart rate above 90 beats/minute; respiratory rate greater than 30 breaths/minute; abnormal leukocyte count (white blood cell count below 4000/ml or above 12000/ml).

ii. **Sepsis**, defined as SIRS in response to a confirmed or suspected infection.

iii.   **Severe Sepsis**, defined by sepsis accompanied with organ dysfunction,

         hypoperfusion (low oxygen levels in the tissue) or hypotension (low blood

         pressure)

iv.   **Septic Shock**, which is defined as severe sepsis with persistent hypotension that

         does not respond to adequate fluid replacement.
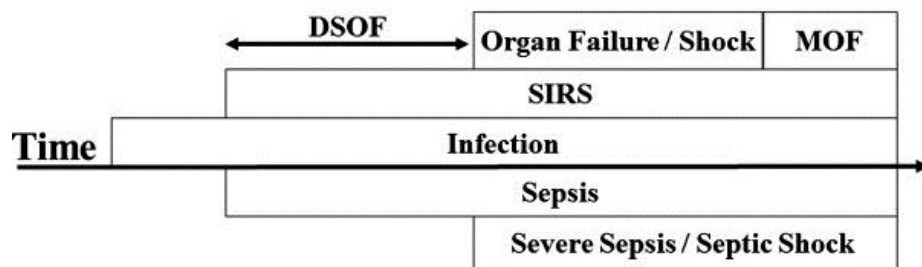
Fig. 1.1.1: Schematic representation of the progressive course of infection. Sepsis without organ failure or shock in the early stage progresses to severe sepsis or septic shock in the advanced stage. Sepsis was defined as an infection with systemic inflammatory response syndrome (SIRS). Severe sepsis and septic shock were defined as sepsis with any organ failure and sepsis with shock, respectively. Duration of SIRS before organ failure (DSOF) was defined as the duration from the first recognition of SIRS to the first recognition of multiple organ failure (MOF) or septic shock. From *Sugita H. et al. International Journal of Emergency Medicine, 2012.*[12]

Owing to factors such as immunosuppression treatment, increased frequency of invasive procedures, the aging population, and the rise in multi-drug resistant bacteria, blood stream infections by microorganisms causing sepsis are one of the leading causes of death worldwide and the incidence of sepsis has been continuously increasing, tripling the number of sepsis-related deaths over the past 20 years.[13] In Europe and the United States, sepsis causes more than 400 000 deaths every year, costing an estimated US$17 billion in the USA and €8.2 billion in Germany every year.[14,15] For bloodstream infections, a study carried out by Kumar *et al.* showed, that already 5 hours after the occurrence of first symptoms of sepsis, the mortality rate rises to 50% if no appropriate therapy is initiated.[16]

In addition to mortality rates directly associated with sepsis, delays in establishing an appropriate treatment strategy also lead to an increased chance of long-term consequences to organs and tissues. Patients who survived sepsis bear an under-recognized risk of physical and cognitive impairment and suffer a more-than-doubled risk of dying in the next 5 years compared with hospitalized controls.[17]
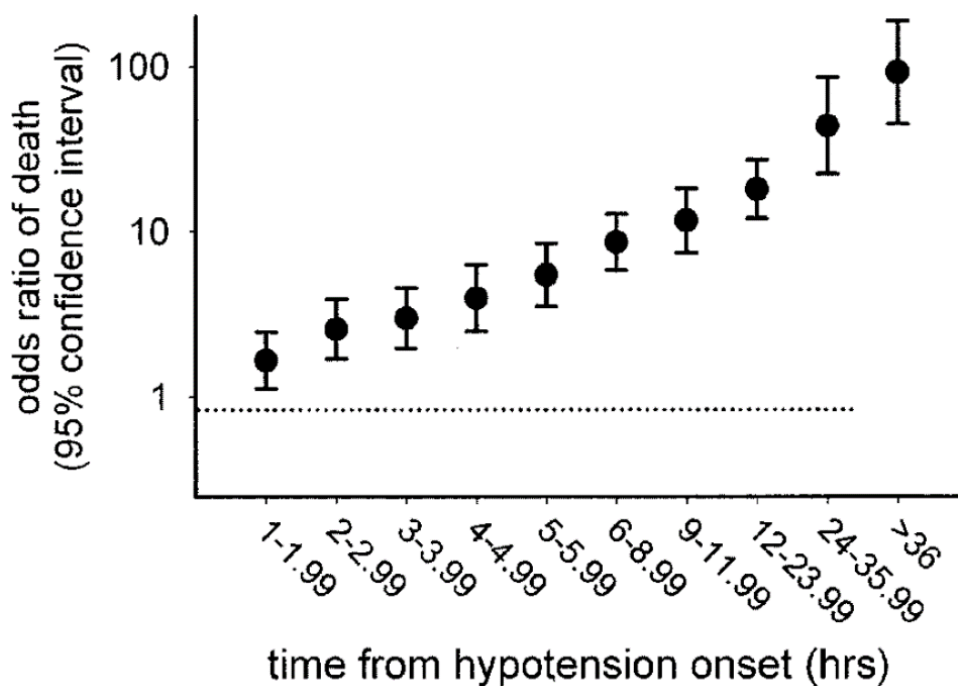
Fig. 1.1.2: Mortality risk (expressed as adjusted odds ratio of death) with increasing delays in initiation of effective antimicrobial therapy. Bars represent 95% confidence interval. An increased risk of death is already present by the second hour after hypotension onset (compared with the first hour after hypotension). The risk of death continues to climb, though, to >36 hrs after hypotension onset. From *Kumar R. et al., Crit. Care Med., 2006.*[16]

As early and appropriate treatment is key to survival of sepsis and patient outcome, broad spectrum antibiotics are given intravenously within the first hour of recognition of clinical signs defining SIRS. These clinical signs however, are also common to many other medical conditions, leading to significant misuse of antibiotics. In addition, the further spread of antibiotic-resistant bacterial strains, such as methicillin resistant *Staphylococcus aureus*

(MRSA), carbapenem-resistant *Enterobacteriaceae* (CRE) or multi resistant *Clostridium difficile*, enforces the early use of species specific antibiotics.[18] With respect to the collateral damage to the patient when using broad spectrum antibiotics inappropriately, the spread of antibiotic resistant bacteria and the necessity for targeted therapy, this underlines the enormous need for fast and accurate diagnosis.

1.1.1 Blood Stream Infection Diagnosis

Worldwide, every four seconds one death is caused by an inappropriately treated blood stream infection. Appropriate, thus immediate and targeted treatment can only be administered if the cause of an infection is recognized and diagnosed early. The present empirical approach of treatment is indicative of our inability to diagnose early enough and leads to misuse of broad-spectrum antibiotics. Rapid identification (ID) and antimicrobial susceptibility testing (AST) of the causative agent(s) of BSI are thus the most important tasks of the clinical microbiology laboratory since this information is essential for clinicians to select the most appropriate antimicrobial therapy.[19]

Starting with the gold standard for BSI diagnosis, the blood culture method, the following section will give an overview of the most promising diagnostic approaches such as MALDI-TOF, molecular biology-based techniques (PCR, Microarray, and Sequencing) as well as developments to implement those technologies in fully automated point of care (POC) devices.

1.1.2 Blood Culture

Till today, blood culture is considered the gold standard in the diagnosis of bloodstream infections and to differentiate systemic inflammatory response (SIRS) form sepsis. A typical procedure consists of taking a patient's blood sample (20-30 ml), which is distributed in culture bottles containing various broth media in aerobe and anaerobe culture bottles. Inoculated bottles are then cultivated for pathogenic growth at 37°C and growth is monitored by turbidity and CO_2 measurements. For fast growing pathogens, such cultivation takes 1-5 days, in case of slow growing pathogens such as fungi or mycoplasms, cultivation can take up to 14 days. Positive cultures are subsequently prepared for Gram staining to differentiate pathogens by ocular inspection based on Gram

staining color, shape and growth pattern. Next, in order to test for antibiotic susceptibility (AST), positive blood cultures are seeded on agar plates with several antibiotic patches and grown for 24 hours and 48 hours for aerobic and anaerobic bacteria, respectively.
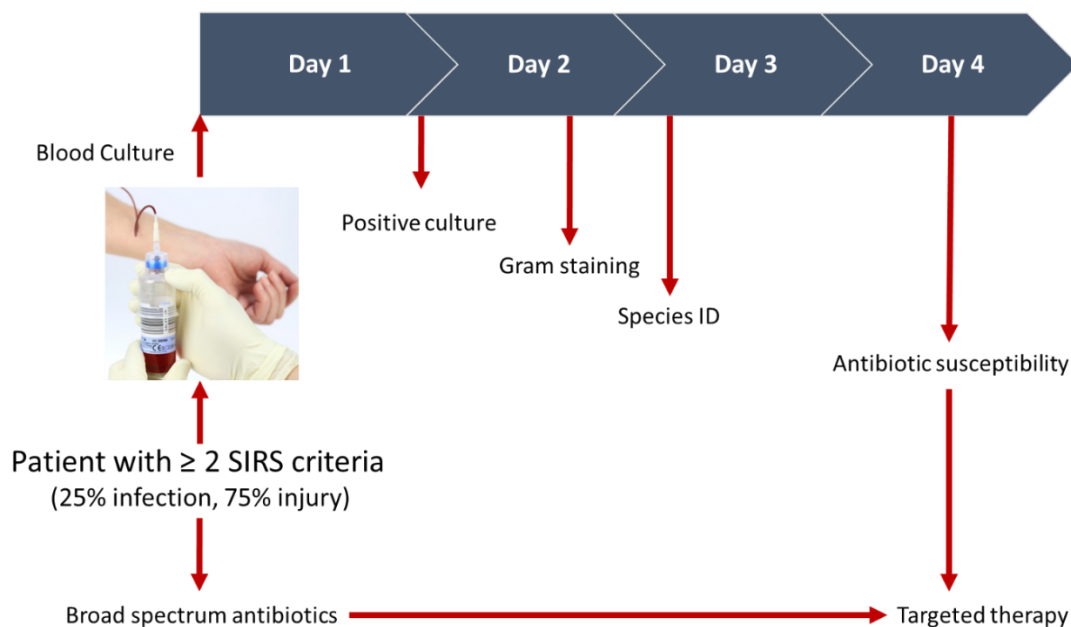
Fig. 1.1.3: Schematic workflow of the blood culture procedure done in clinical microbiology laboratories today. Due to the long time to result, caused by culturing, plating, re-plating of cultures, biochemical staining procedures and phenotypic antibiotic susceptibility testing, broad spectrum antibiotics are given in a first-guess approach. Before administration of targeted therapy, often multiple blood cultures are initiated to confirm results.

Although blood cultures and AST are currently also performed with fully automated instruments that detect microbial growth by the analysis of CO_2 release using fluorescent or colorimetric sensors (e.g. BioMêrieux BacT/ALERT 3D, VITEK 2) or by sensing pressure changes in the bottle headspace due to the consumption and production of gases, the overall time to result of blood cultures is far too long to allow physicians to make immediate treatment decisions.[20]

Fig. 1.1.4: The BacT/ALERT® 3D instrument from BioMêrieux is a state-of-the-art, automated microbial culture and detection system. The system is based on the detection of CO_2 released by actively proliferating bacteria into the liquid media. CO_2 lowers the pH in the growth media, which in turn produces a color change in a sensor in the vial, detected by a reflectometric unit in the instrument. Picture taken www.biomerieuxconnection.com.

Fig. 1.1.5: The Vitek 2 automated ID/AST instrument from BioMêrieux. The disposable reagent cards have 64 wells that each contain an individual test substrate. Substrates measure various metabolic activities such as acidification, alkalinization, enzyme hydrolysis, and growth in the presence of inhibitory substances. An optically clear film present on both sides of the card allows for optical read out using different wavelengths in the visible spectrum to measure either turbidity or colored products of substrate metabolism. Picture taken from www.biomerieuxconnection.com .

In addition to the long time to results, the risk of contamination leading to false positive results, the occurrence fastidious or nonculturable pathogens resulting in false negative findings and an overall high variance in reported sensitivities of 60 - 90% at best are significant clinical problems of the blood culture method.[21–23]

1.1.3 MALDI-TOF-based Diagnosis

In order to shorten the turnaround time required for diagnosis of BSI, Matrix-associated Laser desorption ionization-time of flight (MALDI-TOF) mass spectrometry has been introduced to clinical microbiology laboratories. MALDI-TOF is a widely used mass spectrometry technique for the analysis of biomolecules based on their mass/charge ratio. Briefly, small amounts of sample from positive blood cultures or isolated microbial colonies are co-crystallized on a steel plate with a low-mass organic compound (e.g. formic acid), which assists microbial lysis and supplies protons during ionization (Fig. 1.1.6). The sample-matrix crystal is then irradiated by an UV laser beam for a short time, leading to sublimation of the sample-matrix crystal into a gas phase and followed by ionization of the biological compounds (Fig. 1.1.6). Soft ionization is critical for the identification and characterization of microorganisms, as it allows the analysis of large biomolecules, such as ribosomal proteins and proteins responsible for antimicrobial resistance (e.g. Beta-lactamase). Once ionized, the analytes are accelerated into the mass analyzer where they move through the time of flight tube and reach detectors based on their mass/charge (m/z) ratio. As ribosomal proteins and protein compositions are unique to respective microbial groups, species and even subspecies, different spectra will be generated, allowing for discrimination between closely related organisms.[24,25] Recorded spectra are then compared to databases of defined reference spectra, allowing for microbial identification.
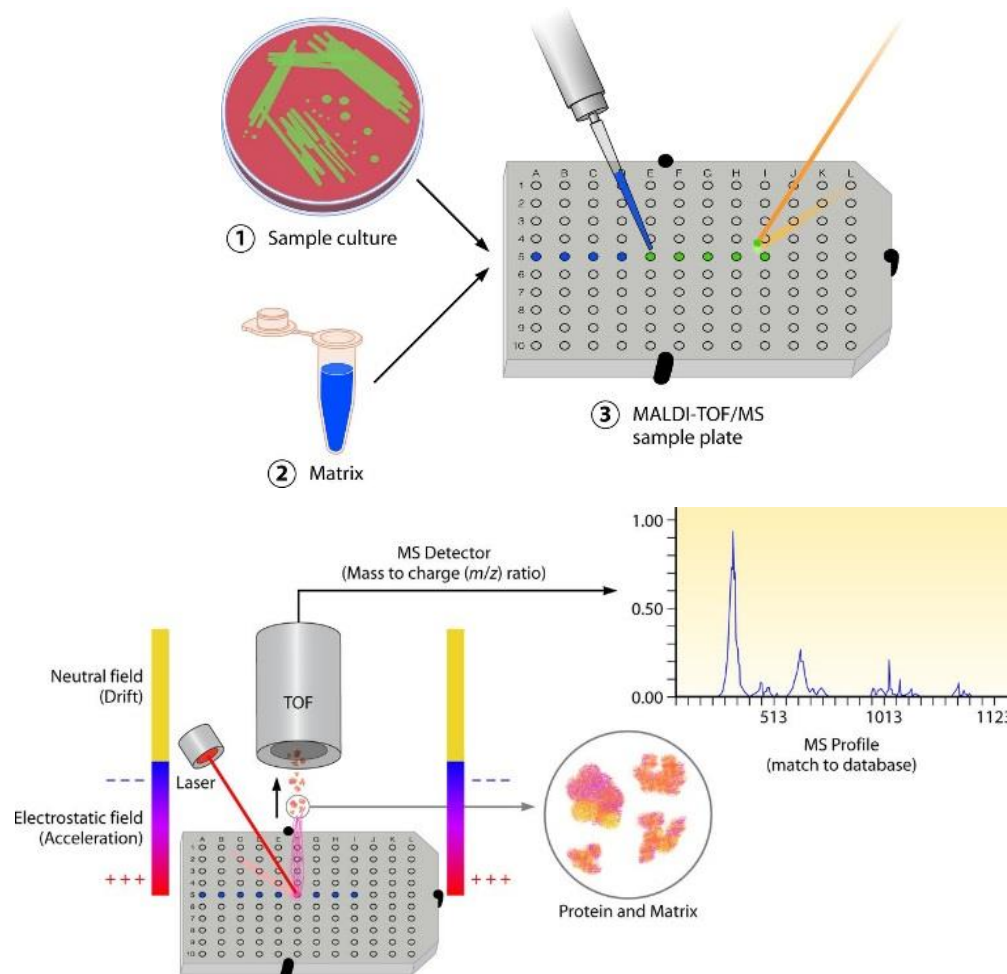
Fig. 1.1.6: General schematic for the identification of bacteria and yeast by MALDI-TOF MS using the intact-cell method. Bacterial or fungal growth is isolated from plated culture media (or can be concentrated from broth culture by centrifugation in specific cases) and applied directly onto the MALDI test plate. Samples are then overlaid with matrix and dried. The plate is subsequently loaded into the MALDI-TOF MS instrument and analyzed by software associated with the respective system, allowing rapid identification of the organism. Once appropriately processed samples are added to the MALDI plate, overlaid with matrix, and dried, the sample is bombarded by the laser. This bombardment results in the sublimation and ionization of both the sample and matrix. These generated ions are separated based on their mass-to-charge ratio via a TOF tube, and a spectral representation of these ions is generated and analyzed by the MS software, generating an MS profile. This profile is subsequently compared to a database of reference MS spectra and matched to either identical or the most related spectra contained in the database, generating an identification for bacteria or yeast contained within the sample. From *Clark AE et al., Clinical Microbiology Reviews, 2013.*[26]

Although detection of antibiotic resistance using MALDI-TOF MS is still in development, due to the low cost per sample analyzed, the relatively simple processing, the rapid turn-around time (< 1 hour) and the large database for species and genus identification available, MALDI-TOF is already integrated into the diagnostic pipeline in many clinical microbiology laboratories. However, the use MALDI-TOF MS for BSI diagnosis has also its limitation. Foremost, blood culture is still needed to enrich bacteria, which again prolongs the time from sampling to result. In addition, early work has shown a high degree of variation of the spectra of microorganisms recorded under different culture conditions and among studies performed in different laboratories.[27]

1.1.4 Molecular Biology-Based Diagnosis

In order to increase the speed of diagnosis and to improve sensitivity of detection of pathogens in blood compared to the gold standard blood culture method, molecular biology-based detection techniques have been developed. By shortening the time required for pathogen identification from days to hours and allowing for detection of organisms missed by blood culture, those molecular methods have the potential to provide significant clinical benefits for the management of patients with sepsis.
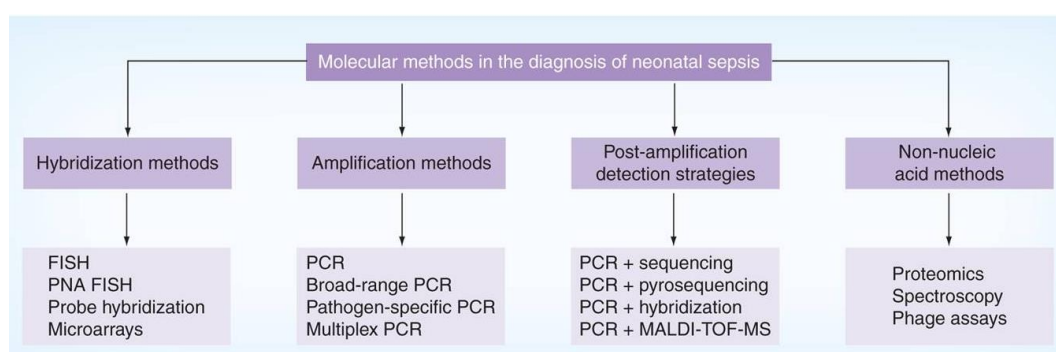
Fig.1.1.7: Molecular biology based methods in the diagnosis of sepsis. From *Venkatesh M. et al., Expert Reviews of Anti-infective Therapy, 2010.*[28]

1.1.4.1 PCR-based Diagnosis

The majority of molecular biology based methods for the detection of pathogens in blood are nucleic acid tests (NAT), which rely on the amplification and/or detection of pathogenic DNA and RNA. The most common technology used is based on the polymerase chain reaction (PCR), introduced by Kary Mullis in 1983.[29] PCR-based pathogen detection is enabled by the ability of the reaction to selectively amplify specific regions of DNA, allowing to detect even minute amounts of pathogen DNA in a sample. Depending on the design of the primers, organism specific PCR or broad range PCR are two basic approaches that have been taken. For the latter, primers targeting highly conserved regions in the 16S rRNA gene and the 23S rRNA gene, as well as internal transcribed spacer (ITS) region between the 16S and the 23S rRNA genes of bacteria and the 18S and 5.8S ribosomal genes in fungi, are used to cover a broad range of pathogens. In addition, multiplex PCR uses multiple primer sets for bigger coverage or more discrimination between species. Using primers targeting antibiotic resistance genes, resistance genotypes can be detected.[30] With the introduction of real-time PCR, it was possible to continously observe the amplification of the sequence of interest throughout the process through the use of fluorescent dyes or flourescently labled probes that bind to specific sequences. Thus, amplification, product detection and analysis is achieved in a single reaction vessel. Furthermore, several sequence-specific probes with different fluorescent reporters can be added to the reaction, allowing for simultanious determination of multiple products.[5] The SeptiFast assay from Roche, the SepsiTest kit from Molzym, the GeneXpert from Cepheid as well as Analytik Jena's VYOO kit and Seegene's Magicplex sepsis real-time Assay are commercial examples for the use of this method in sepsis diagnosis.

1.1.4.2 Microarray

Another method for detcting PCR products found in literature and on the market is the microarray technology. Here, short species and antibiotic resistance gene sequences, termed probes, are immobilized at known positions on a solid carrier by spotting. The PCR products are labeled with a fluorophore during primer extension and bind to the probes by hybridization. After binding and washing, the micoarray is scanned with a high sensitivity CCD camera and computerized image based analysis is used to determine the relative abundance of nucleic acid sequences in the sample. The microarray method for pathogen and antibiotic resistance marker identification can be found in products like Prove-it Sepsis from Mobidiag, Verigene from Nanosphere Inc.or the Hybcell from CubeDx.

1.1.4.3 Fluorescence In-Situ Hybridization (FISH)

A PCR independent molecular biology based technique used for pathogen charaterization is called fluorescenct *in-situ* hybridization (FISH). Here, specific fluorochrome-labeled oligonucleotide probes targeted to rRNA are directly hybridized in fixated cells on a glass slide and visualized microscopically. Althogh more than 95% of bacteria and yeast commonly found in blood can be identified in less than 3 hours, this method is restircted to identify pathogens from positive blood culture only.[20] Due to the relative high costs, the elaborate protocol and the need for sophisitcated fluorescence microscopy equipment, this method is not yet widley used in the clinical context.

1.1.4.4 Sequencing

Culture-independent molecular assays can rapidly identify pathogens in whole blood and compared to conventional blood culture, are more likely to have a clinical impact in future. Nonetheless, the clinical utility of the current assays is limited because of the predefined pathogen detection panels used in some tests and the limited information provided on antimicrobial susceptibility.[31] The revolution in bench-top next-generation sequencing (NGS) technologies (e.g., Illumina MiSeq and Life Technologies Ion Proton) have made genome sequencing faster and cheaper and there is growing interest in applying these technologies for routine clinical microbiology.[32] Using NGS to identify pathogens directly from clinical samples could enable characterization of viable, dead and viable but non-culturable bacteria as well as fungi, viruses and acompanying antimicrobial resistance or virulence markers. NGS is now commonly used in research and in reference laboratories for outbreak investigations, such as *Escherichia coli* O104:H4, *Staphylococcus aureus* and *Clostridium difficile* and *Salmonella typhi*.[31] In future, NGS is believed to be routinely applied in clinical microbiology laboratories. With Illumina and Pacific Biosciences beeing the current big players interested in this area, Oxford Nanopore Technologies Inc. have developed a new generation of nanopore-based single molecule sequencing. Their MinION device is the size of a large USB stick and is designed to provide real-time data streaming and improved simplicity. This will allow pathogen identification within minutes, thus demonstrating the great potential of sequencing for application in infectious disease diagnostics and epidemiology.

1.1.5 Point-of-Care Developments

Although molecular biology based techniques theoretically offer crucial advantages compared to culture dependent methods such as shorter turnaround time, higher specifictiy and high throughput screening possibilities, current developments face major challenges. Due to the complexity of most methods, multiple processing steps have to be performed by highly trained personal. The laborious working procedures lead to pooling of samples, which prolonges time-to-result. Another pitfall ascociated to the complexity of the assays is the susceptibility to contamination during processing. Compared to the culture method, the costs per analysis using molecular biology based techniques are roughly a factor 10 higher, in part due to the use of costly reagents.

In order to adress these challeges, enclosed sample-to-result systems have been developed and are a subject of highly active research. By using microfluidic approaches, disposable cartridges and system integration strategies, fully automated systems could cost effectively support physicians with all required information without the need of centralized laboratories and labor-intensive use of highly trained personal.

The most famous example of an already commercialized sample-to-result system which is already broadly used in US American hospitals is the GeneXpert System form Cepheid Inc.
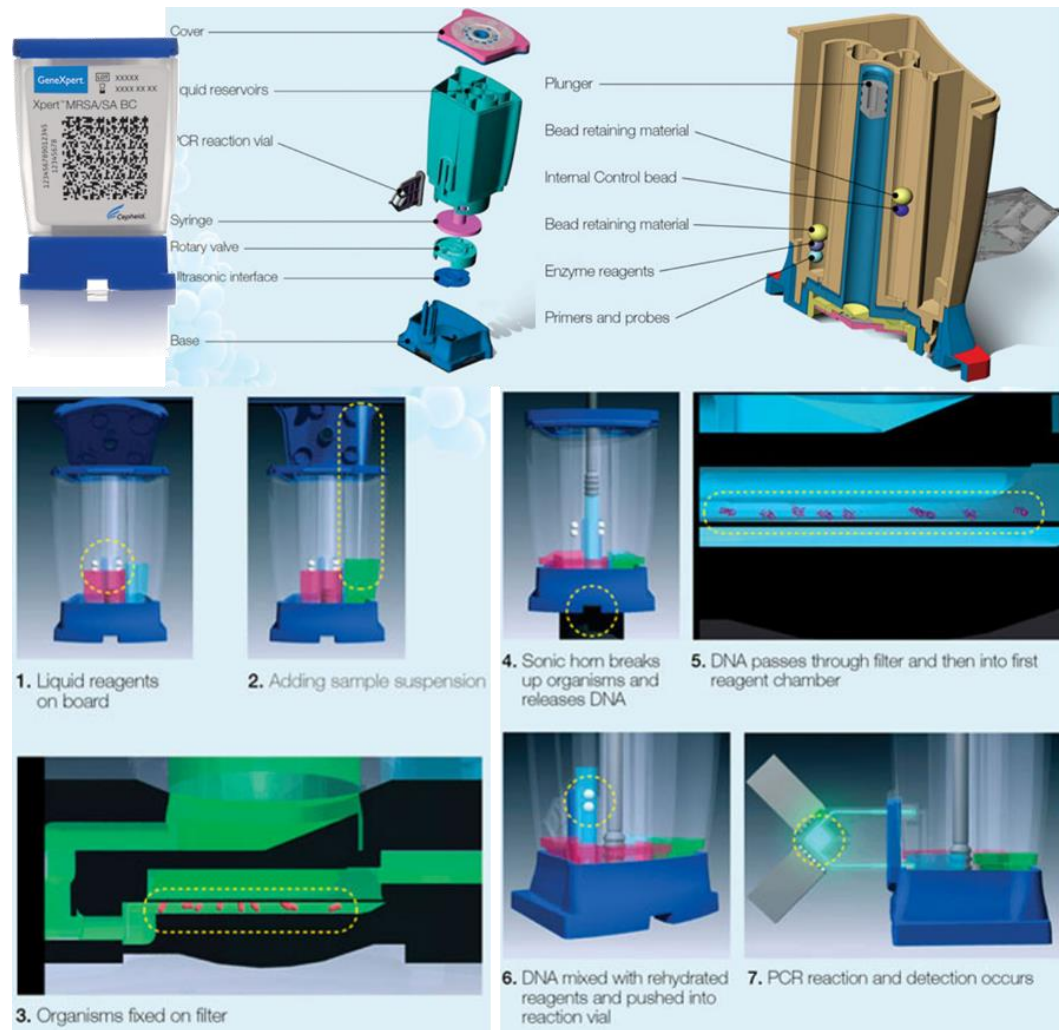
Fig. 1.1.8: The GeneXpert Cartridge from Cepheid and the working principle of the sample-in-result-out workflow. All necessary reagents are stored in lyophilized form in the cartridge (1.). A sample, typically a swab is added to the cartridge (2.) and washed. Microorganisms from the sample are captured on a filter (3.) and lysed via an ultrasonic horn (4.). DNA passes through the filter into the reaction camber (5.) and mixed with rehydrated reagents (6.). A real-time PCR reaction takes place in the cartridge and monitored via detection of fluorescence signals (7.). Taken from *http://www.cepheid.com*

The Cepheid GeneXpert consist of an all-in-one cartridge with enzymes and buffer stored in the cartridge in dry bead format. In 30-40 minutes, the sample is filtered, pathogens are lysed on a filter through ultrasonication, DNA is amplified and detected by real-time PCR.[33] Single cartridges are available for the detection of e.g. MRSA/SA, *C. difficile*, or vanA/VRE detection, thus, although cartridges can be read out in parallel in large multi-

cartridge holding base units, the Cepheid GeneXpert is not specifically designed for general sepsis/BSI detection. Additionally, due to the relative poor limit of detection (LOD) of 610 colony forming units (CFU)/ml for *S. aureus*, positive blood cultures are still needed as sample material.[34,35]
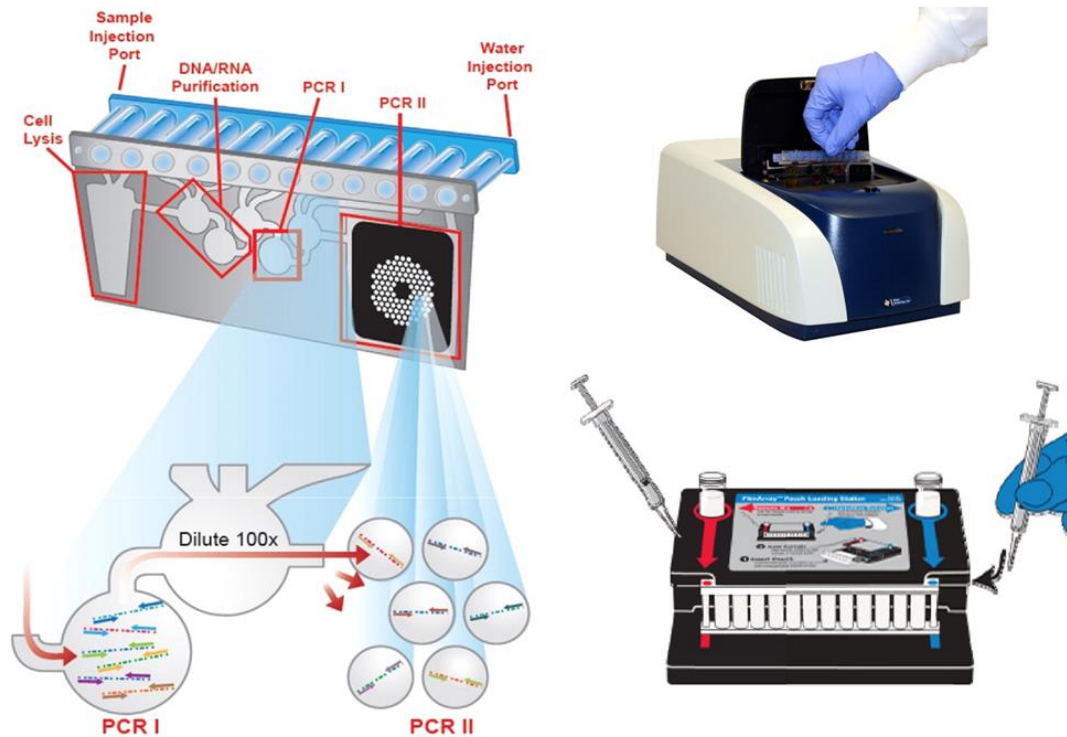
Fig. 1.1.9: The BioFire FilmArray from bioMérieu. Taken from http://www.biomerieux-diagnostics.com/filmarrayr-multiplex-pcr-system

Another commercially available fully integrated and automated system is the BioFire FilmArray from bioMérieux. In contrast to Cepheid's GeneXpert, the FilmArray targets 24 pathogens (8 genus/species of Gram-positive, 11 genus/species of Gram-negative, 5 species of *Candida*) and three antibiotic resistance genes mecA, vanA/B, and *Klebsiella pneumoniae* Carbapenemase (KPC) associated with bloodstream infections in parallel. The FilmArray pouch contains all reagents necessary for sample preparation, amplification and detection. After adding the sample and a hydration solution, the FilmArray instrument first extracts and purifies nucleic acids from the sample and then amplifies the target genes in a large volume, multiplex, reverse-transcriptase first stage PCR. To detect

products from first stage PCR, individual single-plex second-stage nested PCRs for all target genes are performed in individual wells. Amplification of the second stage PCR is monitored in real-time using a dsDNA intercalating fluorescent dye. Post-PCR melting curve analysis is then performed to identify the specific pathogens and resistance genes. The FilmArray platform is a closed diagnostic system which requires 2 min hands-on time and about 1 h turnaround time. However, only one sample can be analyzed at a time and positive blood cultures need to be used as sample instead of blood.[31]

In contrast to the limited number of commercially available integrated pathogen detection solutions, a wide plethora of academic publications are available in the field of POC infection diagnosis.
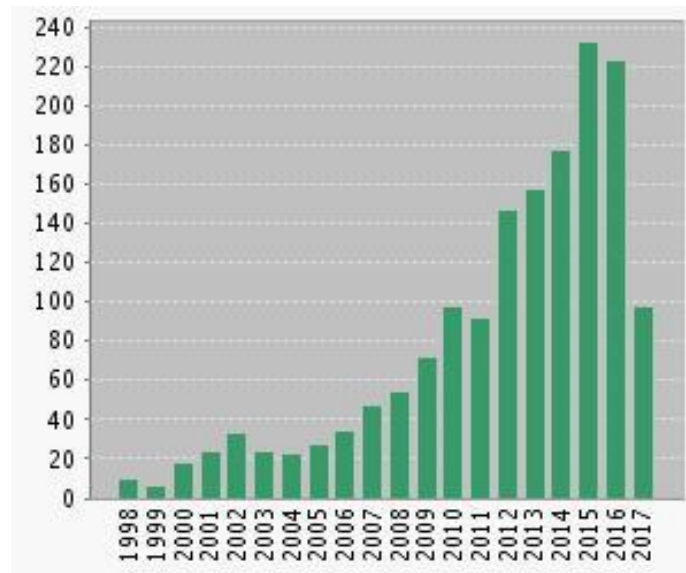
Fig. 1.1.10: Number of publications per year concerning "point of care infection diagnosis". Taken from http://www.webofknowledge.com

In general, techniques to achieve detection, quantification and characterization of pathogens present in samples can be summarized to target the following:

      (a) Whole pathogen(s)

      (b) Metabolites released or consumed

      (c) Genetic material or proteins specific to the target pathogen

Although highly integrated chips are presented which make use of electrochemical[36,37], fluorescence[38–40], amperometric[41,42] or magnetic detection techniques[43], the implementation of these developments into clinical workflows is still missing. One reason is their complex and expensive chip designs, which oppose economic views regarding their disposable nature. In another aspect, the study designs do often not reflect clinical scenarios and only represent simple proof-of-concepts, such as the use of pure culture colonies as starting materials such as in Yeung *et al*.[44] Regarding microfluidic chips, another challenge which is encountered is the low volume of the starting sample material, typically in the μl-range, used in such reports in order to enable processing on chip.[45–49] To have real clinical impact, the onset of bacteremia, bacterial loads of 1 CFU/ml blood or even below, needs to be detected reproducibly. Thus, the low sample volume processed in such examples, significantly reduces the chance to reliably detect early onset of BSI. In addition to the low abundance of analyte, the complexity of the sample blood represents another major challenge for the developments in the field of molecular diagnosis in general. In contrast to the low number of pathogens per one milliliter of blood, which needs to be detected, billions of blood cells are present which interfere with many analytical and preparation technologies and results in low specificity and false negative or positive results. Thus, although impressive advances have been made in the field of lab-on-a-chip and the integration of detection technologies on microfluidic platforms, only recently it was realized that sample preparation is the key issue for successful developments in BSI detection.

BSI Diagnosis Approaches	Advantages	Disadvantages
Blood culture	Gold Standard Routinely used Phenotypical AST Identification from large sample volumes	Labor-intensive Time-consuming Viable but noncultureable pathogens Low sensitivity Risk of contamination
MALDI-TOF	Routinely used Simple processing Fast analysis time Cost efficient Identification from large sample volumes	Needs blood culture Low reliability in species and antibiotic resistance identification Risk of contamination
Molecular biology based diagnosis	Routinely used No cultivation necessary Fast analysis time Specificity	Costs Labor-intensive Low sample volumes Sensitivity Risk of contamination
POC	Full automation No cultivation necessary Fast analysis time No risk of contamination	Early in development Incomplete workflow integration Low processible sample volumes Low LOD

Table 1.1: Overview of the advantages and disadvantages of today's blood stream infection diagnosis approaches.

1.2 Sample Preparation for Blood Stream Infection Diagnosis

Although the above described technologies would allow for more sensitive and specific detection of pathogens including viable but non-culturable bacteria, they still need improved automation and complete workflow integration to replace the gold standard blood culture method. But by far the biggest challenge in applying these technologies to blood stream infection diagnostics is the detection of tiny amounts of pathogens in the vast amount of human blood material, which can only be solved by an appropriate, but currently missing, sample preparation technology.[50–52] Investigating scientific literature, it is evident that a lot of research was conducted during the last 10 years to develop, optimize and automate new technologies for the identification of pathogens, particularly microfluidic lab-on-chip nucleic acid based assays. Only recently, it has been realized that sample preparation, especially for complex samples, is the major bottleneck. This complexity resembles the search for the needle in the haystack: in case of nucleic acid based detection of bacteria in septic human blood, the ratio of human to bacterial DNA is $10^{10}:1$ which results in low sensitivity, specificity and reproducibility.[31] Available sepsis diagnostic products such as the above discussed FilmArray from BioFire Diagnostics LLC., Verigene from Nanosphere Inc. or the GeneXpert from Cepheid Inc. as well as the MALDI-TOF systems from Bruker and Biomerieux circumvent this problem of low analyte/high background concentration by using only positive blood culture. The dependence on culture-enriched samples, however, has several disadvantages: i) long turn-around time, ii) loss of viable but non-culturable pathogens and iii) risk of contamination. A much more efficient solution is to separate pathogen DNA (or cells) from human DNA (or cells). Thus, different sample preparation strategies to increase sensitivity are currently investigated, focusing on the separation of eukaryotic and prokaryotic cells previous to bacterial cell lysis e.g. by size exclusion, dielectrophoresis, acoustic separation or antibody-coupled magnetic beads.[53] Size exclusion using filters is problematic

especially when large volumes (mL range) of blood need to be processed, as clogging necessitates sophisticated and expensive device designs.[54–56] Dielectrophoresis and acoustic separation using standing waves has yet to be shown to be reproducibly achievable in biological samples and to work for milliliter volumes as the slow capture and small transverse dimensions produce extremely low throughput.[57–63] Antibody-coupled beads on the other hand are expensive for routine diagnosis and also cause problems concerning storage stability, epitope screening and binding efficiency. Hence, the acquisition of nanoMR Inc, a company developing such a strategy for pathogen capture from blood, by DNA Electronics, a company developing point-of-care semiconductor DNA sequencing, for US$24 million in 2015 is quite surprising, but confirms the strong need for a strategy to solve the problem of sample complexity.[64] Another pitfall of these strategies is that they all aim at actively capturing the pathogen in the sample which bears the risk of incomplete recovery, specifically critical with a low pathogenic load in addition to omitting intracellular pathogens. Instead of being target specific, a better strategy is to specifically reduce the human background. One commercial development using eukaryotic specific chemical cell lysis and enzymatic human DNA digestion prior to bacterial lysis is the MolYsis Kit from Molzym, which has been shown to significantly increase the specificity and sensitivity of PCR results by reducing the human background.[52,65] However, concerns have been raised over the specificity of the chemical eukaryotic lysis step indicated by up to 80% loss of bacterial DNA from Gram-negative species.[66,67] Another commercially available product for reducing human DNA is the Looxter Enrichment Kit from SIRS-Lab, which makes use of unmethylated CpG island motifs to separate human from pathogen-borne DNA. Compared to the MolYsis kit, however, reduction of human DNA was shown to be not as efficient due to human DNA fragments not containing methylated CpG motifs. Besides having issues with bacterial loss or incomplete removal of human DNA, both products need multi-step protocols involving chemical and enzymatic additives, which are time-consuming, labor intensive, costly, and restricted in sample volume scalability. In addition, feasibility to integrate those methods into a fully automated POC device could not be demonstrated yet.

1.3 Electric Field Induced Cell Lysis

As a comprehensive state-of-the-art concerning the use of electric fields in biotechnology would go beyond the scope of this thesis due to the broad range of applications (transfection, molecule separation, cell fusion, tissue ablation, sterilization, cell perforation, lysis and rupture), this section will focus on electric field induced cell lysis and it's potential as sample preparation technology for BSI diagnosis. Briefly, the use of electric fields for biotechnological applications goes back to the first patents in the area of sterilization and food processing from Doevenspeck in the 1960s.[68] First profound theories of the electric field action on biological cells were developed by Sale and Hamilton in the late 60s.[69] Investigating the effect of electric fields on microorganisms, lysis was observed at 3.1 kV/cm to 17 kV/cm. Using equations already described by J.C. Maxwell for calculating the conduction through a suspension of spheres[70], Sale and Hamilton calculated the transmembrane potential using a model in which the cell was considered to be a conductive sphere isolated from the external conductive medium by a thin dielectric layer, the cell membrane (Fig. 1.3.1).
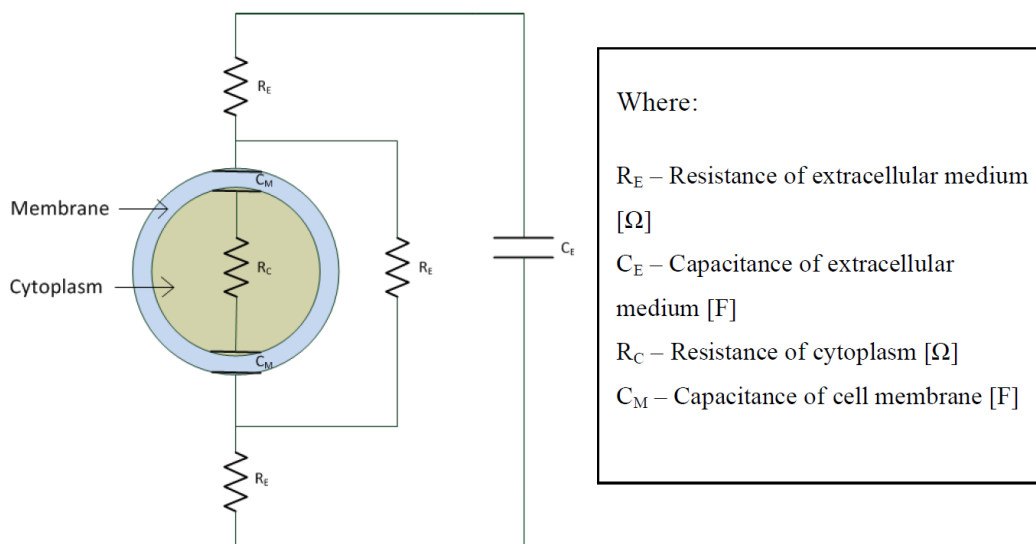
Fig. 1.3.1: Equivalent circuit representation of a cell in suspension. From *Shah DF, Development of a microfluidic device. University Toronto, 2010.*

The *Schwan Equation* is still found routinely in literature to derive values for the electric field induced transmembrane potential ($\Delta\Psi_m$),

$$\Delta\Psi_m = \frac{3}{2}ER\cos(\theta) \qquad (1)$$

where E is the applied electric field, R is the radius of a spherical cell, 3/2 corresponds to the form factor of a sphere and θ is the polar angle measured between the center of the cell and the direction of the electric field.

With resulting transmembrane voltages in the range of 0.7 V and 1.15 V, Sale and Hamilton suggested that an external electric field may cause "*conformational changes in the membrane structure resulting in the observed loss of its semipermeable properties*". Today, several theoretical models exist to explain the process of electroporation. Although still under debate, the most common theory is the transient aqueous pore mechanism hypothesis proposed by Weaver *et al.*[71] and expanded by others[72,73], in which a pulsed external electric field results in polarizing the membrane and increasing its electrical conductivity while inducing thermal fluctuations, which together lead to a rapid rearrangement of localized structures. As a result, hydrophobic pores appear randomly on the surface of the membrane which transform into aqueous pathways, or reversible hydrophilic pores, due to further lipid bilayer rearrangements under the stress of the transmembrane potential (Fig. 1.3.2).
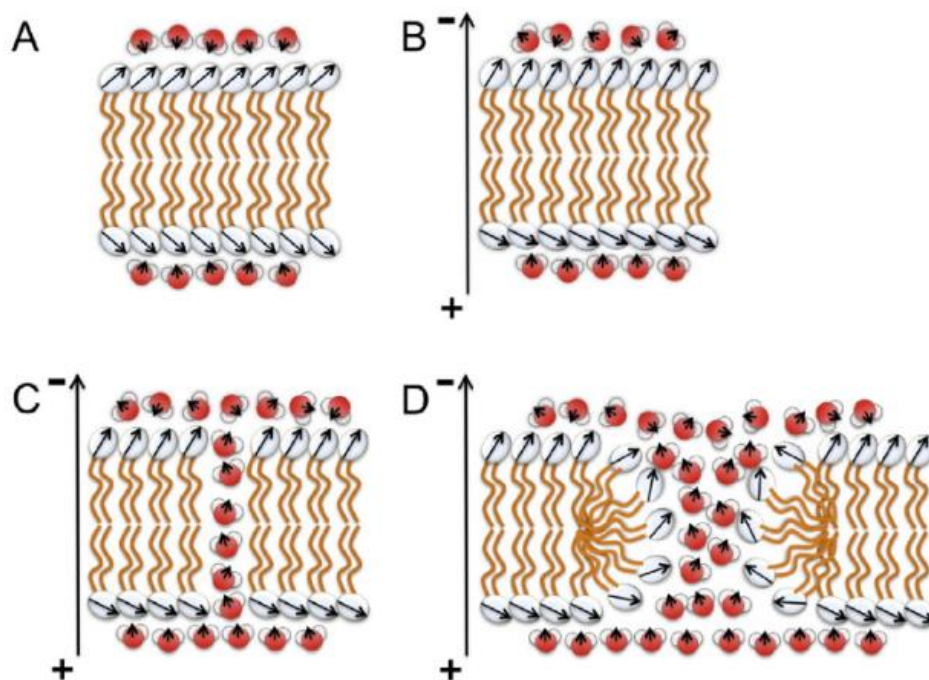
Fig. 1.3.2: Pore formation following electric field exposure. Lipid tails are shown in orange, headgroups are shown in grey. Water molecules are shown in grey (hydrogen) and red (oxygen). Dipole orientation is indicated by arrows. (A) Before application of an electric field, water dipoles close to the membrane point towards the hydrophobic core of the membrane. (B) After initiation of an electric field, orientation of the water dipoles on the cathodic membrane side is enhanced, whereas orientation at the anodic side is weakened. (C) Suddenly, a closed water wire forms across the membrane. (D) The channel expands to a hydrophilic pore by intrusion of additional water molecules and rearrangement of the lipids. Taken from *Kirsch, Bockmann, Biochimica et Biophysica Acta, 2016*[74]

Single, or a combination of a train of DC pulses is typically used for reversible electroporation. This term indicates the closure of the electric field induced pores after pulsing, which is important for retaining the viability of the cells. This is of exceptional importance for one of the most widely used electric field application in biotechnology: the manipulation of cells by introduction of external cargo into cells, such as DNA.

Contrary, irreversible electroporation refers to breaking open the cell by disintegration of the plasma membrane using brief, high electric fields that induces a transmembrane

potential in excess of the threshold value. This phenomenon has also been referred to as electrical lysis, electrical breakdown or electrodisruption.[75–77]
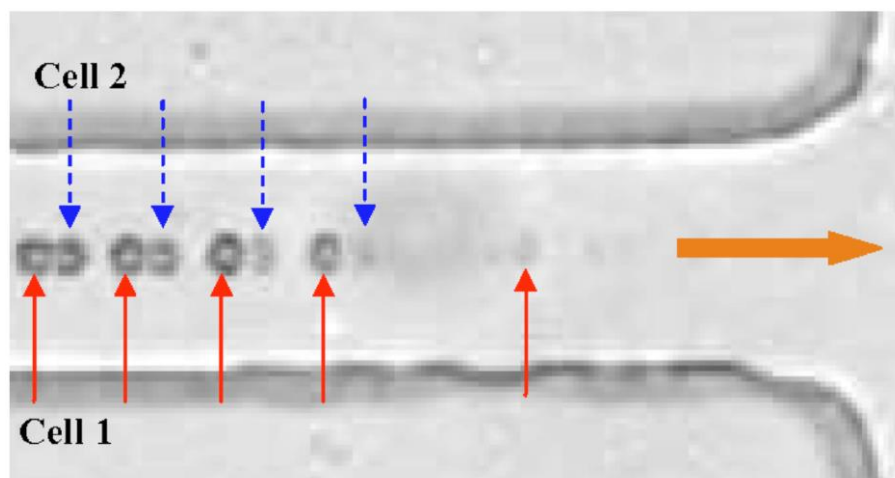
Fig. 1.3.3: Superimposed image of two red blood cells (highlighted as cell 1 and cell 2) illustrating the typical process of electrical lysis in the microchannel constriction. The block arrow indicates the flow direction in the channel. The electric field is applied parallel to the flow direction. From *Church C. et al., Biomicrofluidics, 2010.*[78]

With the advent of microfluidics and single cell analysis techniques, irreversible electroporation gained more and more attention as promising alternative to other cell lysis strategies due to the rapid operation, low power requirement, low cost, simplicity of integration and automation. Several review articles will give the dedicated reader a good overview of the different designs including 2D and 3D electrode arrangements.[79–81] Although an electric field produced by a direct current (DC) source can lead to single cell lysis, bubble formation, electrode decomposition and pH changes as a result of exceeding the water electrolysis threshold pose dramatic problems especially in microfluidic approaches.[75,82,83] Consequently, alternating current (AC) is more generally used as a source to generate the electric fields necessary for cell lysis as several reports argue that electrochemical reactions are efficiently reversed at frequencies above 1 kHz.[78,84–86] As the cell is modeled as spherical capacitor, the simplified Schwan equation from (1) has to be modified to include a term for the charging time[87]:

$$\Delta\Psi_m = \frac{\frac{3}{2}ERcos(\theta)}{1+i\omega RC_m(\rho_i+\frac{\rho_e}{2})} \qquad (2)$$

with $\Delta\Psi_m$ being the change in the transmembrane potential, C_m being the membrane capacitance per unit area , ω being the angular frequency of the external field ($2\pi f$) and ρ being the resistivity of the interior (index *i*) and exterior (index *e*) of the cell and *i* being the imaginary unit.

Obviously, the transmembrane potential induced by an electric field and thus the onset of membrane poration and cell lysis is dependent on cell size and membrane composition. Following this consideration, mammalian cells, such as blood cells which are in the size range of 7 – 15 µm, are more susceptible to electric fields than pathogenic cells, such as bacteria, that have a cell size in the range of 0.1 to 5 µm and possess a rigid cell wall. Several reports support this theory. Bacterial inactivation is typically observed above electric field strength of 10 kV/cm[88,89] whereas the onset of blood cell lysis is observed at electric field strengths > 1 kV/cm.[79,90–92] Interestingly, however, although a large number of reports can be found concerning the lysis of different cell types and cell organelles through the application of electric fields[89,93,94], no report on microfluidic cell-specific lysis in a mixture consisting different cells or in biological samples could be found.
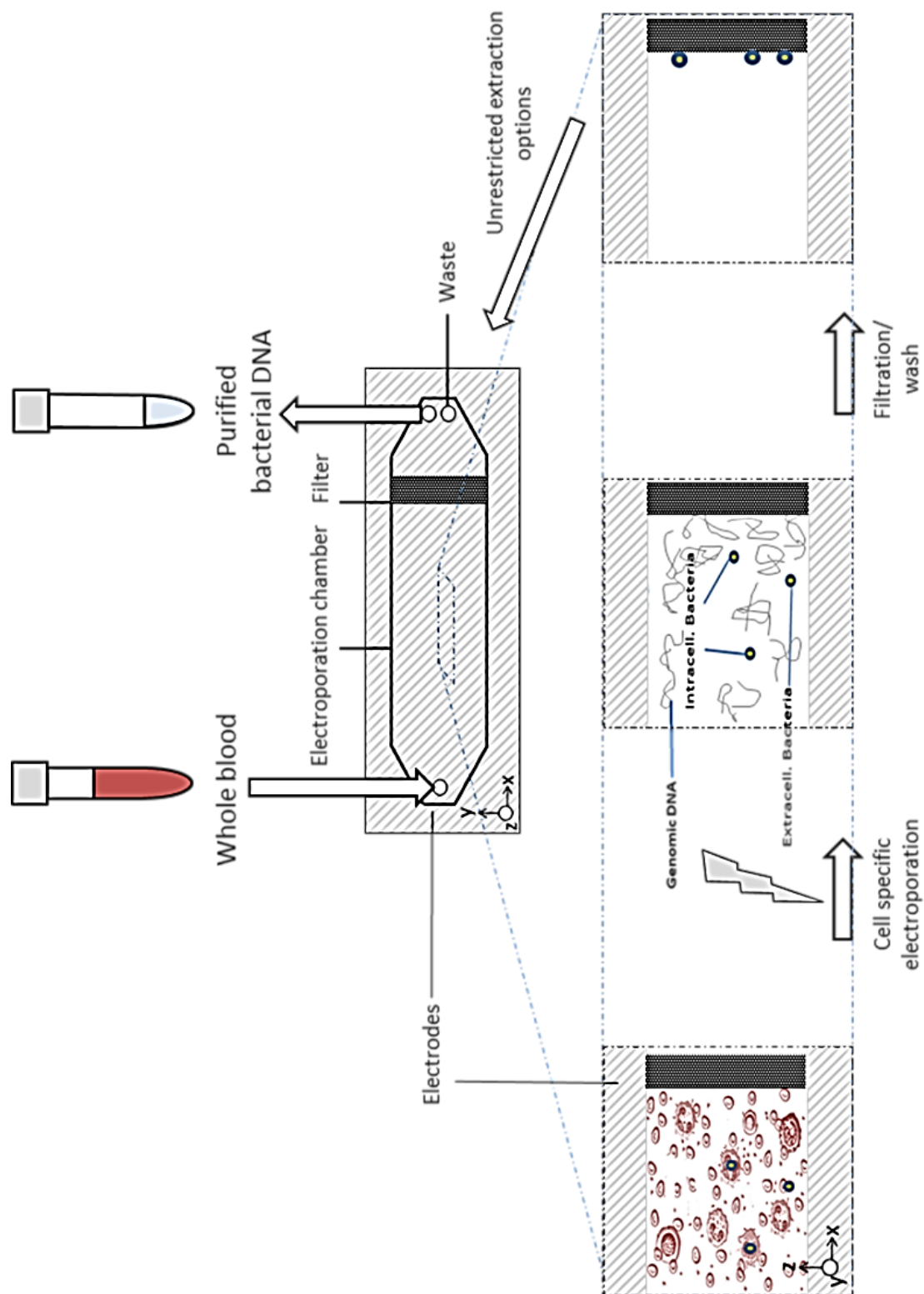
Chapter 2

Concept

In the first months of the thesis, after an in-depth review of the relevant literature, the problem of inefficient sample preparation was identified as the bottleneck for a new generation of BSI detection technologies. Several ideas were developed to specifically separate human from pathogenic cells or DNA. For further investigation of the ideas, criteria concerning possible future applicability had to be met such as robustness and reproducibility, background specificity (no loss of pathogens), possibility to concentrate the analyte from milliliters of sample to a processing volume in the µl range, low cost production and operation, throughput scalability, processing time and ease of automatization. The use of electric fields fulfills these criteria as a simple, cost-effective possibility for specific cell lysis that can be implemented and up-scaled for LOC devices. The basic principle of the idea is depicted in Figure 2.1.

In a microfluidic chip comprising of two parallel plate electrodes, sample is introduced in a continuous flow fashion. By choosing the right electric field parameters, human blood cells are lysed without compromising pathogen integrity. After lysis of human blood cells, free human DNA and inhibitors for molecular biology based down-stream techniques, such as heme, can be washed away and pathogens residing in septic blood can be captured on a filter, thus allowing to incorporate a significant up-concentration step. Subsequently, the captured and purified pathogens can either be removed from the filter for cell-based analysis (e.g. MALDI-TOF) or lysed on-chip using elevated electric fields to obtain intracellular molecules such as nucleic acids for molecular biology based analysis techniques.

Fig. 2.1: Schematic workflow of the idea to use electric field cell-specific sample preparation for the purification of blood borne pathogens. Taken from *Wassermann KJ. et al., WO2015044191.*[95]

Chapter **3**

Methods, Results & Discussion

3.1 Direct Electrode Contact Leads to Unspecific Cell Lysis

3.1.1 Introduction

To evaluate the idea of using electric fields for cell specific lysis, a literature research was conducted to find first parameters as starting point to test and establish the method of electric field induced cell lysis. Genomic DNA isolation through electric field induced lysis has been repeatedly reported.[96–99] Different susceptibilities of cells and cell-organelles to electric fields are reported in literature with *E. coli* being considered one of the most susceptible microorgansims.[72,75,78,79,89,92,93,,94,100–107] Figure 3.1.1 gives a summary of literature values for electric field induced cell lysis from individual reports performing DC electric field induced cell lysis of lymphocytes, erythrocytes and *E. coli* , respectively.
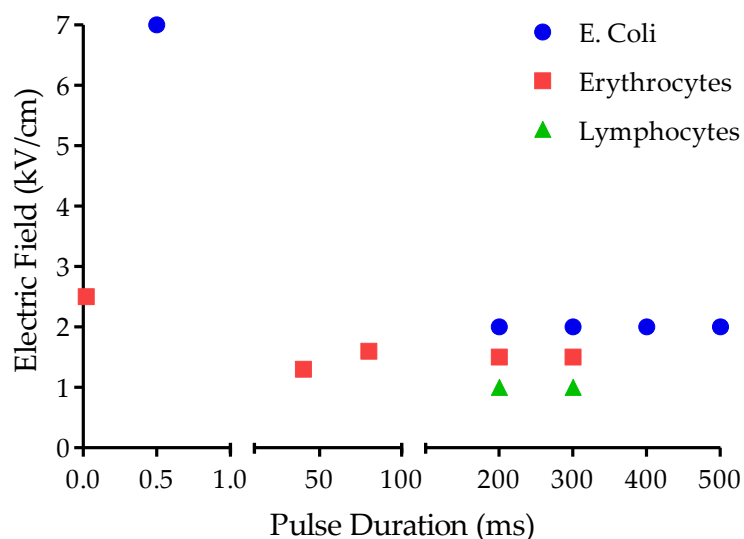
Fig. 3.1.1: Parameters for electric field induced cell lysis using DC electric field pulses taken from literature show a clear trend for cell specific electric field effects.

It has to be noted that different electrode designs, electrode materials, incomplete description of experiments and buffer systems reported, hamper a direct comparison of these literature values. Due to these reasons, DC electric field studies were compared as studies using AC electric fields are even more diverse in respect to the influencing parameters. However, when plotting the individual reported values for the onset of cell lysis, an obvious trend in the differences in the lysis susceptibility of these different cell

models can be seen. Interestingly however, all derived values originated from studies on single cell types, thus cell-specific lysis by electrical fields in an inhomogeneous cell suspension has not been shown. Additionally, Albritton *et al.*[108] and Jensen *et al.*[109] describe the use of electrical fields for unspecific lysis of cells in biological samples and in the patent application of Lu *et al.*[111] unspecific lysis of cells in a microfluidic channel by applying a direct current is described. Of note, Cheng *et al.*[112], Iliescu *et al.*[113] and Tai and Lee[114] use dielectrophoresis prior to electrical lysis to gain specificity.

As the concept of pathogen isolation from blood was envisioned to be realized in a microfluidic flow-through device, focus was set on using alternating current electric fields to circumvent bubble formation and more complex workflows including pulsing aperture and flow rate synchronization. Square AC (sqAC) wave signal with a frequency between 1 kHz to 1 MHz was chosen for the first experiments regarding electric field induced cell lysis in respect to reports arguing higher lysis efficiency compared to sinusoidal signals[110] and the inhibition of bubble formation and electrode dissolution at frequencies above 10 kHz, an often described limitation of using electric field applications especially in microfluidic devices.[84,85]

3.1.2 Materials & Methods

3.1.2.1 Cell Preparations

Human lung fibroblasts (received from AKH Vienna), were cultivated in DMEM medium (Gibco, Life Technologies) with 10% fetal bovine serum (FBS; Thermo Fisher Scientific Inc.) and 1% Pen/Strep Antimycotic (Gibco, Life Technologies) in T75 flasks (Corning Inc.). Cells were grown in a 37°C CO_2 incubator (Heracell VIOS 160i) and split in a 1:3 ratio when a confluence of 70-80% was achieved. For the experiments, cells were washed with 1x phosphate buffered saline (PBS; 10x PBS, Thermo Fisher Scientific Inc.) followed by trypsinization (0.25% Trypsin EDTA, Thermo Fisher) for 5 minutes at 37°C. Cells were harvested, washed, counted and resuspended in 1x PBS to a final cell concentration of 10^6 cells/ml for experiments.

Blood was withdrawn from a healthy volunteer, collection was performed with the K2EDTA Vacutainer system from BD. Blood samples were immediately stored at 4°C and used for a maximum of 5 days. For the leukocyte experiments, whole blood was diluted in a 1:4 ratio with 1x erythrocyte lysis buffer prepared from a 10x concentrate (20.77 g ammonium chloride, 2.5 g of potassium hydrogen carbonate in 250 ml ultrapure water, pH of 8.0 was adjusted by adding 0.5 ml of 0.5 M EDTA). After a 10 min incubation at room temperature, the suspension was centrifuged for 5 min at 500 g. Supernatant was withdrawn and the procedure was repeated until a clear white cell pellet was visible. The leukocyte cell pellet was then suspended in 250 mM sucrose in ultrapure water to a final cell concentration of $2x10^6$ cell/ml.

Kanamycin resistant *E. coli* were grown over night in Luria-Bertani (LB; Carl Roth) medium supplemented with 50 μg/ml Kanamycin sulfate (Sigma Aldrich) in a shaking incubator at 37°C the day before the experiments. Next day, bacterial cell counts were determined by measuring the absorbance at 600 nm using a NanoDrop. Dilutions were made in 250 mM sucrose in ultrapure water and the final concentration of *E. coli* spike-in

in the leukocyte or whole blood dilution was adjusted to 10^3 cells per treatment volume. After the experiments, samples with spiked-in *E. coli* were plated on LB Agar (Carl Roth) with 50 µg/ml Kanamycin sulfate and incubated over night at 37°C.

3.1.2.2 Electrode Design and Device Assembly

Electric cell lysis units (ECLU) with transparent electrodes were constructed by using two ITO glass slides (ITO Coated Glass Slides, 4-8 Ω, Cytodiagnostics Inc.) with the ITO covered side facing each other. Using a scalpel, a 55 µl chamber was cut into a 100 µm thick silicon foil (Thermosilikonfolie KU-KE-11, Aavid Kunze GmbH) and sandwiched between the two ITO glass slides. The assembly was fixed using paper clips. To manually inject sample into the ECLU, two holes were drilled into the top electrode using a diamond covered glass drill before assembly. Nanoports (Nanoport Std 6-32 coned connector and fitting for 1/32" OD tubing, IDEX Health & Science LLC), PTFE tubing (0.4 mm ID, 0.8 mm OD, Scantube) and a syringe connected to the tubing via a cannula was used for sample manipulation and washing. Adherent copper tape was used to preserve the ITO surface as alligator clips were used for electrical connection.

For lysis experiments done with copper electrode material, rectangular electrodes were cut out of standard PCB boards using a diamond covered circular saw blade. For a more efficient testing of parameters, a batch design was used. Chamber forming foils of 50 µm (Thermosilikonfolie KU-KG-50, Aavid Kunze GmbH) or 25 µm (PEEK foil, DuPont) thickness were used for experiments with 2 kV/cm or 4 kV/cm, respectively.

In case of experiments performed with PTFE covered copper electrodes, electrodes were first thoroughly cleaned with ultrapure water, isopropanol and acetone for 15 min each in an ultrasonic bath. After drying the electrodes using pressurized air, electrodes were spray coated in a hood with PTFE (Polytetrafluoroethylene, Fluoropan T-20, Klüber GmbH), followed by a 30 min incubation at 70°C to assist solvent evaporation. To monitor coating quality, the electrical resistance was measured of each batch assembly before lysis experiments.

3.1.2.3 Experimental Setup

Experiments with the ITO chips were performed as follows. The chip connected to the function generator (DG4012, Rigol Technologies Inc.) was placed onto an inverted microscope, a cell suspension prepared as described in *3.1.2.1 Cell preparations* was loaded into the chip via a syringe and Teflon tubing until the chamber was filled, lysis parameter was tested and observed under the microscope. After the experiment, the cell suspension was withdrawn from the chamber, the chamber was washed with 100 µl PBS and added to the withdrawn cell suspension, 100 µl PBS was also added to the controls. Suspensions were loaded onto a hemocytometer (Thoma hemocytometer, Laboroptik Ltd.) and cells were counted manually under an inverted microscope.

Experiments performed in the batch design using copper electrodes were performed as follows. A silicon foil forming 20 µl chamber was placed on the bottom electrode, 15 µl sample was manually pipetted onto the center of the bottom electrode, the top electrode was placed on top, a small steel weight was used to fix the assembly and the electrodes were contacted using alligator clips connected to the function generator.

After the lysis experiment, cells were withdrawn from the electrode surface manually by a pipette. Cells were transferred to a hemocytometer and counted manually under an inverted microscope. Electrodes were washed by repeated flushing of the surface with ultrapure water.

3.1.2.4 Readout

Cell counts of the stock cell suspension (Control) or the non-exposed 0 V control were set to 100%, percent cell lysis was calculated as percent of cell number in the treated samples relative to the controls. Each parameter was tested at least three times.

Bacterial spike-in experiments were evaluated by colony count after incubation of the inoculated agar plates over night at 37°C.

3.1.3 Results

3.1.3.1 Establishment of Electric Field Induced Cell Lysis Using Fibroblast Cells

The very first encounters with Bioelectronics were done using indium tin oxide (ITO) coated glass as electrodes. The reason for choosing this type of electrode material was the chance to microscopically visualize cells when voltages are applied and to get a direct read-out of the wide plethora of parameter possibilities that could be tested. First experiments were done using fibroblast cells immersed in phosphate buffered saline and a chamber designs as depicted in Figure 3.1.2. According to literature, strong pH changes and bubble formation at frequencies below 1 kHz were observed[84,85,115], thus lysis experiments were done at 20 Vpp and square wave frequencies between 1 kHz and 1 MHz. After 30 seconds exposure, cells were withdrawn from the chamber and cell lysis was determined.
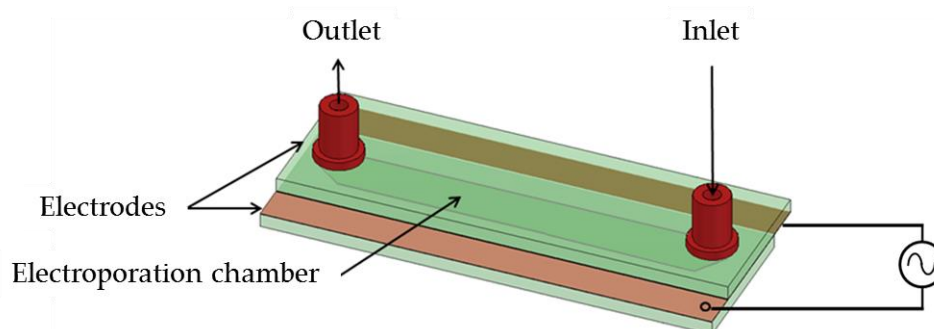
Fig. 3.1.2: CAD design of the used ITO electric field lysis chip. ITO coated glass slides were used as electrodes (green). Fluidic in- and outlets were drilled in the top electrode. A chamber was cut in a 100 μm thick silicon foil used as electrode spacer. Electrical contacts to the ITO surface were established by using a copper adhesive tape and alligator clips.
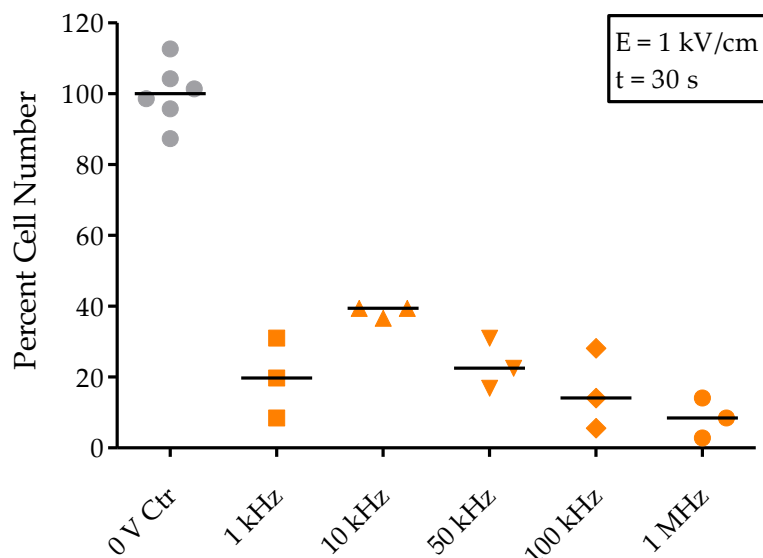
Fig. 3.1.3: Results of first fibroblast cell lysis experiments using the shown ITO electric field lysis chip. A square AC signal of 20 V_{PP} (1 kV/cm) was applied for 30 s with the indicated frequencies. Bars represent the median.

As can be seen in Figure 3.1.3, cell lysis through electric fields could be achieved with the described setup. Fibroblast lysis was most efficient at a frequency of 1 MHz. These pilot studies served to establish electric field induced cell lysis. Thus, next experiments were planned to test the lysis behavior of human leukocytes derived from blood. Although using frequencies above 1 kHz, repeated use of the electrode material lead to loss of ITO transparency and brownish discoloration followed by loss of electrode conductivity. Due to the relatively high cost of ITO glass slides in respect to the number of planned experiments and in respect to possible future market requirements, the electrode material was changed to copper-coated printed circuit boards (PCB) for the next experiments.

3.1.3.2 Leukocyte Cell Lysis with Electric Fields

The final goal of developing a new sample preparation strategy for infection diagnosis from whole blood is to significantly reduce the human DNA background for more sensitive and specific pathogen detection using molecular biology based techniques. As the majority of cellular DNA found in blood is carried by leukocytes, removal of leukocyte borne DNA is the first key challenge. After electric field induced cell lysis could be achieved in experiments with fibroblasts, the next crucial point was to address the possibility to achieve significant electric field induced leukocyte lysis without compromising bacterial integrity. Interestingly, no literature reports could be found in this respect.

Additionally, as Pucihar *et al.* argue for higher electric field efficiency in solutions of lower ionic strength[105], PBS was substituted for a low ionic strength isoosmolar 250 mM sucrose solution in ultrapure H_2O. A schematic of the experimental setup is depicted in Fig. 3.1.4.
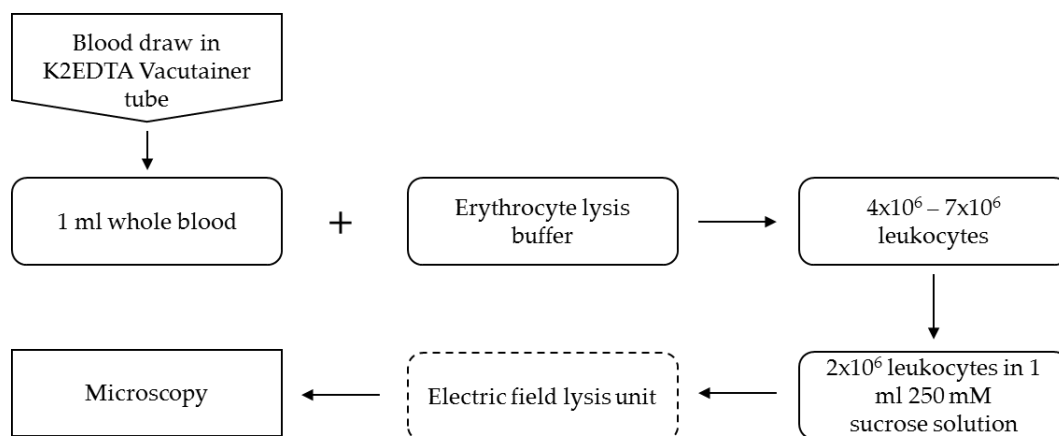
Fig. 3.1.4: Schematic illustration of the experimental workflow. From a 1 ml EDTA blood sample, leukocytes were isolated by repeated incubation in erythrocyte lysis buffer, pelleted leukocytes were suspended in isoosmolar sucrose solution and immediately used for lysis experiments.

In order to test the lysis efficiency, leukocytes were isolated from whole blood, suspended in 250 mM sucrose solution and then exposed for 60 seconds to electric fields in the

stationary batch design depicted in Figure 3.1.5. The ITO electrodes were substituted by more cost efficient rectangular copper electrodes cut out from PCB boards.
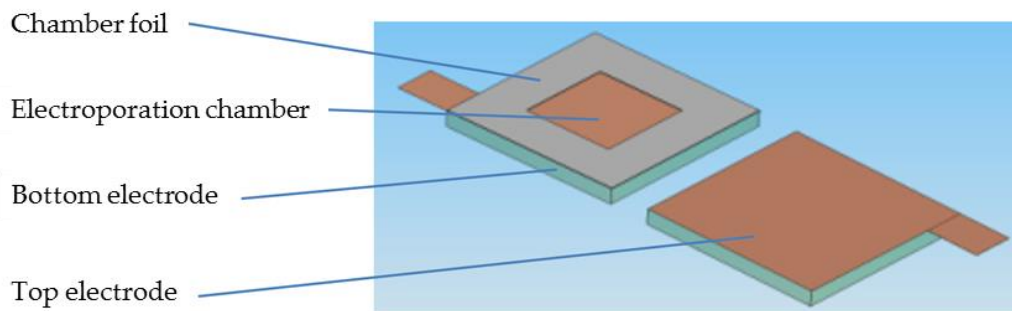
Fig. 3.1.5: Schematic of the stationary ELCU comprising copper coated PCB boards. The chamber-forming silicon foil (grey) also acts as electrode spacer. A 50 µm and a 25 µm thick foil was used, resulting in 2 kV/cm and 4 kV/cm maximum electric field strength for experiments with leukocytes and whole blood, respectively.

As shown in Figure 3.1.6, efficient leukocyte cell number reduction could reproducibly be achieved, showing up to 76,7% reduction in total cell number at square wave alternating voltages of 20 V$_{PP}$ at 1 MHz for one minute.
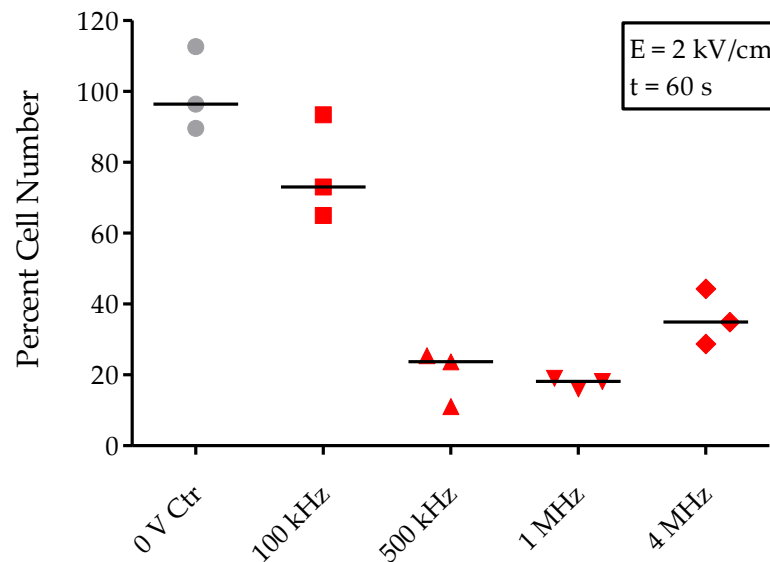
Fig. 3.1.6: Frequency dependent human leukocyte cell lysis at an electric field strength of 2 kV/cm in the stationary ECLU. Cells were exposed to a square AC of 20 V$_{PP}$ for 60 s at the indicated frequencies. Bars represent the median of three individual experiments.

3.1.3.3 Bacterial Spike-in Experiments

To test if lysis is specific to human leukocytes, spike-in experiments were performed by adding kanamycin resistant *Escherichia coli* to the leukocyte solution with a final concentration of 10^3 bacteria per 15 µl sample for each parameter.
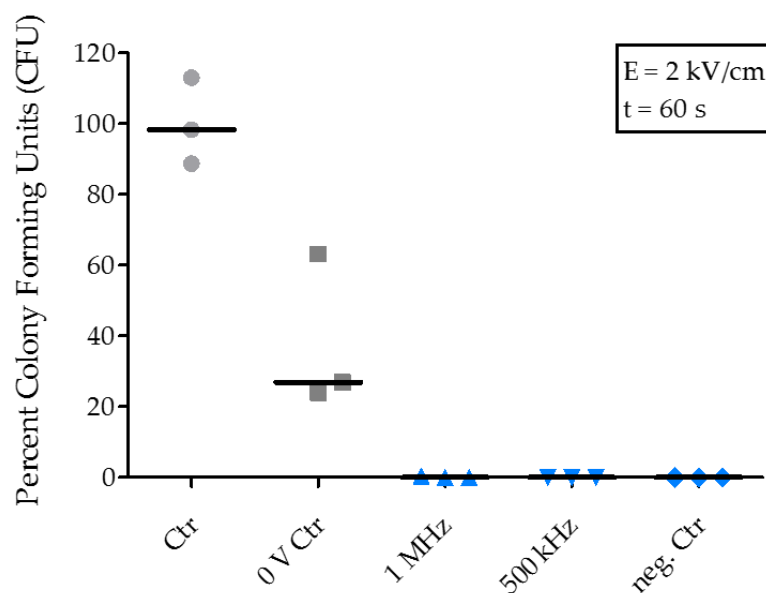
Fig. 3.1.7: Spike-in experiment using kanamycin resistant *E. coli* spiked into the human leukocyte suspension and exposed to a square AC of 20 V_{PP} for 60 s at the indicated frequencies. Sample was withdrawn from the initial cell mixture (Ctr) or the stationary ECLU (0 V Ctr, 1 MHz, 500 kHz) and plated on Ager plates with 50 µg/ml kanamycin. A negative control (neg. Ctr) was included representing a leukocyte suspension without bacterial spike-in. Bars represent the median bacterial colony counts after three individual experiments.

Two detrimental effects could be observed during these spike-in experiments. First, using the current strategy, selective human blood cell lysis was not achieved as shown by the complete loss of bacterial viability at 1 MHz and 500 kHz electric field exposure. Second, comparing the number of colony forming units of control and 0 V control, an electric field independent effect on bacterial viability must exist.

It was supposed that this electric field independent effect of bacterial loss was either due to incomplete removal of bacteria from the electrode surface or due to the direct contact of bacterial cells with copper. Indeed, a report by Mathews *et al.* describes the negative effect of contact to cooper surfaces on bacterial viability.[116]

To prevent direct contact between the copper electrode and the cell suspension and to improve sample retrieval, a hydrophobic PTFE (Polytetrafluoroethylene, Teflon) spray coating was tested next.
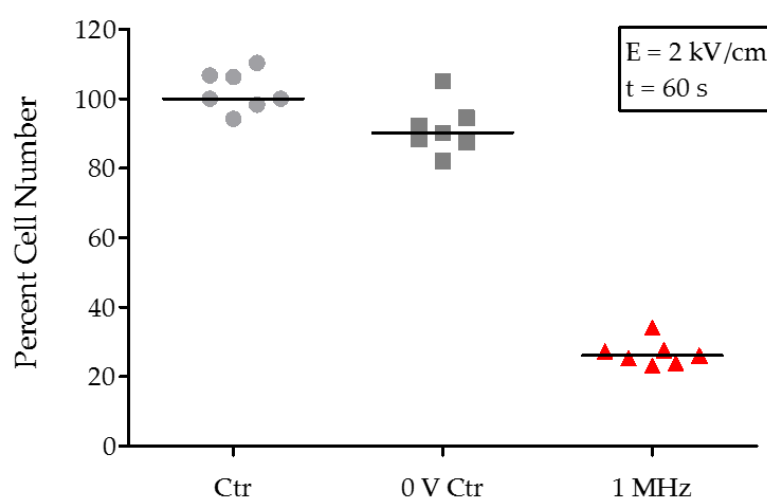
Fig. 3.1.8: Human leukocyte lysis at an electric field strength of 2 kV/cm in the stationary ECLU comprising PTFE coated copper electrodes. Cells were exposed to a 1 MHz square AC of 20 V_{PP} for 60 s. Bars represent the median of seven individual experiments.

Using a PTFE passivated electrode surface, leukocyte cell lysis comparable to non-passivated electrodes was observed (Fig. 3.1.8). In contrast, the results of the spike-in experiments show unaltered bacterial viability in the electric field exposed sample when compared to the 0 V control (Fig. 3.1.9). The manual withdrawal of the sample from the electrode surface again lead to a high variance and a reduced number of colony forming units in the 0 V control samples compared to the control. Compared to the values of Fig. 3.1.7, however, an improvement due to the PTFE coating could be observed. The slight increase in bacterial colony forming units in the electric field exposure sample compared

to the 0 V control sample on the other hand might originate from electrophoretic forces which further reduces adhesion of bacteria to the surface during the one minute treatment.
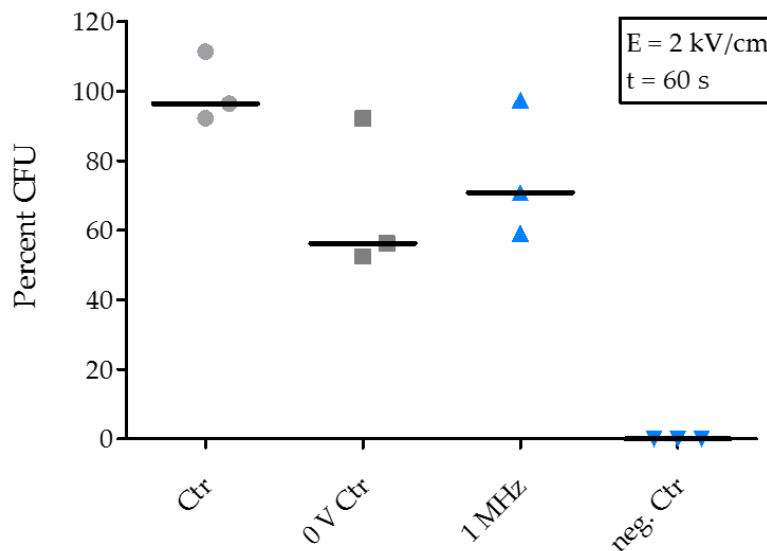
Fig. 3.1.9: *E. coli* spike-in experiment using PTFE-coated copper electrodes shows increased bacterial viability compared to experiments using non-passivated electrodes. A 20 V_{PP} square AC was applied for 60 s. Bars represent the median of three individual experiments.

As this was the first proof-of-principle for cell-type specific lysis in a complex sample, the idea of using electric fields as a new strategy for sample preparation to sensitively and specifically detect blood borne pathogens was further pursued.

3.1.3.4 Whole Blood Cell Lysis with Electric Fields

In order to reduce final protocol complexity, the next goal was to realize whole blood cell lysis utilizing the PTFE passivated electrodes. To achieve the necessary higher electric field strengths for erythrocyte cell lysis, the 50 μm thick silicon spacer foil forming the chamber was replaced by a 25 μm PEEK (Polyether ether ketone) polymer foil. As the maximum output voltage from the function generator used was 20 V_{PP}, the reduction of the electrode distance to 25 μm resulted in the maximum electric field strength of 4 kV/cm.
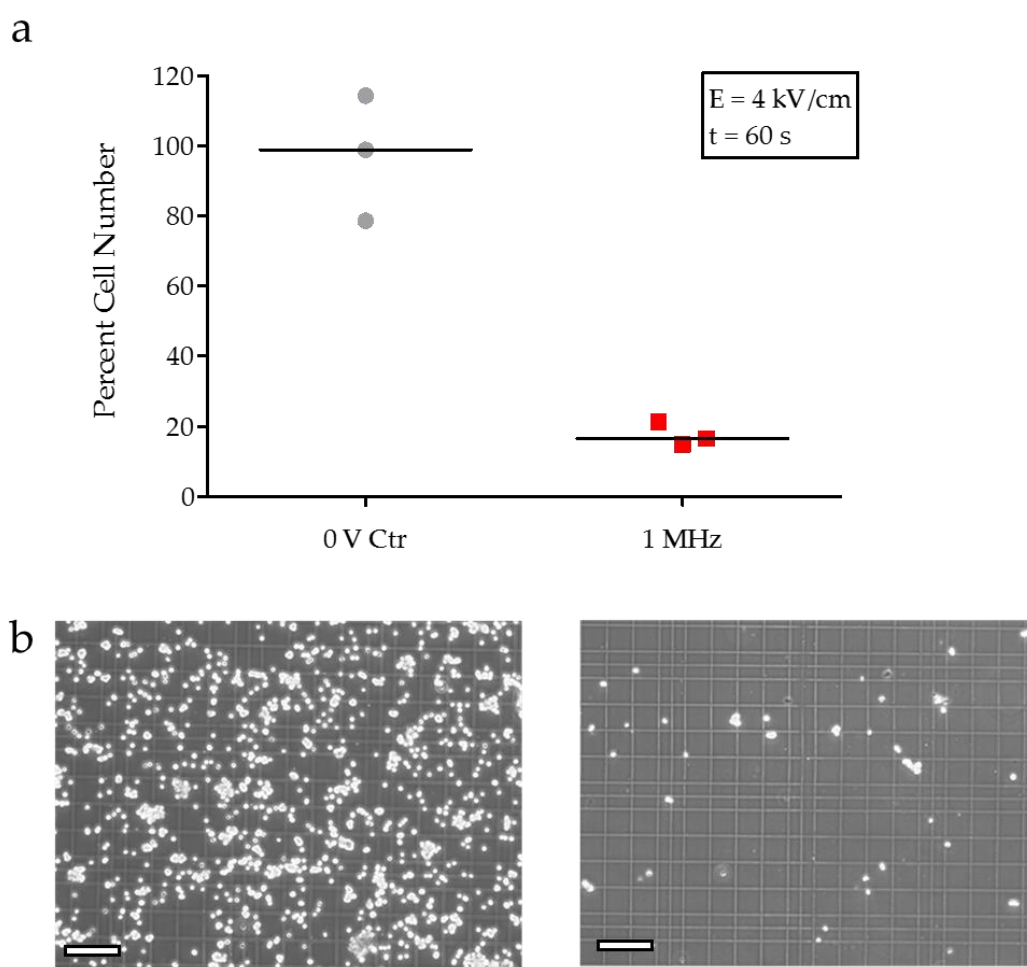
Fig. 3.1.10: (a) Increasing the electric field strength to 4 kV/cm results in effective whole blood cell lysis. Bars represent the median of three individual experiments. (b) Micrograph of 1:100 diluted whole blood without exposure to electric fields and after 60 s at 20 V_{PP} sqAC (scale bar: 100 μm).

Experiments using the 25 μm thick PEEK foil showed efficient whole blood cell lysis at an electric field strength of 4 kV/cm. Figure 3.1.10 shows that a 83% whole blood cell lysis was achieved using a square AC of 1 MHz for less than 1 minute. In addition, the elevated electric field strength did not significantly affect bacterial spike-in viability, as can be seen in Figure 3.1.11.
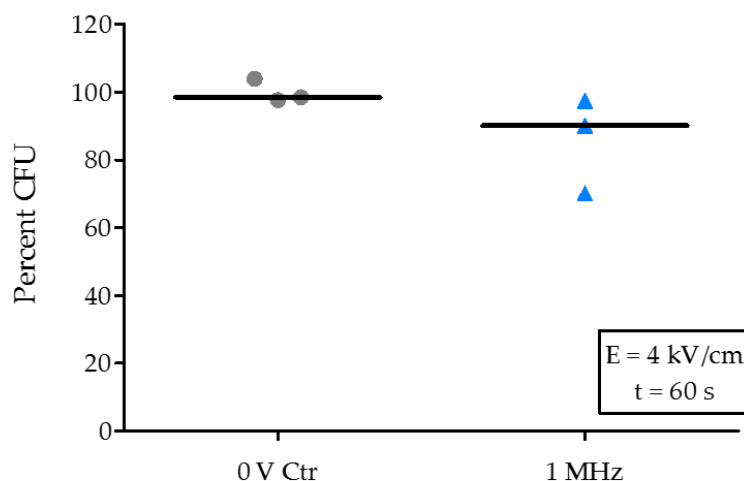
Fig. 3.1.11: *E. coli* spike-in experiment confirming efficient whole blood lysis at 4 kV/cm (20 V_{PP} sqAC, 1 MHz, 60 s) does not significantly affect bacterial viability. Bars represent the median of three individual experiments.

Although the strategy of reducing cell adherence and contact to the electrode surface seemed promising, the use of PTFE spray coating had some major drawbacks. First, leukocyte lysis and *E. coli* viability was only reproducibly achieved with certain sets of electrodes. Second, the adhesion of the coating to the electrode was not permanent and washing of the electrodes after each parameter test lead to a visible removal of the passivation, thus electrodes could only be used for a limited number of experiments. Overall, the spray application lead to bad reproducibility and an inconsistency of the quality of the passivation.

As the PTFE passivation on top of the electrode adds a resistive element, the quality of the passivated electrodes before lysis experiments was evaluated by measurements of the overall resistance after assembly and before testing a parameter. Results showed low

reproducibility of the electrical parameter and a correlation with variances in the results of the lysis experiments. Only a limited number of prepared electrodes achieved a total resistance above 1 MΩ, which was the threshold level were electrodes were considered fully coated. Electrodes which showed resistance below this level lead to unspecific lysis of blood cells, thus simultaneously affecting bacterial spike-in viability as shown in Figure 3.1.12.
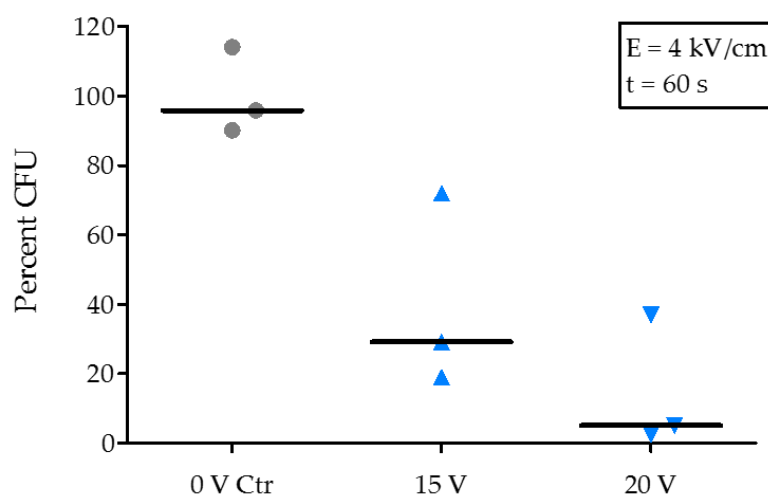
Fig. 3.1.12: *E. coli* spike-in experiment using a deficient PTFE electrode coating shows reduced bacterial viability after applying 15 V_{PP} and 20 V_{PP} at 1 MHz sqAC for 60 s. Bars represent the median of three individual experiments.

The first reason to introduce a PTFE passivation on the electrode was to inhibit cell adhesion and direct contact of bacterial cells with the copper electrode. As a locally deficient PTFE coating would still prevent adhesion and direct contact with the electrode by most bacterial cells, the significant loss of bacterial viability was expected to be due to another effect.

A direct contact of the electrode with the cell suspension, however, would indicate unspecific effects due to pH changes, joule heating and electrolysis when applying high voltages. Although it is often stated in literature that joule heating and electrochemical effects do not play a role when alternating currents above 1 kHz are applied, the gained results and the fact that no reports on microfluidic cell specific lysis with electric fields in

complex biological samples could be found urged for a deeper investigation on the role of electrode passivation for electric field applications in biology.

3.2 Capacitive Coupled High Frequency Electric Fields Lead to Specific Cell Lysis

3.2.1 Introduction

First proof-of-principle experiments for the selective and rapid lysis of human blood cells by electric fields have been demonstrated repeatedly in a stationary batch design based on copper electrodes with Teflon passivation (3.1). Due to the non-specific electric field effect when using non-passivated electrodes or deficient coatings, electrode passivation was expected to be decisive for the successful specific lysis of human cells using electric fields for the enrichment of pathogens from a blood sample. Thus, at this point, the role of a passivation layer and its respective electrical characteristics had to be studied.

As cells are suspended in an electrolyte and electric potentials are applied to non-passivated electrodes, it was thus hypothesized that electric field effects are superimposed by non-specific secondary effects caused by a substantial charge transfer at the electrode/electrolyte interface, leading to electrochemical reactions which induce electrode decomposition, electrolysis, pH changes and bubble formation as well as joule heating. Likewise, Saulis *et al.* showed the release of Al ions from the Al electrode to the electroporation buffer, which was accompanied by significant changes in the pH of the solution.[117] Similarly, Kim *et al.* showed significant pH changes at the electrode surface induced by electrolysis during electroporation.[91] Although it is often argued that electrochemical effects do not influence electric field effects when alternating currents above 1 kHz are used, cytotoxic effects of cell-free culture medium due to electrochemical oxidation processes were demonstrated after exposure to nanosecond pulses by Pakhomova *et al.*[118] Additionally, An *et al.* investigated the hydrolysis of water and could show the generation of hydrogen ions and pH gradients at the electrode in the frequency range of 5 kHz and 12 kHz.[119] Thus, the effect of electrochemical reactions at the electrode surface might be reduced at higher frequencies due to fast reversal of the reactions. In microfluidic approaches however, were the majority of the cells are in close proximity to the electrode surface, these effects might still play a major role. Also the data from 3.1 demonstrating non-specific electric field effects even at frequencies of 500 kHz and 1 MHz, implicated the importance to inhibit or at least significantly reduce direct charge transfer

at the electrode/electrolyte interface. One strategy to circumvent adverse bubble formation, heating and electrochemical reactions is to increase the distance between electrodes. Lee and Cho used a DC electric field across a long channel with an orifice to concentrate the electric field locally.[75] Kim *et al.* encased one electrode in a glass capillary to locally separate variations in pH from the cell-containing suspension.[91] In both concepts however, a considerable part of the applied electric energy is converted into electrochemical reactions at the solid to liquid interface, representing significant losses and thus preventing an exact control of the electric field strength within the sample. Furthermore, both strategies are accompanied by the need to apply high voltages due to large electrode distances while affecting only a small population of cells at a time. To increase through-put and efficiency, microfluidic flow-through designs with planar electrodes and large effective electric field areas would have a great impact for lab-on-chip and point-of-care applications and the reduction of the electrode distance to the μm-range would drastically reduce the required voltages. For small electrode distances, however, diffusion length and electrical resistance of the fluid in the inter-electrode space is drastically reduced. For non-passivated electrodes the influences of secondary faradaic current based effects therefore increases in such a configuration. This is especially important for flow through designs were successive pulses need to be applied for longer durations. Hence, for a drastic reduction of the superimposing faradaic current based effects, focus was set on the investigation and the optimization of the passivation layer.

3.2.2 Materials & Methods

3.2.2.1 Cell Preparation and Handling

Blood was withdrawn from a healthy volunteer, collection was performed with the K2EDTA Vacutainer system from BD. Blood samples were immediately stored at 4°C and used for a maximum of 5 days. For the experiments, whole blood was diluted 1:100 in 250 mM sucrose in ultrapure water.

Kanamycin resistant *E. coli* were grown over night in Luria-Bertani (LB) medium with 50 µg/ml Kanamycin sulfate in a shaking incubator at 37°C the day before the experiments. Next day, bacterial cell counts were determined by measuring the absorbance at 600 nm using a NanoDrop. Dilutions were made in 250 mM sucrose in ultrapure water and the final concentration of *E. coli* spike-in in the 1:100 whole blood dilution was adjusted to 2-$5x10^2$ cells per 15 µl treatment volume. After the experiments, samples with spiked-in *E. coli* were plated on LB Agar with 50 µg/ml Kanamycin sulfate and incubated over night at 37°C.

3.2.2.2 Device fabrication

For the bare gold electrodes, 5 nm chrome and 200 nm gold were deposited on square glass slides using high-vacuum thermal evaporation.

Polymer passivated electrodes were fabricated by spin coating a square-cut printed circuit board (PCB) substrate with AZ6612 photoresist (MicroChemicals GmbH) at 5000 rpm for 1 minute followed by a post bake at 125°C for 50 s on a hotplate. To ensure uniform thickness of the passivation layer, the outer 2 cm were cut-off after coating.

For the SiO_2 passivated electrodes, P/Bor doped 2" Si-wafers (0.01-0.02 Ωcm) with a 50 nm thermal oxide layer (Active Business Company GmbH) were diced to form square

electrodes using a blade saw. Contacts were created on the backside of the wafer by removing the thermal oxide with hydrofluoric acid. To reduce the semiconductor/metal interface resistance, the silicon surface was mechanically roughened with sand paper prior to the deposition of 5 nm chrome and 200 nm gold by high-vacuum thermal evaporation. The wafers were then mounted on massive aluminum blocks using conductive silver paste.

For all experiments, a 25 μm PEEK foil was used as electrode spacer framing a 20 μl chamber in the middle of the electrode surface.

3.2.2.3 2″ SiO₂ Flow-through Chip

Silicon wafer (P/Bor doped 2″ Si-wafers, 0.01-0.02 Ωcm, with a 50 nm thermal oxide, Active Business Company GmbH) was laminated (Renz HT330L) with a 30 μm or 55 μm thick Ordyl negative dry resist at 110°C. In the clean room, wafers were soft baked for 1 min on a 95°C hot plate followed by UV contact exposure using a mask comprising the channel geometry and a mask aligner. After an additional minute on a 95°C hotplate, channels were produced using an SU-8 developer and an ultrasonic bath. Fluidic in- and outlets were created by sandblasting the wafers using a rubber mask. The in- and outlets were used to align the top wafer according to the channels on the bottom wafer. Chips were bonded using the laminator repeatedly. To electrically contact the chips, the oxide was removed from the top and the bottom wafer by sandpaper prior to the deposition of 5 nm chrome and 200 nm gold by high-vacuum thermal evaporation. Nanoports were mounted above the fluidic in-and outlets to finalize the production of SiO₂ flow-through chips.

Capacitance of ECLUs was measured with an LCR meter (B&K Precision, Model 875B) at a given fixed frequency of 119 Hz.

3.2.2.4 Experimental Setup and Data Analysis

A function generator (Rigol 4102) connected to a voltage amplifier (Falco WMA-300) was used as a power source. Voltage and current (via a 1 Ω resistor as indicated in the Figure captions) was monitored with an oscilloscope (Rigol DS1104B) as seen in Figure 3.2.1 (b).

For the experiments, 15 μl of a 1:100 blood dilution in isoosmolar 250 mM sucrose in ultrapure water with and without spiked-in *E. coli* were manually pipetted onto the bottom electrode. The PEEK foil and the upper electrode were manually assembled and fixed in position. A high frequency signal with 1 MHz and varying voltage amplitudes was applied for 3 seconds or 1 minute for the gold or the passivated electrodes, respectively. After treatment, the sample was aspirated from the electrodes. For the analysis of blood cell lysis, the cell suspension was transferred to a hemocytometer and bright field images were taken with an inverted microscope equipped with a digital camera. Cell counts were done using ImageJ's automatic particle count.[120]

Spike-in experiments were evaluated by standard bacterial colony count after incubating the inoculated Agar plates over night at 37°C.

3.2.3 Results

3.2.3.1 Non-passivated Gold Electrodes Confirm Unspecific Lysis

To confirm the unspecific effects originating from direct contact of the cell suspension with the electrode and to exclude copper-based effects, electrical cell lysis with blood samples and spiked–in *E. coli* were performed using non-passivated gold electrodes at a frequency of 1 MHz.
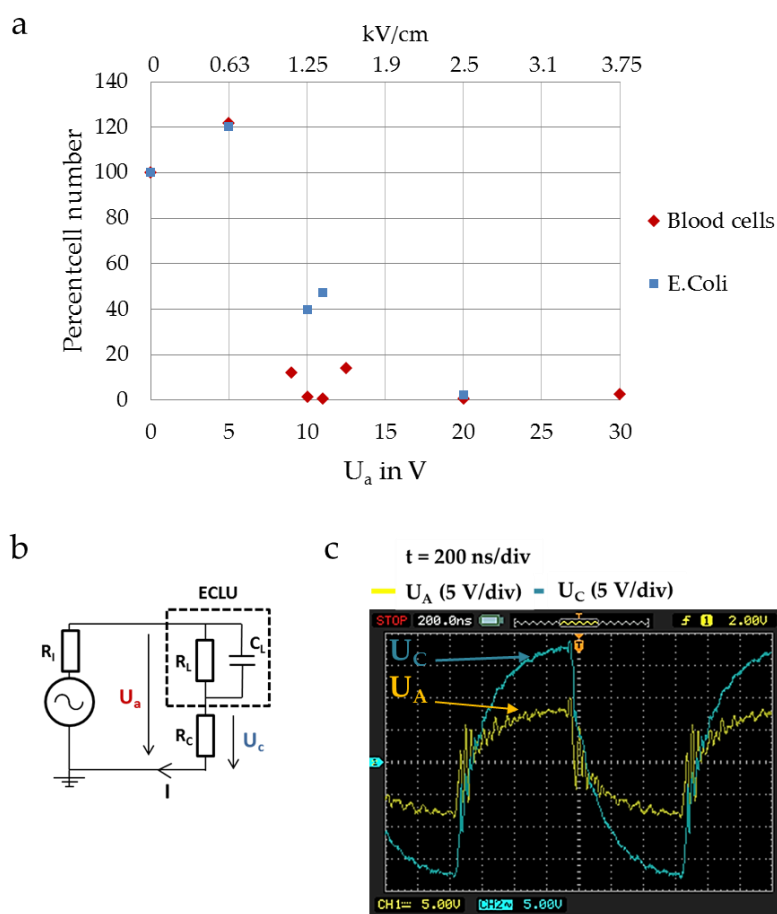
Fig. 3.2.1: (a) Non-specific lysis of human blood cells and spiked-in *E. coli* using bare gold-electrodes. **(b)** Measuring circuit. ECLU: Electric cell lysis unit, U_A: applied voltage (sqAC), U_C: voltage proportional to current, I: current, R_C: resistor for current measurement, R_L: resistance of lysis cell, C_L: capacitance of lysis cell, R_I: internal resistance of function generator. **(c)** Voltage and current plot, U_c is proportional to the total current *I* (voltage at a 1 Ω resistor in series to the ECLU).

Figure 3.2.1 a shows efficient lysis of human blood cells already at 7 V applied. Taken the chamber design, this corresponds to electric field strengths of 2.8 kV/cm. This value is comparable to values found in literature in respect to erythrocyte cell lysis.[75,90] Again, also the spiked-in *E. coli* were inactivated at electric field strengths as low as 4 kV/cm resulting in a reduction in the number of colony forming units of 60% compared to the 0 V control measurement. Figure 3.2.1 (c) depicts the voltage and current characteristics of electrodes in direct contact with the fluid sample. The ECLU comprising of two bare electrodes exhibits RC-characteristic with the current in phase with the voltage. Thus, the dominant load is due to ohmic losses through the liquid resulting in faradaic current.

3.2.3.2 Polymer-based Coatings Result in Electric Field Shielding

As the spray application of the Teflon coating resulted in neither a reproducible, homogeneous layer thickness nor in a coating for repeated use, both the homogeneity and the durability of the electrode passivation had to be improved.

To circumvent problems with poor adhesion of the passivation layer, several other strategies were tested.

Electrodes were spin coated with DuPont Teflon AF in different concentrations (3%; 1%; 0.6%; 0.3%) in Fluorinert FC-40 or with acrylic resins. Passivation adhesion to electrodes and the consistency of the overall electrical resistance was high but only minor electric field induced effects could be observed, mainly cell fusion and the formation of erythrocyte cell chains (Fig. 3.2.2).
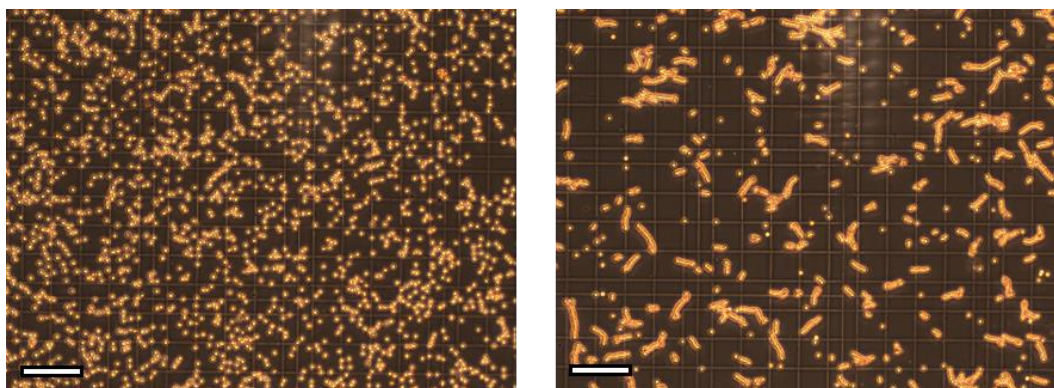
Fig. 3.2.2: Non-treated whole blood dilution (left). Cell fusion and pearl-chain formation observed after applying 30 V, 1 MHz sqAC to Teflon AF spin coated copper electrodes (right). Scale bar is 100 μm.

Figure 3.2.3 shows one example were a photoresist coating of 1 μm thickness was utilized to cover planar copper electrodes from a standard printed circuit board. As displayed in Figure 3.2.3 (b), an insulating electrode passivation results in a current characteristic which is dominated by capacitive behavior. Voltage dependent reduction in total cell number compared to the 0 V control group was observed, however the lysis efficiency of human blood cells was significantly reduced compared to the bare electrodes. Even amplitudes of 40 V resulted in just 52.2% cell number reduction, as shown in Figure 3.2.3 (a).
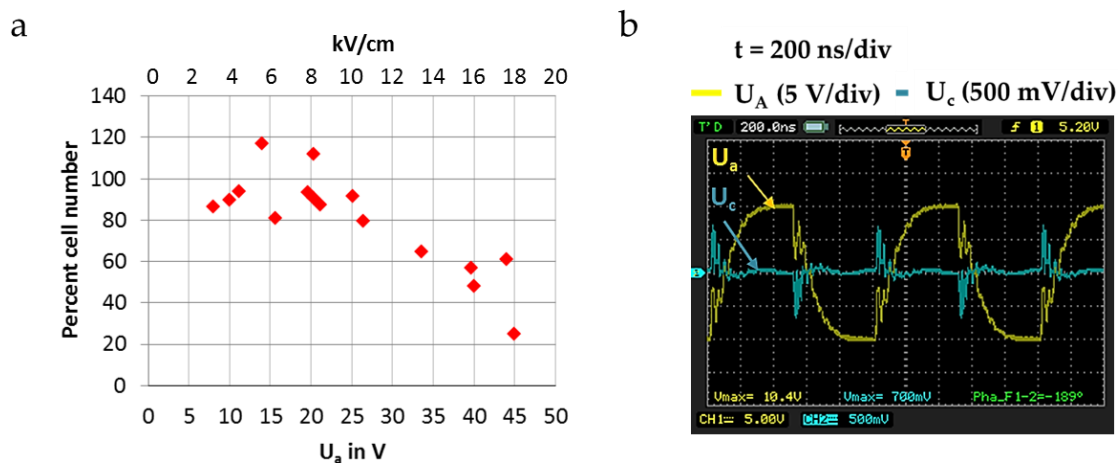
Fig. 3.2.3 (a) Voltage-dependent lysis of human blood cells using copper electrodes with a 1 μm polymer passivation. **(b)** Voltage and current plot, U_c is proportional to the total current I (voltage at a 1 Ω resistor in series to the ECLU).

To find an explanation for the loss of electric field effects, the electrical implications of introducing a passivating coating layer on top of the electrode were studied.
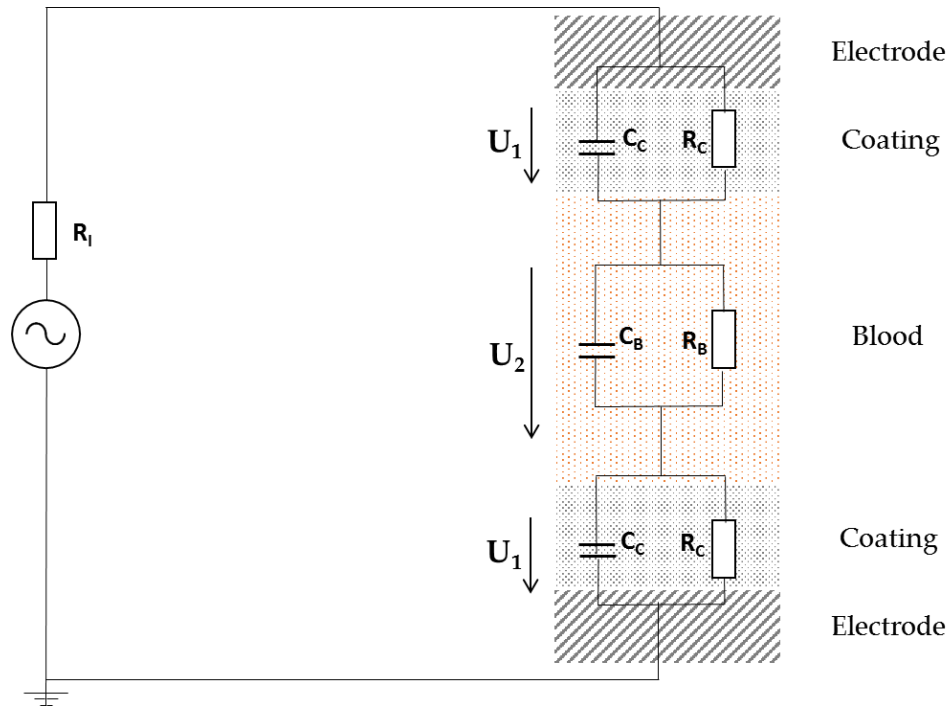
Fig. 3.2.4 Simplified equivalent circuit of the ECLU with electrodes coated by a passivation layer.

As the coating is electrically insulating, the capacitance of the passivation plays a crucial role. The impedances of the liquid and the coatings represent a voltage divider, resulting in a reduction of the voltage across the liquid sample (U_2) and thereby of the electric field experienced by the cell (Fig. 3.2.4).

Thus, the capacitive reactance (x_c) of the coating layer needs to be considered,

$$X_C = \frac{1}{2\pi f C} \qquad (3)$$

where, f is the frequency (Hz) and C is the capacitance of the coating (Farad):

$$C = \varepsilon_0 \varepsilon_r \frac{A}{d} \qquad (4)$$

with ε_0 being the permittivity of free space ($\varepsilon_0 = 8.854 \times 10^{-12}$ F·m^{-1}), ε_r the dielectric constant of the passivation material, A is the surface area of the electrode (m^2) and d is the thickness of the passivation layer (m).

The higher the capacitive reactance, the higher the impedance of the coating which results in a larger voltage drop across the coating (U_1 in Fig. 3.2.4) and a lower electric field experienced by the cell.

Thus, to reduce the capacitive reactance with fixed frequency, the film thickness (d) needs to be reduced or the dielectric properties of the coating (ε_r) need to be increased.

To test this, first, lowering of the coating thickness was addressed.

3.2.3.3 Cell Specific Lysis using Thin-film Electrode Passivation

To reduce the coating thickness, the ECLU was designed with heavily p-doped silicon wafers with a 50 nm thin SiO$_2$ passivation layer (Fig. 3.2.5).
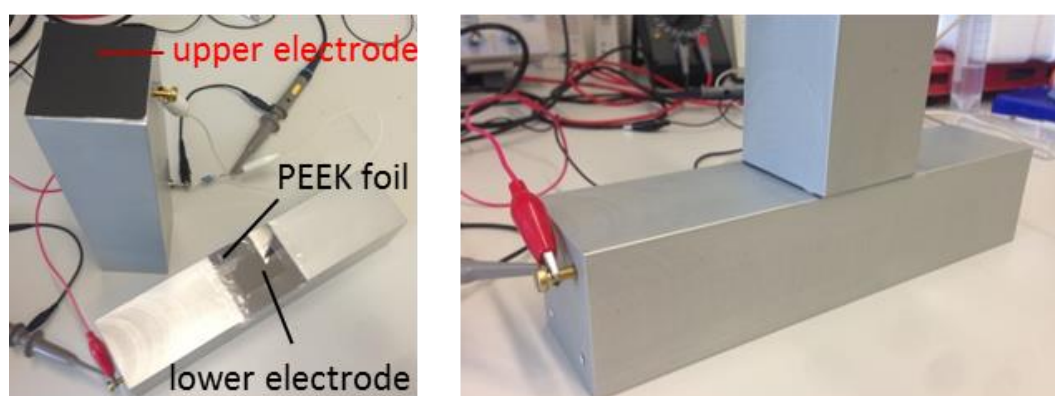
Fig. 3.2.5: Stationary ECLU comprising p-doped silicon electrodes with a 50 nm SiO$_2$ passivation layer mounted on aluminum blocks.

As shown in Figure 3.2.6, voltage dependent lysis of blood cells can be observed at lower voltages in comparison to the polymer passivated electrodes (Fig. 3.2.3). Additionally, as can be seen in the voltage and current plot (Fig. 3.2.6 b), capacitive current characteristic is achieved. The deviation of the square wave signal towards a saw-tooth shape is caused by a prolonged time constant due to a capacitance of the 50 nm SiO_2 passivation and the 1 MHz frequency of the applied signal in combination with the low power output of the function generator.
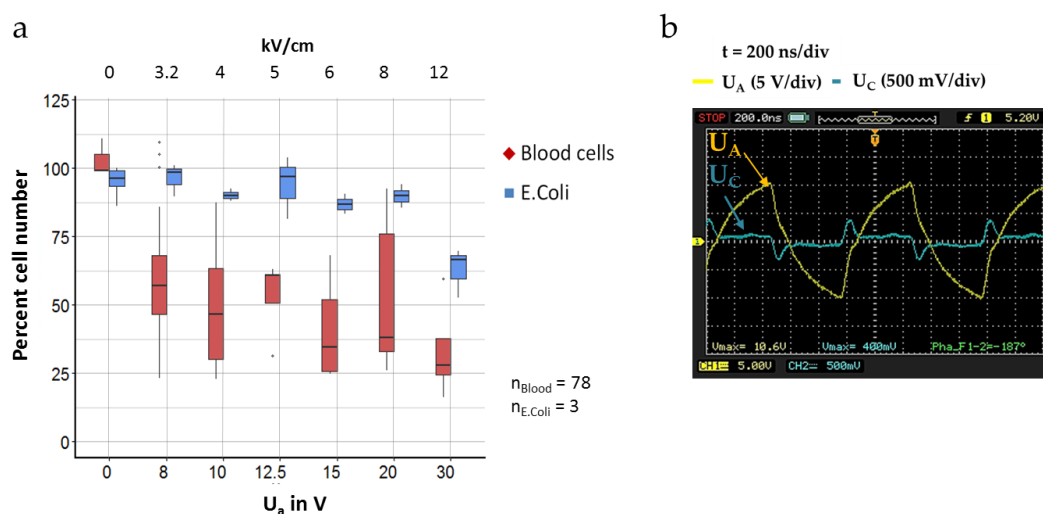
Fig. 3.2.6 Cell lysis using SiO_2 passivated electrodes (a) Voltage-dependent lysis of human blood cells (N_{Total}=78) in comparison to the survival rate of the spiked-in *E. coli* (*N*=3 per voltage value) presented as box plot. **(b)** Voltage and current plot, U_c is proportional to the total current *I* (voltage measured at a 1 Ω resistor in series to the ECLU).

With this set-up, cell-type specific lysis of human blood cells without significantly compromising the spiked in bacteria is demonstrated in the range between 8 and 20 V. The median of the number of total blood cells is reduced to 57% or 34%, whereas more than 97% and 90% of the spiked-in bacteria remained viable at 8 V and 15 V, respectively. The onset of human blood cell lysis at 8 V and the onset of significant viability reduction of *E. coli* at 30 V correspond to electrical field strengths of 3.2 kV/cm for human blood cells and of 12 kV/cm for *E. coli* with the developed ECLU. These values are in the range of the

reported values for the induction of a threshold TMP for erythrocytes (2.2 kV/cm)[75,90,121] and *E. coli* (10 kV/cm).[88,89]

The apparent increase in cell number after applying low voltages in Figure 3.2.1 and Figure 3.2.3 as well as the high variance in lysis rates in Figure 3.2.6 can be explained by the manual withdrawal of the samples from the electrode surface, especially concerning the hydrophilic surface of the SiO_2 set-up.

The data gained from the experiment with AZ6612 polymer passivation demonstrate that the electric field induced in the liquid and, therefore, experienced by the cells is strongly influenced by the parameters of the coating. As passivation layers are introduced, they act as a voltage divider in combination with the impedance of the liquid and the voltage drop across the passivation layer is proportional to its reactance. The lower the thickness of the layer or the higher its dielectric constant, the higher the capacitance and the lower the reactance, resulting in a lower voltage drop in the passivation layer itself. This could practically be confirmed by using a 50 nm SiO_2 passivation of highly p-doped silicon as electrode material. In contrast to the 20 times thicker polymer passivation, effective and selective lysis could be observed at lower voltages.

3.2.3.4 SiO_2–based Flow-through Electrical Cell Lysis Unit

To circumvent problems with manual sample withdrawal and to increase sample throughput, a flow-through device based on 2" heavily p-doped silicon electrodes passivated with 50 nm SiO_2 was designed and fabricated using optical lithography and a 35 µm dry resist forming the channel walls sandwiched between two wafers by lamination. Figure 3.2.7 shows the channel design (channel width is 500 µm), the constructed flow-through prototype and voltage/current plots when a square wave signal with 10 V at 1 MHz is applied.
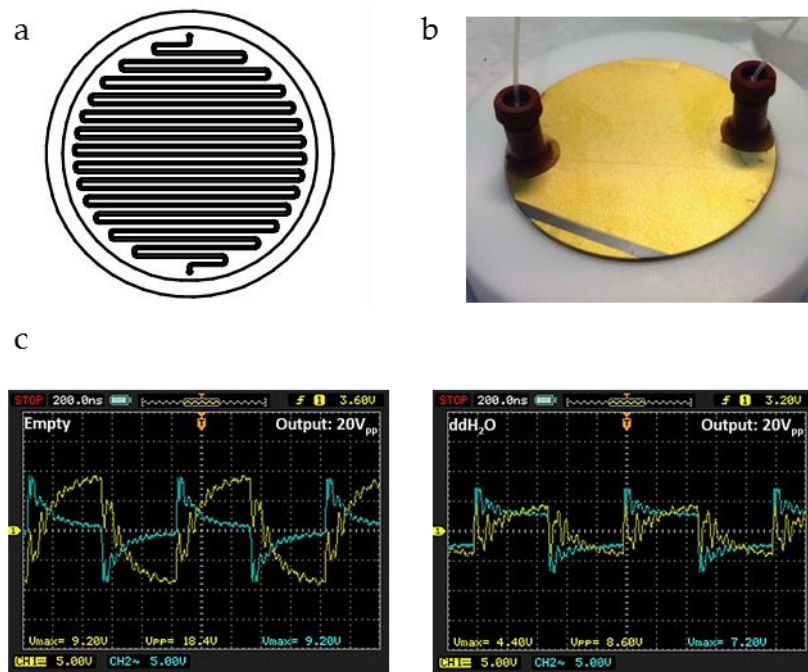
Fig. 3.2.7: (a) Mask design for the production of a 500 μm wide microfluidic channel in a dry resist laminated between two 2″ p-doped silicon wafers. **(b)** Final silicon flow-through ECLU with gold sputtered surface for low resistance contact to the silicon wafer. **(c)** Voltage (yellow) and current (blue, voltage at a 1 Ω resistor in series to the ECLU) plot when applying 20 V_{PP} to an empty chip (left) and after introduction of a blood dilution (right).

After successful fabrication and fluidic tests, the electrical characteristics were measured. The introduction of fluid into the flow-through chip lead to a significant increase in overall capacity compared to air, resulting in large charging currents and heating of the device. With 110 nF, the measured capacity of the ultrapure water-filled SiO_2 flow through device was significantly higher than the calculated overall capacity of 17 nF which was also measured using the SiO_2 stationary batch design filled with water (Fig. 3.2.8).

a

Stationary SiO$_2$ (25µm)
A = 600 mm²   C = 17 nF

Flow through SiO$_2$ (35µm)
A = 433,3 mm² C = 110 nF

Flow through SiO$_2$ (55µm)
A = 433,3 mm² C = 110 nF

b **Calculation**

	A (mm²)	C	
Wafer	2026,83		1,4 µF
Air (frame)	436,4		0,39 nF
Ordyl	1156,6		3,8 nF
Channel	433,3	Air:	0,21 nF
		Water:	17 nF
		SiO$_2$:	291 nF

C $_{Channel}$ = 15 nF

c **Measurement**

	Flow Through (nF)	Stationary (nF)
Air	5	1
EtOH	132	4
H$_2$O	136	10
Sucrose	140	12

No ε_r-dependency in the flow through

Fig. 3.2.8: (a) Comparison of the measured values of capacitance in the stationary design and the flow-through silicon ECLU with different inter-electrode distances. **(b)** Calculation of the overall capacitance of the silicon flow-through ECLU. **(c)** Measurement of the overall capacitance using solutions with dielectric constants.

As the surface area and thus the volume of the flow through device was lower than that of the batch design ($A_{Flow through}$ = 433 mm², $A_{Stationary batch design}$ = 600 mm²), this significant change in overall capacity was surprising. SEM imaging of the cross section of a SiO$_2$ flow through prototype excluded a bias originating from fabrication and confirmed the desired channel height (Fig. 3.2.9 c). Also, the overall capacitance was independent of the channel height as it did not change when a SiO$_2$ prototype with a 55 µm thick dry resist was investigated (Fig. 3.2.8 a). Most interestingly, the overall capacitance was also independent of the dielectric constant of the solution filling the channel (Fig. 3.2.8 c). In contrast, using the stationary batch design, water (ε_{Water} = 80) more than doubled the overall capacity of the system when compared to an ethanol-filled chamber ($\varepsilon_{Ethanol}$ = 24.5).

In order to explain the dominance of the capacitance represented by the SiO$_2$ passivation layer, an equivalent circuit was built on a bead board comprising two 220 nF capacitors representing the passivated silicon electrodes and a 22 nF capacitor parallel to a potentiometer representing the fluid in the channel (Fig. 3.2.9 a).
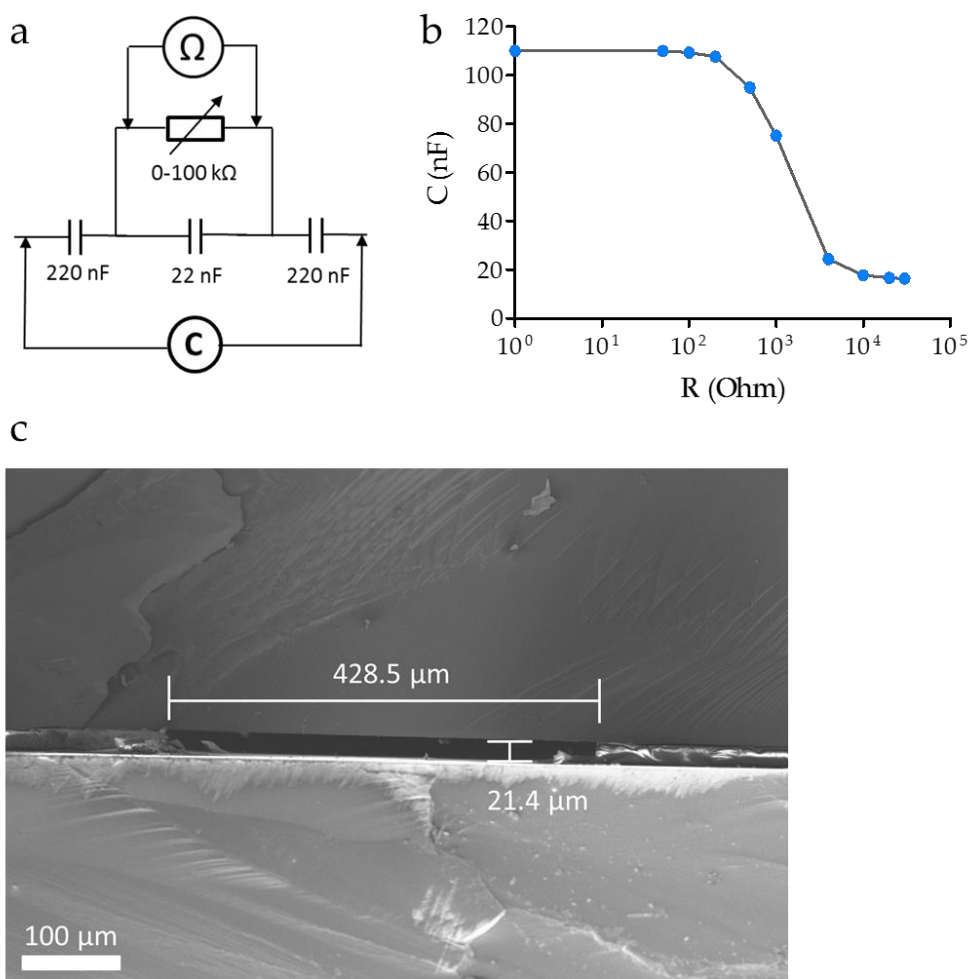
Fig. 3.2.9: (a) Equivalent circuit bread board assembly for the measurement **(b)** of the overall capacitance in dependency of the channel resistance. **(c)** Channel height was confirmed by electron microscopy imaging of a cross section of a silicon flow-through ECLU.

When the resistance is below 1 kΩ, the capacitor representing the fluid was shunted and the capacitance of the electrode passivation dominated. However, as the resistance of ultrapure water at an electrode distance of 35 μm with a surface area of 433.3 mm² was calculated to be 14.7 kΩ, the capacitance of the fluid was expected to dominate the overall capacitance. Due to the simple electrical model, a final conclusion about the surprising occurrence of fluid independent capacity of the overall system could not be satisfyingly be drawn at this point. However, impedance spectroscopy for the investigation of an improved system was performed at a later stage (see chapter 3.3.3.7) which reasoned the

dominance of the passivation layer capacitance. Due to parallel advances concerning the use of novel passivation strategies, focus was set on a more promising approach for cell specific lysis by electrical fields, which is discussed next.

3.2.3.5 Alternative Thin-film Passivation Strategies

The strategy of using silicon wafers as electrodes would have set the ground for highly reproducible devices due to the well-established semiconductor technologies including surface oxidation processing. However, due to the potential commercial applicability of electric field based sample preparation for blood stream infection diagnosis, the impact of costs for industrial realization had to be considered early. As a successful development must lead to a disposable device, the use of silicon wafers would significantly increase material costs, making this technology unattractive for commercial uptake. Thus, an applicable development strategy aiming at reduced material costs was required. In addition, such a cost effective thin film passivation of the electrodes had to further improve lysis efficiency. Thus, a profound examination of technologies and protocols from the field of material science was performed. A wide plethora of possibilities were investigated regarding the use of thin-film electrode passivation. First, self-assembly monolayers on aluminum and gold electrodes using APTES (3-Aminopropyltriethoxysilane), MPTES (3-Mercaptopropyltriethoxysilane), 1H,1H2H,2H-Perfluorodecyltriethoxysilane, Hexamethyldisiloxane, as well as commercial silanization products (eg. Evonik Dynasylan Glymo) were produced, but showed poor insulating characteristics in addition to restricted chemical stability at high electric potentials. Also, silica passivation of aluminum following the protocol of Schäuble K., Univ. Köln, 2010[122] exactly, did not result in successful cell specific lysis. In parallel, another strategy aimed at using aluminum oxide passivated electrodes. As such electrodes are routinely integrated in electrolyte capacitors, the company Kendeil Satma P.P.C. kindly supplied some samples of anodically oxidized aluminum foils. Lysis experiments were planned by constructing a flow through electric cell lysis device using two such electrodes and a

double sided adhesive in between forming a chamber (Fig. 3.2.10 a). After injecting sample, however, leakage of the sample through the foil was observed (Fig. 3.2.10 b). To achieve the high capacitance of commercially available electrolyte capacitors, anodic oxidation yielding highly porous aluminum oxide to significantly increase the surface area of the foils is desirable. As can be seen in Fig. 3.2.10 c, a high concentration of nanometer sized pores were observed under the electron microscope.
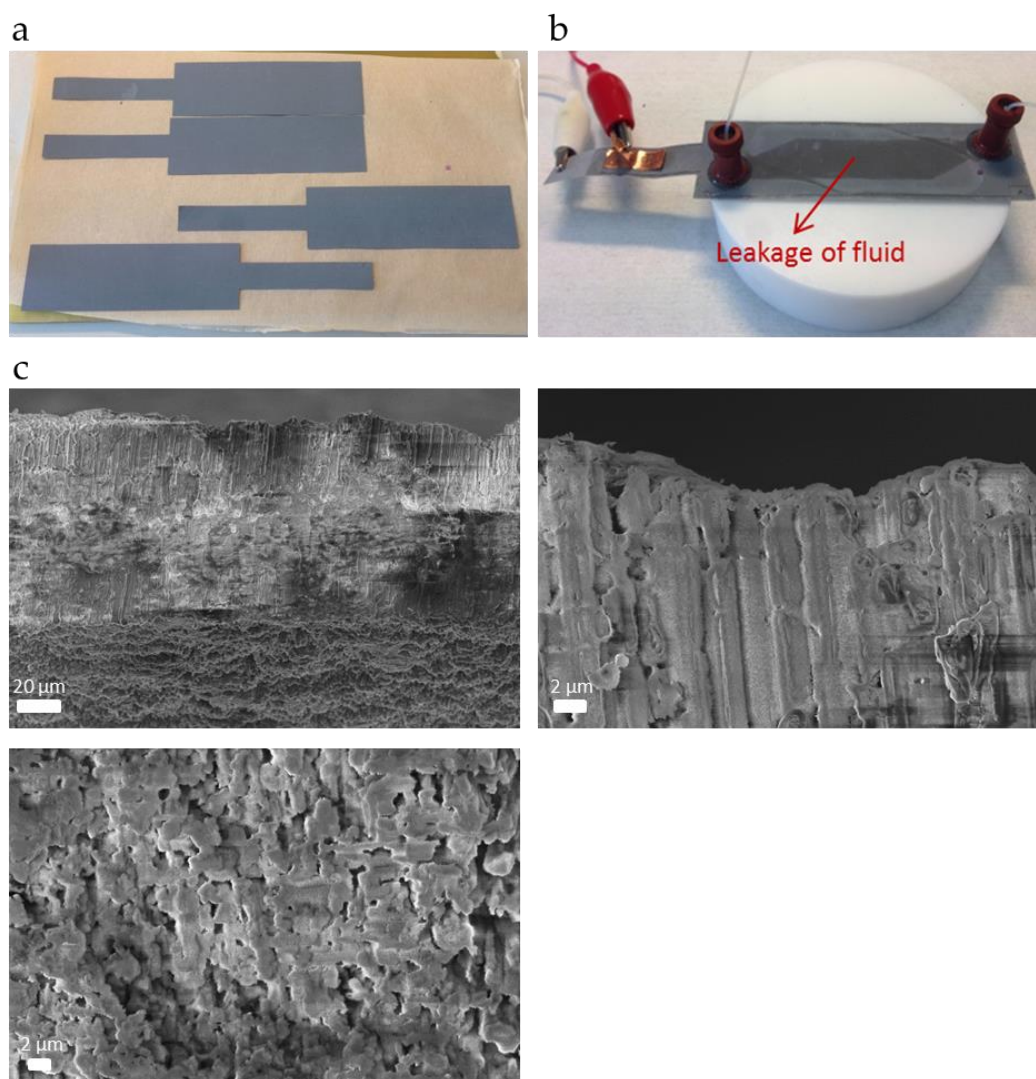
Fig. 3.2.10: (a) Anodically oxidized aluminum capacitor foils as received by Kendeil Satma P.P.C. **(b)** Assembled flow-through aluminum ECLU showing sample leakage through the aluminum foil. **(c)** Electron microscopy images of a cross section and the surface (buttom image) of a foil showing highly structured and rough aluminum oxide surface and a high density of nm-sized pores.

Besides sample leakage, which could be addressed by using a closed core foil, the use of porous aluminum oxide layers are disadvantageous in regard to loss of sample through diffusion as well as to unreproducible effects due to inhomogeneous electric fields.

In parallel, another strategy was pursued regarding the use of an optimized passivation strategy for the development of a cost effective sample preparation technology for BSI diagnosis, which lead to promising results early.

3.3 High-k Dielectric Electrode Passivation Enables Reproducible and Cell Specific Lysis at Low Frequencies, Low Voltages and at Low Cost in a Microfluidic Flow-Through Device

3.3.1 Introduction

As described in 3.2, the impedances of the liquid and the passivation layers represent a voltage divider where the voltage across the liquid sample and thereby the electric field experienced by the cell is reduced when the passivation impedance increases. Therefore, the electrical passivation characteristics represent the bottleneck in capacitive coupling electric fields for cell lysis where the reactance of the passivation layer needs to be minimized. With a 50 nm silicon oxide thin film as electrode passivation, electric field induced cell specific lysis has been achieved. However, lysis efficiency was low, which was expected to result from inefficient electric field coupling originating from the low dielectric constant of the SiO_2 passivation layer (ε_r = 3.9). To address this, the electrical properties of the passivation layer needed to be tailored further. The first strategy to minimize the capacitive reactance of the passivation layer was to reduce the coating thickness. Lowering the passivation layer thickness resulted in a trade off with coating homogeneity and the risk of dielectric breakthrough for most materials. Hence, the strategy was to reduce the capacitive reactance by increasing the dielectric constant of the passivation layer. This offers the advantage of efficient electric field coupling into the sample with thicker and thus more stable coatings.

Due to their high dielectric constant, high-k materials (ε_r > 3.9) promise to achieve ohmic decoupling of the electrode material from the liquid sample but at the same time provide low capacitive reactance and hence a high electric field in the sample. Titanium dioxide (TiO_2) as passivation layer was chosen due to two main reasons. First, chemically inert and biocompatible titanium dioxide with dielectric constants of 60-110, depending on the crystal structure (brookite, anatase or rutile)[123], can be produced by oxidation of titanium.[124] Second, grade 2 titanium (commercially pure titanium, cpTi, 99.2% purity) represents an attractive electrode substrate because of good electrical conductivity, excellent mechanical properties, cost effectiveness and its wide spread use in the biomedical field.

The use of a high-k dielectric TiO_2 electrode passivation was thus investigated next.

3.3.2 Materials and Methods

3.3.2.1 Fabrication and Characterization of High-k Passivated Titanium Electric Cell Lysis Unit

Grade 2 titanium foils were cut, inlet and outlet ports were drilled using a 0.8 mm drill followed by deburring and cleaning with a series of acetone, ultrapure water and 2-propanol washes in an ultrasonic bath for 10 minutes each. Thermal oxidation was done in a muffle furnace (L 9/11 P330, Schaefer & Lehmann) at indicated temperatures and a temperature rise time of 2 hours. After thermal oxidation, the furnace temperature was allowed to cool down to room temperature before the samples were withdrawn. Oxide thickness was measured at lateral cuts using scanning electron microscopy (Zeiss SUPRA 40 Field Emission Scanning Electron Microscope, Zeiss). Microfluidic ECLUs were constructed using two titanium sheets thermally oxidized for 3 hours at 650 °C and a double-sided 81.3 μm thick adhesive tape (Arcare 90445, Adhesive Research) in between forming a 10 μl chamber. The chamber geometry was cut into the adhesive tape using a scalpel. Fluidic in- and outlet connectors were realized using NanoPorts (NanoPort Std 6-32 Coned 1/32, IDEX) and the oxide layer was locally removed by a diamond file on the opposite sides until surface resistance was below 1 Ω for an efficient electric contact. For voltage and current plots a function generator (DG4102, Rigol) connected to a voltage amplifier (Falco WMA-300, Falco Systems) was used as a power source. Voltage and current (via a 2 Ω resistor) was monitored with an oscilloscope (DS1104B, Rigol).

3.3.2.2 Electric Field Induced Lysis Experiments

Whole blood was withdrawn from healthy volunteers using EDTA or citrate collection tubes (Vacuette, Greiner Bio One) and immediately stored at 4 °C. Each blood sample was used for a maximum of one week. For the experiments, whole blood was diluted 1:100 in

isoosmolar sucrose solution (250 mM sucrose in ultrapure water) unless otherwise indicated. A 1 ml blood dilution sample was transferred to a 1 ml syringe (Omnifix-F, Braun) and applied with the indicated flow rate to the ECLU by a syringe pump (Fusion 200 Touch, KR Analytical Ltd). To discriminate between parameters, at least 5 times the chamber volume (10 µl) was allowed to pass through the device after each parameter change and before an aliquot was collected for analysis. For blood cell lysis measurements, the cell suspension was transferred to a hemocytometer (Thoma, Optik Labor) and bright field images were taken with an inverted microscope (CKX41 Fluo V2, Olympus) equipped with a digital camera (Prosilica GT, Allied Vision). Cell counts were performed using ImageJ's automatic particle count function.[120] For bacterial spike-in experiments, Kanamycin resistant *E. coli* and *L. fermentum* were added to 1 ml 1:100 whole blood dilution in 250 mM sucrose solution to a final concentration of 10^4 CFU/ml. As small cell numbers are resulting in larger variances, the bacterial cell concentration was chosen to account for possible dilution inhomogeneity and to better discriminate for electric field effects. After every voltage change, 100 µl sample was allowed to pass through the ECLU before 100 µl sample was collected. A 10 µl aliquot was transferred to a hemocytometer to confirm blood cell lysis. For bacterial spike-in analysis, 90 µl of the sample was plated on LB agar plates with 50 µg/ml Kanamycin and incubated over night at 37°C aerobically for *E. coli. L. fermentum* spike-in samples were plated on MRS-Agar plates and incubated for 3 days at 35 °C anaerobically. Bacterial viability was evaluated by colony counting. The percent of bacterial cell viability was referenced to a control which was not exposed to electric fields (0 V in Fig. 3.3.9 b). To control for post-experiment contamination during plating and incubation, a negative control (Fig. 3.3.9 b) consisting of 100 µl 250 mM sucrose solution without spiked-in bacteria was included and plated in parallel. For the dilution and conductivity dependent lysis experiments, whole blood was diluted as indicated in 250 mM sucrose or PBS and solution conductivity was measured using a conductivity meter (LAQUAtwin, Model B-771, Horiba).

3.3.2.3 Electrical Characterization and Leakage Current Measurements

ECLUs were constructed with passivated titanium, non-passivated titanium sheets and gold coated glass slides. The fluidic chamber was filled with PBS, ultra-pure water or 250 mM sucrose solution. Electrodes were connected to a DC power supply (Rigol DP832) with a multimeter (Fluke 289) and a 1 kΩ resistor in series. DC voltages were applied and the corresponding currents measured by the multimeter were recorded.

3.3.2.4 Universal pH Indicator Readout

To illustrate pH changes at the electrode/solution interface, non-passivated and passivated electrodes were inserted 20 mm apart into a multichannel pipette tub (Model JHA027), attached and sealed by hot glue. Electrodes were connected to the circuit on the bottom side while the tub reservoir on the top side was filled with universal pH indicator (Fisher Scientific, 422435000). A DC voltage of 30 V was applied using a power supply (Rigol DP832). The reservoir was photographed after 3 seconds to visualize any changes in pH by color transition of the pH indicator.

3.3.2.5 Diode Characteristics

Diode characteristic was recorded with a DC power supply (Rigol DP832) in series with a 1 kΩ resistor and a multimeter (Fluke 289) connected to a passivated and non-passivated titanium sheets through a copper tape on top of a conductive silver paste covering 90 mm^2 of the surface of the sheets defined by an adhesive film. The other pole of the DC power supply was connected to the base metal, respectively (see Fig. 3.3.1).
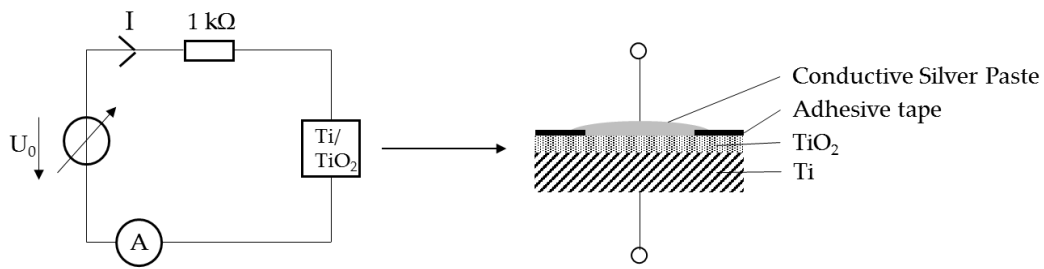
Fig. 3.3.1: Equivalent circuit and schematic of the measurement of the passivation's diode characteristics in both polarities. Voltage was applied and the resulting current was recorded.

3.3.2.6 Impedance Spectroscopy

Impedance measurement of the flow-through ECLU was done using a potentiostat (PGSTAT30, Autolab). The potentiostat was connected to the ECLU filled with solution and AC voltages of 10, 100 and 500 mV RMS were applied in the frequency range between 10 Hz and 1 MHz. After the measurement, the software "NOVA 1.11" was used for data analysis, data presentation and curve fitting on the measured impedances based on equivalence circuit models.

3.3.3 Results

3.3.3.1 Generation of High-k Titanium Metal Oxide Layers

Several techniques to produce TiO_2 in rutile phase from titanium material can be found in literature. Besides plasma oxidation techniques, anodic oxidation and thermal oxidation are widely established.[125] To test the feasibility of TiO_2 electrode passivation, thermal oxidation was further considered due to the simpler setup and the lower number of process parameters found in literature compared to anodic oxidation. As the resulting oxide thickness of similar works varied significantly (e.g. 2 μm oxide thickness after oxidation of cpTi at 600°C of 1.5 hours[126] compared to 300 nm after oxidation of cpTi at 600°C for 2 hours[124]), the dependency of oxide thickness and structure with changing oxidation time and temperature was first investigated to establish an in-house protocol.

As can be seen in Figure 3.3.2, the oxide thickness increases linearly in the investigated temperature and time interval, ranging from several hundred nm to up to 4 μm when oxidized at 650°C or 750°C, respectively. To test the passivation layer characteristics of the differently oxidized titanium electrodes, stationary batch experiments for whole blood cell lysis were conducted (not shown). Electrodes that were oxidized below temperatures of 650°C and below 2 hours of oxidation time, exhibited incomplete ohmic decoupling of the electrode from the fluid samples which was indicated by ohmic current in the I/V plot. Electrodes oxidized at temperatures above 700°C formed brittle multi-layer laminated oxides. Using 650°C on the other hand yielded 400-600 nm thick oxide layers with good reproducibility and mechanical stability. To minimize oxide defects, the temperature rise time was optimized. Titanium oxidation yielding a high percentage of defect-free passivated titanium electrodes was achieved with a temperature rise time of 2 hours, a hold time of 3 hours at 650°C, followed by a cooling period to room temperature of 15 hours.
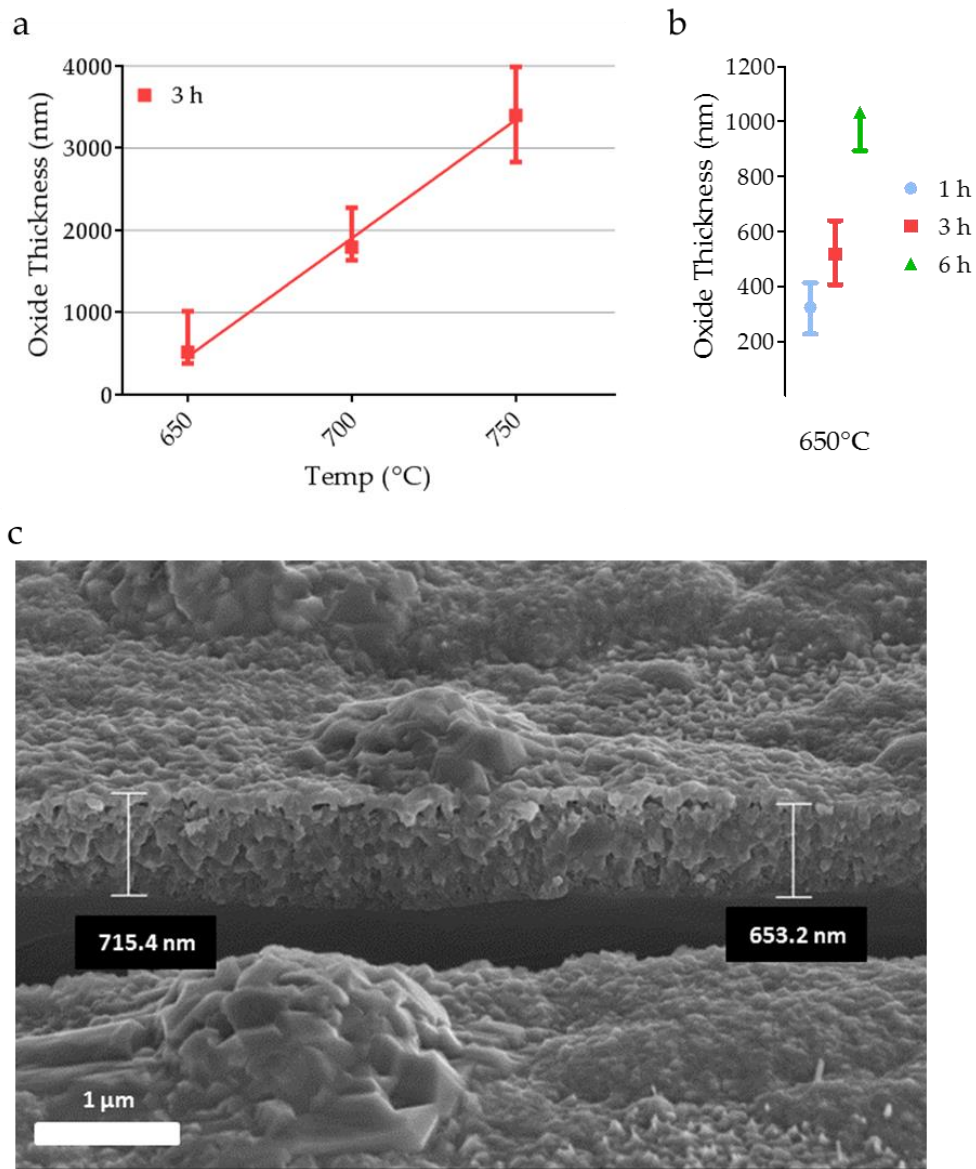
Fig. 3.3.2: Fabrication and characterization of high-k TiO_2 passivated electrodes. **(a)** Temperature dependency of oxide thickness in the range between 650 °C and 750 °C under atmospheric pressure, *N*=4. **(b)** Oxide thickness after thermal oxidation at 650 °C for 1, 3 or 6 hours, *N*=3. Data points represent the median, error bars represent standard deviation. **(c)** SEM image of a TiO_2 layer generated at 650 °C for 3 hours at a manually induced breaking edge of a thermal oxidized titanium sheet.

3.3.3.2 Flow-Through Electric Cell Lysis Unit with Thermally Oxidized Titanium Electrodes

After promising batch experiments using thermally oxidized 100 μm thick cpTi sheets as electrodes, a microfluidic flow-through chip was constructed utilizing an 81 μm thick double sided adhesive tape forming a 10 μl flow through chamber (Fig. 3.3.3).
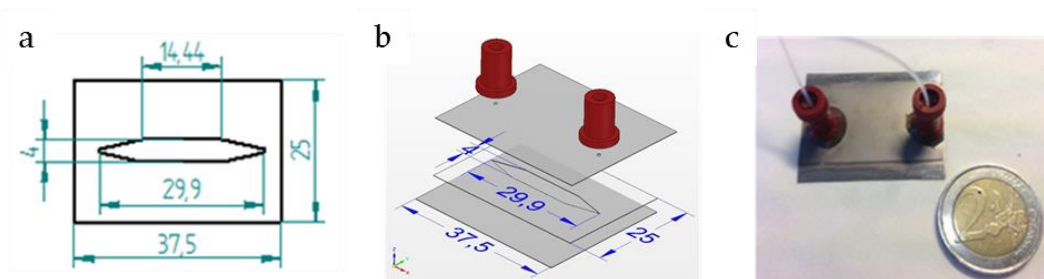
Fig. 3.3.3: Flow-through electric cell lysis unit (ECLU) with Ti/TiO$_2$ electrodes. **(a)** Template for the double sided adhesive foil forming the flow chamber. **(b)** Schematic of the assembly. **(c)** Assembled flow-through ELCU. All dimensions in mm.

Again, as with the SiO$_2$ flow-through chip (see 3.2.3.4), after assembly of the titanium flow-through prototype, the capacity increased from 18 nF to 80-160 nF compared to the batch device used for first control experiments. Using the established lysis parameter of 1 MHz sqAC voltage signal, the capacitive loading current lead to a significant heating of the electrodes which was not observed at frequencies below 2 kHz at 40 V applied. Of note, high frequencies were chosen in the beginning of the thesis to decrease electrochemical effects and to efficiently reverse electrochemical reaction according to the literature when using non-passivated electrodes. Using an electrode passivation however, charge transfer due to electron tunneling is reduced, minimizing faradaic current and electrochemical reactions at the electrode/liquid interface. Thus, this allows for the use of low frequency alternating currents, liberating electric field applications from the restriction to use only high frequencies.

3.3.3.3 Electrical Characterization of Ohmic Decoupling Efficiency

To confirm this, a DC voltage of 30 V was applied to thermally oxidized and to non-passivated titanium electrodes separated at a distance of 2 cm. The gap between the electrodes was filled with a universal pH indicator to visualize the electrochemical reactions at the electrode surface. As can be seen in Figure 3.3.4, bubble formation and pH changes are observed in less than 3 seconds after applying a direct current to non-passivated electrodes. Although a natural oxide layer of 3-8 nm thickness instantly forms on titanium[127], this layer is too thin for complete ohmic decoupling and to significantly reduce charge transfer. In contrast, even after several minutes, no pH changes and no bubble formation were observed in the case of passivated electrodes strongly indicating the inhibition of direct charge transfer at the electrode/electrolyte interfaces.
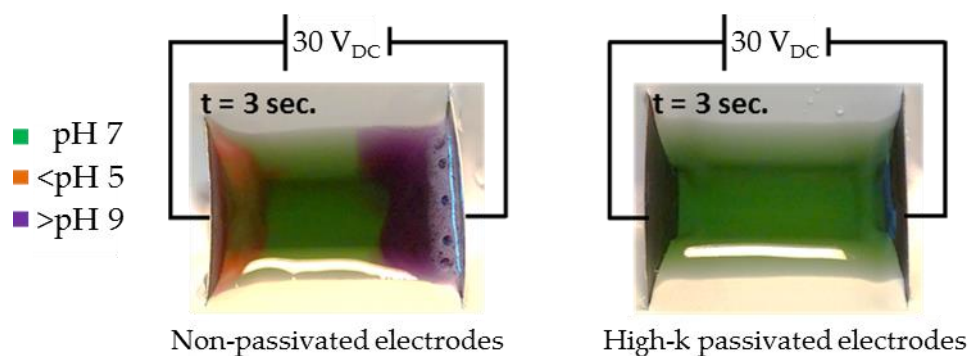
Fig. 3.3.4: Bubble formation and pH changes illustrated with a universal pH indicator at the electrode/electrolyte interface in less than 3 seconds when applying 30 V to non-passivated electrodes separated by 2 cm. In contrast, no color change or bubble formation can be observed for high-k passivated electrodes.

To further confirm the passivation characteristics, the leakage current was measured using ECLUs constructed of gold, non-passivated and thermally oxidized titanium electrodes.
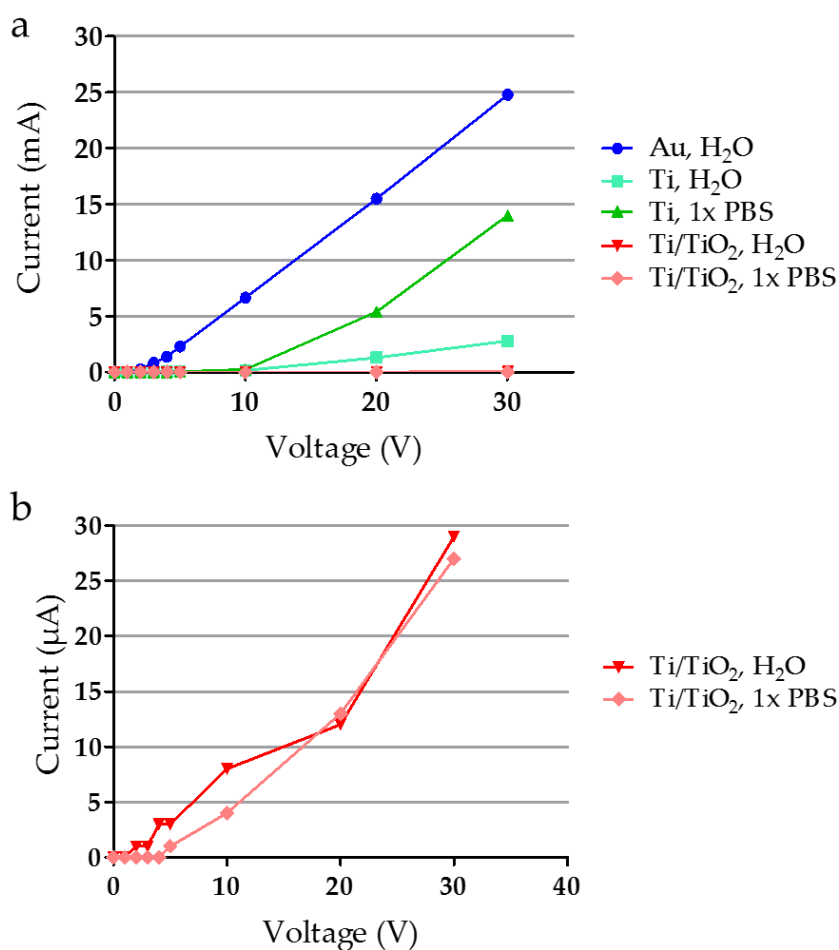
Fig. 3.3.5: Current-voltage characteristic of the electrical cell lysis device with different electrode and buffer combinations. **(a)** Graph depicting leakage current in mA. **(b)** Electrical cell lysis device with thermally oxidized titanium electrodes shows leakage current in the µA range.

A leakage current below 30 µA is observed when a DC voltage of 30 V is applied to the flow-through ECLU comprising Ti/TiO$_2$ electrodes. This value is 3 orders of magnitude smaller than that of the ECLU comprising gold electrodes (Fig. 3.3.5). Also, the leakage current in the devices using the non-passivated electrodes clearly correlates with solution conductivity. Using high ionic phosphate buffered saline (100 Ωcm) or ultrapure water (18 MΩcm) results in leakage current of 14 mA and 2.8 mA, respectively, when 30 V$_{DC}$ are applied to a device with titanium electrodes covered by a native oxide layer. In the device using thermally oxidized titanium electrodes, no significant difference could be observed

between ultrapure water and the highly conductive PBS solution, resulting in 29 µA and 27 µA at 30 V_{DC}, respectively.

Electric decoupling of the electrode material from the fluid sample by introducing an electrically insulating passivation is the essential step to circumvent the secondary effects originating from faradaic current passing through the electrolyte. To illustrate this, Figure 3.3.6 (a) depicts a simplified equivalent circuit comprising an ECLU consisting of two parallel electrodes with or without a passivation layer in contact with the cell suspension in between. Figure 3.3.6 (b) shows simulation results for two non-insulated electrodes with ohmic contact to the fluid sample (R_P represents the transfer resistance between the blank electrode and the liquid). In this case the interface is dominated by the ohmic part leading to faradaic current through the sample accompanied by a significantly lower potential at the electrode due to a high load in the range of the internal resistance of the power source. Figure 3.3.6 (c) shows corresponding simulation results for passivated electrodes (R_P represents the resistance of the insulating passivation layer). The I/V diagram reveals capacitive characteristic, hence, only a short loading current from the power source to the electrode occurs (i.e. no faradaic current between the electrodes through the electrolyte). The capacitor configuration enables an efficient ohmic decoupling of analyte and metallic electrode and allows to establish an accurate controllable electric field inside the liquid sample affecting the cells of interest.
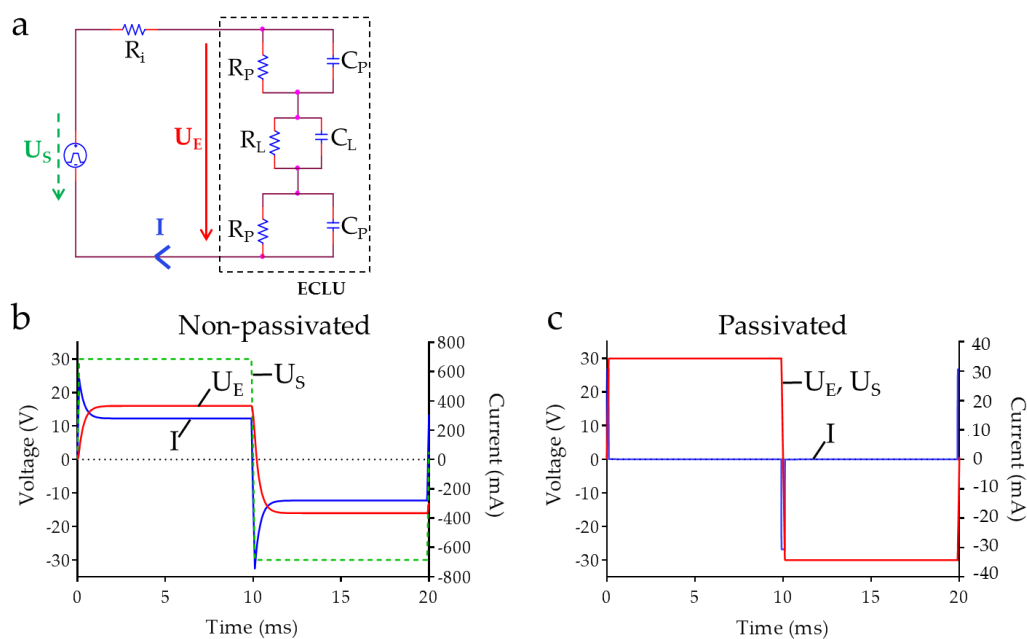
Fig. 3.3.6: I/V-simulation and measurements of the lysis device with non-passivated and passivated electrodes. Equivalent circuit **(a)** comprising of an AC source with internal resistance ($R_i = 50\ \Omega$) and a model of the electric cell lysis unit (ECLU) including the passivation layer (R_P, C_P) and the cell-containing liquid sample ($R_L = 57\ \Omega$, $C_L = 1.1\ \mu F$). U_S: voltage of the AC source, U_E: voltage at the ECLU, I represents current. **(b)** Simulation results of U_S, U_E and I for non-passivated electrodes with a low transfer resistance between electrode and fluid sample ($R_P = 0.1\ \Omega$, $C_P = 180\ nF$). **(c)** Simulation results of U_S, U_E and I for electrodes with an electrically insulating passivation layer ($R_P = 3\ M\Omega$, $C_P = 180\ nF$).

To evaluate the passivation quality and current characteristics for an AC voltage, PBS was injected into the ECLU (Fig. 3.3.7 a) and a voltage of 30 V, 50 Hz square wave AC was applied. Of note, the voltage/current characteristics recorded (Fig. 3.3.7 b) shows clear capacitive loading current of the titanium electrode, followed by a sharp decline to baseline current noise, again confirming efficient ohmic decoupling in accordance to the simulation results (3.3.6 c).
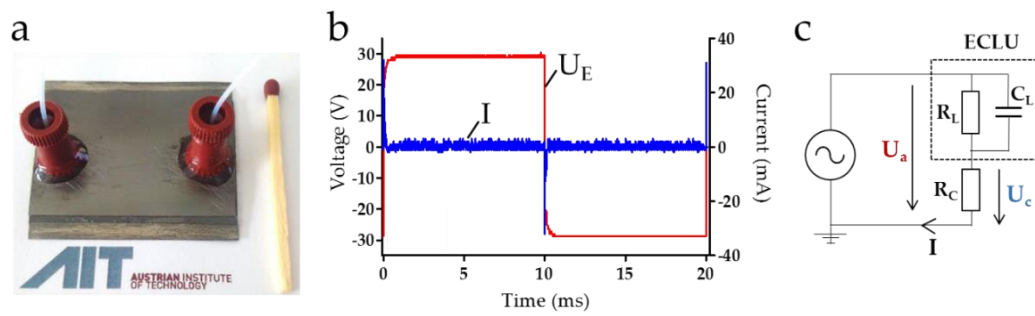
Fig. 3.3.7: I/V-measurements of the lysis device with passivated electrodes. **(a)** Photograph of the microfluidic flow-through ECLU comprising high-k TiO_2 passivated electrodes. **(b)** Voltage and current characteristic of the ECLU from (a), 30 V, 50 Hz square wave, ECLU filled with phosphate buffered saline. **(c)** Measurement circuit. ECLU: Electric cell lysis unit, U_E: applied voltage, U_C: voltage proportional to current, I: current, R_C: 2 Ω resistor for current measurement, R_L: resistance of lysis cell, C_L: capacitance of lysis cell.

Due to the low frequency, ohmic current would be observable using high ionic buffers if ohmic coupling would be given, thus the capacitive behavior confirmed stability of the TiO_2 layer in the microfluidic setup. As the capacitive reactance using a high-k metal oxide is reduced, efficient cell lysis should be observable as the electric field will be coupled into the liquid sample efficiently. Using a 1:100 whole blood dilution in 250 mM sucrose in ultra-pure water, i) field strength, ii) time and iii) frequency dependent lysis behavior of whole blood cells was investigated next.

3.3.3.4 Impact of Voltage, Time and Frequency on Lysis Efficiency of Diluted Whole Blood

Figure 3.3.8 (a-c) depicts the dependence of blood cell lysis on the voltage, flow rate and frequency. Microscope images of the cell suspension after application of 0, 18 and 20 V at 50 Hz square wave at a flow rate of 100 µl/min are shown in Figure 3.3.8 (d). Reproducible and expectable results were gained concerning the voltage and flow rate dependency of whole blood lysis efficiency. Lysis efficiency was recorded with a reduction in cell number of 73.3% at voltages as low as 15 V and 97.1% at 20 V, corresponding to electric fields of 1.85 kV/cm and 2.47 kV/cm, respectively. The onset of whole blood lysis at electric fields above 1.85 kV/cm fits to earlier reports[75,78,90,97] and thus demonstrates the efficient coupling of the electric field by the high permittivity of TiO_2. Whole blood cell lysis by electric fields shows linear dependence (coefficient of determination R^2=0.996) in the investigated interval and efficient lysis was observed within seconds, proving the rapidness of electric field induced cell lysis. Using 18 V and a flow rate of 100 µl/min, 90%, 73.1%, 52.5% and 8.8% of cells were lysed at an electric field exposure of 12, 6, 3 and 1.5 seconds, respectively, given the chamber volume of 10 µl. The frequency spectrum (Fig. 3.3.8 c) shows a parabolic behavior in the observed frequency range with maximum median lysis efficiency of 90.5% and 96.3% at 50 and 100 Hz and only 22.7% and 2.8% lysis efficiency at 10 Hz and 1 kHz, respectively. The reason for the parabolic-like characteristics of the lysis rate between 10 Hz and 1 kHz is surprising as no reports describing such behaviors at this low-frequency spectrum could be found. However, as longer pulses and frequencies below 1 kHz are generally considered to cause more detrimental electrochemical effects when using non-passivated electrodes[79,80,85], the lower lysis efficiencies at 10 Hz and 25 Hz compared to 50 Hz and 100 Hz additionally proofs that faradaic current caused effects are successfully diminished using high-k passivation, thus emphasizing electric field effects. In summary, due to the large surface to distance ratio of the electrode design, efficient lysis at low voltages (15-40 V) and a high through-put (2-5 x 10^5 cells/min) was reproducibly achieved.
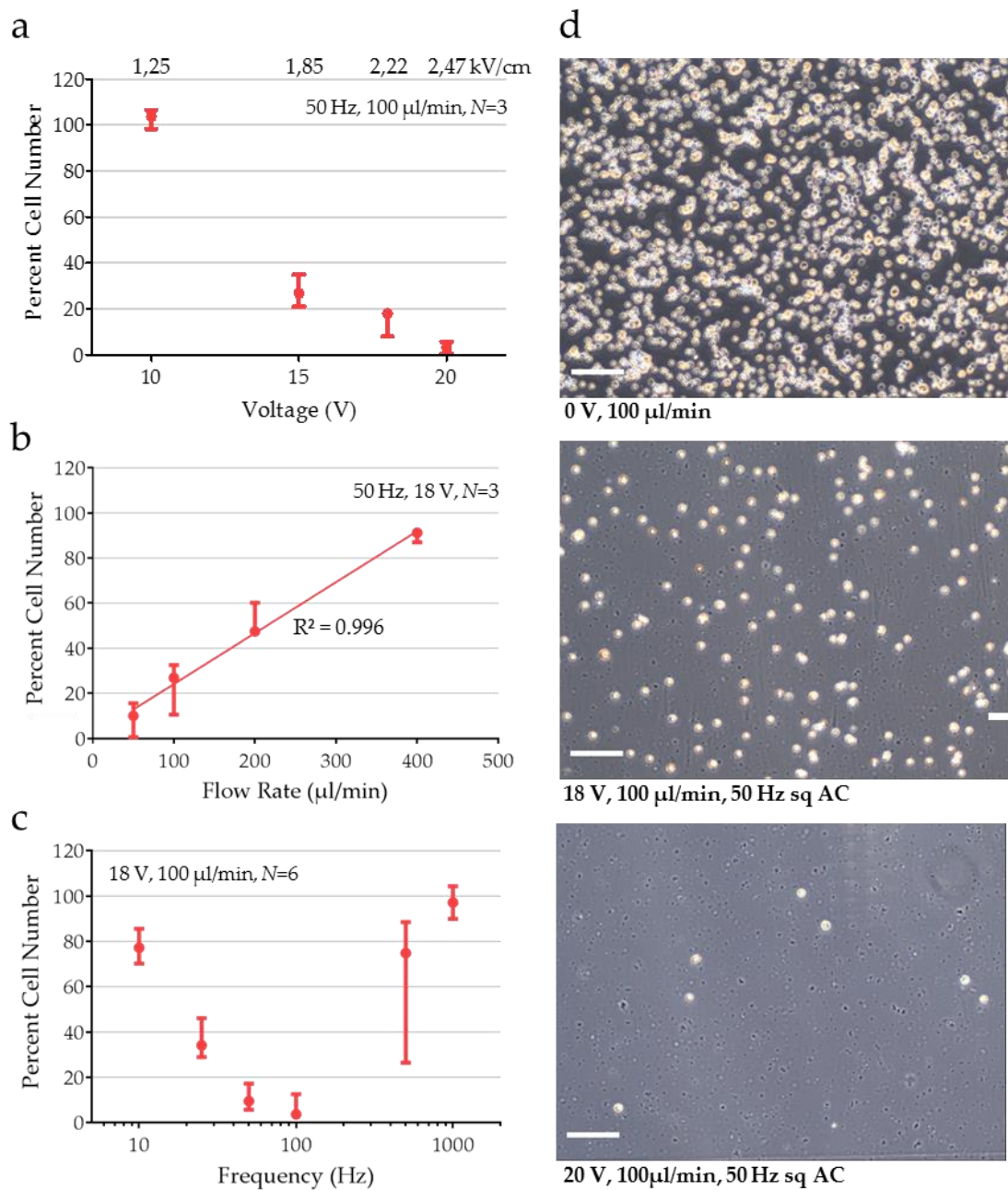
Fig. 3.3.8: Influence of electric field strength, frequency and flow rate on diluted whole blood cell lysis efficiency using the described ECLU. **(a)** Lysis efficiency at different applied voltages (50 Hz, 100 µl/min, N=3). **(b)** Lysis efficiency at different flow rates showing linear dependency (18 V, 50 Hz, N=3). **(c)** Lysis efficiency at different frequencies showing parabolic dependency (18 V, 100 µl/min, N=6). All data points represent the median, error bars depict range. **(d)** Optical micrographs of 1:100 whole blood dilutions after application of 0, 18 and 20 V, 50 Hz square wave at a flow rate of 100 µl/min. Scale bars are 100 µm; R^2: coefficient of determination.

3.3.3.5 Cell Specific Electric Field Induced Lysis

As electric field induced cell lysis is achieved by increasing the transmembrane potential, which depends on the size and composition of the cell (cell wall thickness and rigidity, morphology of intracellular structures as described in *1.4. Electric Field Induced Cell Lysis*), cell type specific lysis can be achieved if secondary current-based effects are successfully suppressed. Thus, the most crucial question which needed to be addressed was, if this strategy allows for cell specific lysis in an efficient and reproducible manner. To answer this, whole blood dilutions spiked with Gram-negative and Gram-positive bacteria were exposed to different electric fields in the described ECLU.

Figure 3.3.9 (a) demonstrates efficient and reproducible whole blood cell lysis. At 40 V, whole blood lysis efficiency was 99.8%, representing the highest efficiency of the tested voltages. Cells pumped through the device immediately after the voltage of 40 V was switched off (0 V post in Fig. 3.3.9 a) showed no significant change in the cell number compared to the 0 V control sample, which proves the instantaneous effect of electric fields on cells. Figure 3.3.9 (a) also demonstrates the robustness of efficient whole blood cell lysis as the data is gained from different experiments done with both EDTA and citrate anticoagluants, samples collected from 2 donors on different days and 3 ECLUs showing a low overall standard deviation in the range of 0,39% for the highest lysis efficiency at 40 V. Figure 3.3.9 (b) illustrates the results of spike-in experiments with Gram-negative *Escherichia coli* and Gram-positive *Lactobacillus fermentum* showing no significant effect of the applied electric fields on bacterial viability. Hence, specificity of electric field induced lysis was achieved, resulting in efficient and reproducible whole blood lysis while bacteria still maintained full viability after treatment. Noticeable, specific whole blood lysis was shown with an efficiency of 99.8% at an electric field exposure time of just 6 seconds, demonstrating the fast dynamics of electric field induced effects.

a

b
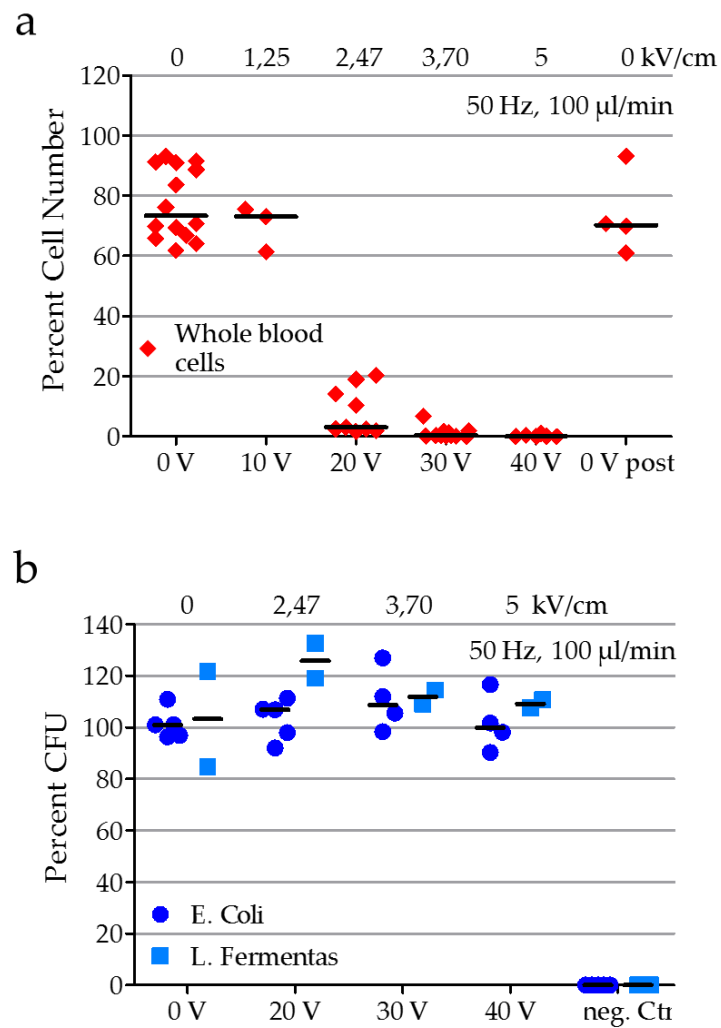
Fig. 3.3.9: High-k electrode passivation enables reproducible cell specific blood cell lysis without affecting bacterial viability. Experiments were done with a 50 Hz square wave at the indicated voltage and a flow rate of 100 µl/min. **(a)** Volatage dependent lysis efficiency of whole blood diluted 1:100 in 250 mM sucrose solution. **(b)** Viability of Gram-positive and Gram-negative bacteria after application of 0, 20, 30 and 40 V to bacterial-spiked whole blood dilutions determined by colony count.

In addition to the experiments utilizing gold electrodes (Chapter 3.2.3.1) the importance of the passivation layer was again confirmed with non-passivated titanium electrodes (Fig. 3.3.10).
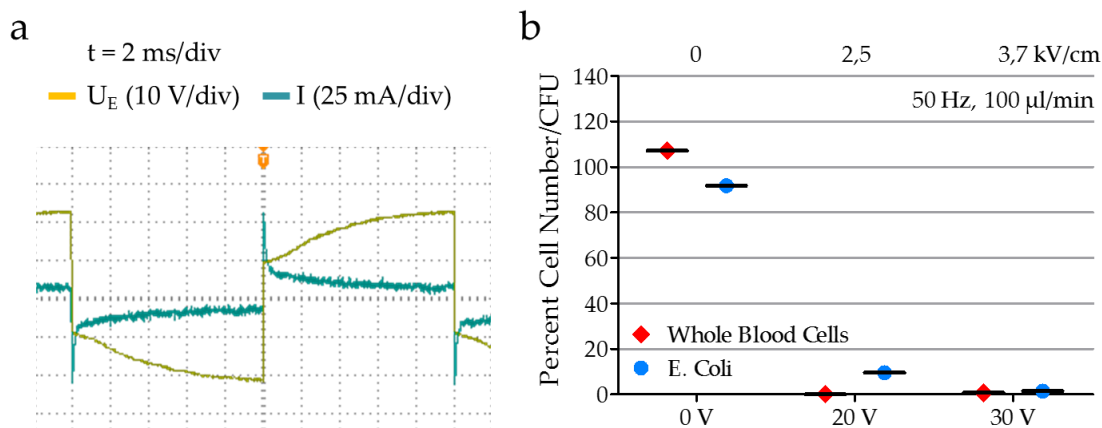
Fig. 3.3.10: Spike-in experiment with non-passivated titanium electrodes confirm unspecific lysis. **(a)** I/V plot during application of 30 V 50 Hz square wave shows faradaic current passing through the liquid sample. **(b)** Lysis efficiency of whole blood cells and bacterial viability after application of a 50 Hz square wave at the indicated voltage to bacterial-spiked whole blood dilutions at a flow rae of 100 µl/min.

In contrast to the experiments with passivated electrodes, cell specific lysis was not achieved. A reduction of *E. coli* viability to 9.6% was observed at an electric field strength of 2.5 kV/cm. This value is below the calculated 10 kV/cm needed to reach a critical TMPs in *E. coli*.[69] Also *E. coli* inactivation has been experimentally shown at values >7 kV/cm in macroscopic batch experiments using AC electric fields[128,129] and the onset of *E. coli* inactivation was observed between 8 and 12 kV/cm using the SiO_2 passivated electrodes in Figure 3.2.6. Again, the natural oxide layer on titanium is too thin for complete ohmic decoupling resulting in faradaic current after the initial capacitive loading (Fig. 3.3.10 a).

3.3.3.6 Dilution and Conductivity Dependent Lysis Efficiency
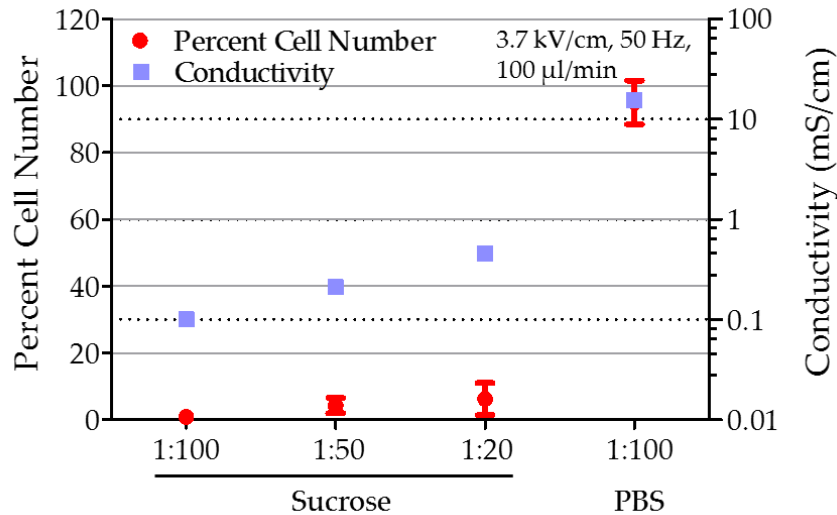
Fig. 3.3.11: Efficiency of whole blood cell lysis depening on dilution and solution conductivity. A 50 Hz square wave signal of 30 V was applied to corresponding blood dilutions. Flow rate was 100 μl/min, $N = 3$.

Focusing on a future application as sample preparation strategy for BSI diagnosis, the influence of reducing the dilution factor on cell lysis efficiency was investigated. As depicted in Figure 3.3.11, after application of a 50 Hz square wave signal of 30 V, lysis efficiency decreased in a dilution dependent manner. Blood cell lysis was recorded with 99.1%, 95.7% and 93.8% at whole blood dilutions of 1:100, 1:50 and 1:20, respectively. Concurrently, also the solution conductivity scaled with the dilution factor with 100 μS/cm, 210 μS/cm and 455 μS/cm for the 1:100, 1:50 and 1:20 whole blood dilution, respectively (Fig. 3.3.11). Obviously, this increase in conductivity originates from the increase in the concentration of blood serum derived ions at lower blood dilutions. To confirm the negative influence of solution conductivity on the lysis efficiency, a 1:100 blood dilution using phosphate buffered saline (PBS) was also exposed to an electric field of 50 Hz square wave, 30 V. As illustrated in Figure 3.3.11, electric field induced cell lysis was completely inhibited. In contrast to the low conducting 250 mM sucrose solution, PBS

represents a high ionic solution, resulting in an overall solution conductivity of 15.4 mS/cm. Considering the simplified equivalent circuit from Figure 3.3.6 (a) an explanation for these observations can be derived. As the electrode passivation and the solution act as a voltage divider, the voltage drop through the sample is proportionally higher at lower conductivity, hence higher resistance of the liquid. Thus, lower electric potentials are required for efficient electric field effects when working with a low conductive medium. In contrast, as faradaic current would increase with increasing electrolyte conductivity, the observed complete inhibition of cell lysis using PBS notably demonstrates the isolation of electric field effects from any influences of faradaic current based effects.

3.3.3.7 Electrical Characterization of the Electric Cell Lysis Unit

A more comprehensive engagement with titanium dioxide raised the question whether the thermally generated oxide is fully insulating or behaves as an n-type semiconductor. In order to get a better understanding of the whole system, an I/V scan was performed for non-passivated and passivated electrodes. Therefore, electrodes were contacted via the base metal and via a silver contact paste covering a surface area of 90 mm^2 (see Fig. 3.3.1). Current was measured at corresponding DC voltages applied.
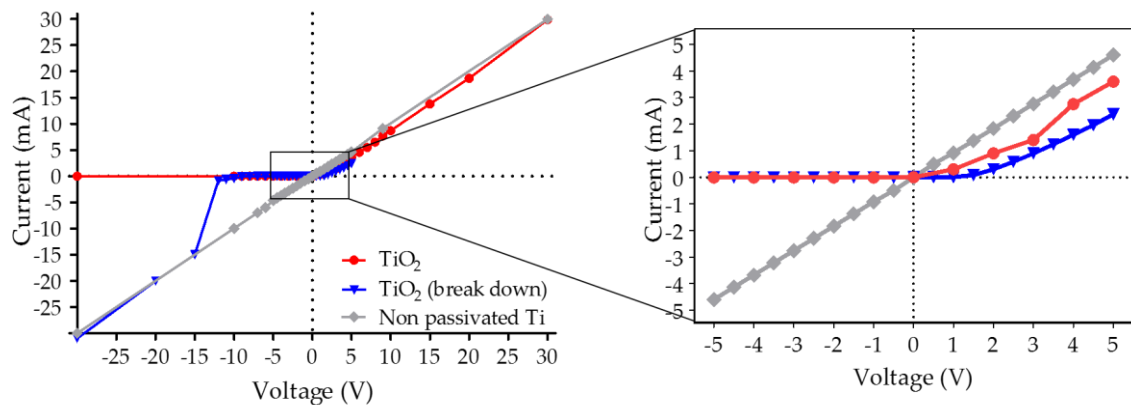
Fig. 3.3.12: I/V diagram of non-passivated (grey) and thermally passivated titanium electrodes (TiO$_2$, red and blue). TiO$_2$ (break down) in blue shows an example of passivation deficiency and dielectric breakdown.

As can be seen in Figure 3.3.12, titanium electrodes without thermal oxidation (grey) show a linear increase in current with the applied DC voltage independent of polarity, thus representing a resistive element. In contrast, passivated titanium electrodes show a current blocking behavior when applying negative potentials, thus acting with n-type semiconducting characteristics. In blue, a titanium electrode with deficient passivation layer shows dielectric breakdown when voltages above 12 V are applied. As such, the TiO$_2$ layer on top of the electrode represent a diode, blocking the current in one direction.

Concerning the assembled ECLU, this suggests that both electrodes represent two diodes in opposing directions, blocking overall ohmic current independent of the voltage polarity. The low leakage current measurements (Fig. 3.3.5), the experiment done with a pH indicator dye showing no electrochemical reactions (Fig.3.3.4), as well as the lysis experiments showing no effect in highly conductive solutions (Fig. 3.3.11) encourage such a model.

To further characterize the ECLU, impedance spectroscopy was performed. The fluidic channel was filled with solutions of different conductivities and the total impedance was measured in the range from 1 Hz to 1 MHz at 500 mV or at 10, 100 and 500 mV at a single solution conductivity for voltage dependent analysis.
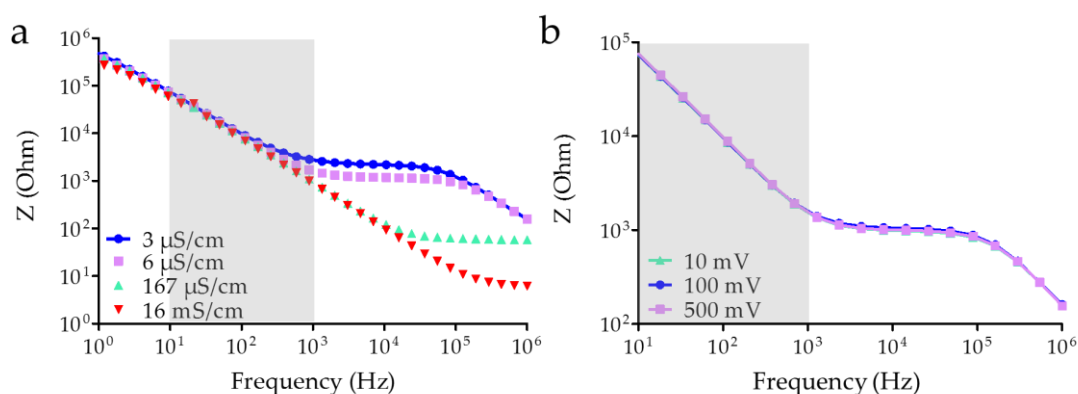
Fig. 3.3.13: Bode plot representation of the impedance spectroscopy done with the high-k passivated ECLU. **(a)** Solution conductivity dependent impedance. **(b)** Voltage dependent impedance.

In the low frequency range between 1 Hz and 1 kHz, the impedance (Z) of the system is determined by the capacity of the TiO_2 layers, which gives the typical linear decrease of Z with increasing frequency (Fig. 3.3.13). With increasing frequencies, the impedance of the passivation becomes lower than the impedance of the solution, resulting in a plateau dependent on the solution conductivity. Starting at 1 kHz, ultrapure H_2O (3 µS/cm) shows a plateau at an impedance ranging from 2.56 to 2.06 kΩ, followed by the 250 mM sucrose solution (6 µS/cm) at 3 kHz and 1.26 to 1.14 kΩ, respectively. The higher conductive solutions, 250 mM sucrose solution with PBS (167 µS/cm) and PBS (16 mS/cm) show a

plateau at 83.8 kHz at 63.13 to 57.77 Ω and at 661.5 kHz starting at 6.35 Ω, respectively. At higher frequencies, the resistance of the low conducting solutions (3 μS/cm and 6 μS/cm) is shunted by the capacitance of the solution, again resulting in a linear decrease of the overall impedance (Fig. 3.3.13 a). The impedance spectrum is thus highly dependent on the solution conductivity. In contrast, total impedance of the system is independent of the value of the applied voltage. Figure 3.3.13 b shows the impedance spectroscopy of the ECLU filled with 250 mM sucrose solution (6 μS/cm) at 10, 100 and 500 mV applied.

As indicated by the grey box in Figure 3.3.13 a, in the operational range of the lysis experiments (10 Hz to 1 kHz), the system is only dominated by the impedance of the passivation layer. The data gained from the impedance spectroscopy also confirms the dominance of the passivation capacitance measured at 119 Hz as discussed in chapter 3.2.3.4. The resistance of the sucrose solution in the range of 1 kΩ also corresponds to the cut-off value identified by the bead board equivalent circuit in Figure 3.2.9, were the capacitance representing the passivation layers dominated the circuit.
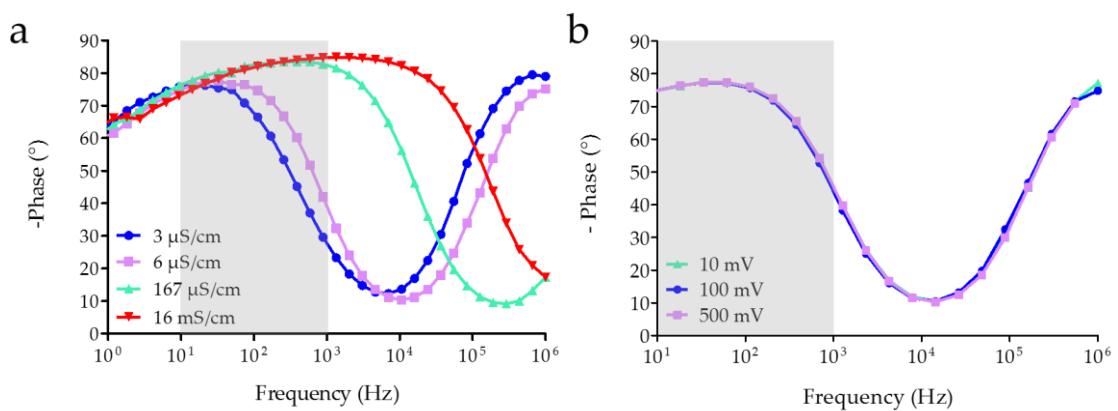

Fig. 3.3.14: Bode phase plot of the impedance spectroscopy done with the high-k passivated ECLU. **(a)** Solution conductivity dependent phase. **(b)** Voltage dependent phase.

As with the total impedance, also the phase angle is highly interrelated with the solution conductivity (Fig. 3.3.14 a). At high frequencies between 10^5 and 10^6 Hz, the lower conductive solutions (3 μS/cm and 6 μS/cm) show capacitive behavior as x_c of the solution is lower than $R_{Solution}$. Higher conductive solutions (167 μS/cm and 16 mS/cm) are

dominated by a resistive behavior in this frequency range. In the medium frequency range between 10^2 and 10^5 Hz, the overall impedance is higher for low conducting media (Fig. 3.3.13 a) but the impedance characteristic is dominated by the resistive part of the solution. In contrast, as the solutions contain more mobile charge carriers, capacitive behavior is observed, showing phase angle values above -80° for the PBS solution (16 mS/cm) in the frequency range between 10^2 and 10^4 Hz. In the low frequency spectrum (1 Hz to 100 Hz), no difference between the solutions is observed as overall impedance is again dominated by the passivation layer. The decrease in the value of the phase angle as low as to -51.73° from 10 Hz to 1 Hz indicates the occurrence of a resistive element parallel to the capacitance of the TiO_2 layer. This result is in accordance to earlier experiments were a leakage current of a maximum of 29 µA has been observed when 30 V_{DC} were applied to the ECLU (Frig. 3.3.5 b).

In order to retrieve first values for the capacitance and the resistance of the passivation layer, the elements of an equivalent circuit were fitted to the impedance spectroscopy data from Figure 3.3.13 (b) with Autolab's Nova Software. Using a circuit as depicted in Figure 3.3.15 (b), with R1|C1 representing the two electrodes and R2|C2 representing the solution, the simulation results are in good agreement with the measurement data (Fig. 3.3.15 a). As such, the passivated electrodes represent an equivalent circuit comprising of a capacitor with 171 nF and a parallel resistor with 233 kΩ.

a

b

Element	Value
R1	$2.33 \times 10^5 \, \Omega$
C1	$1.71 \times 10^{-7} \, F$
R2	$1.01 \times 10^3 \, \Omega$
C2	$1.03 \times 10^{-9} \, F$
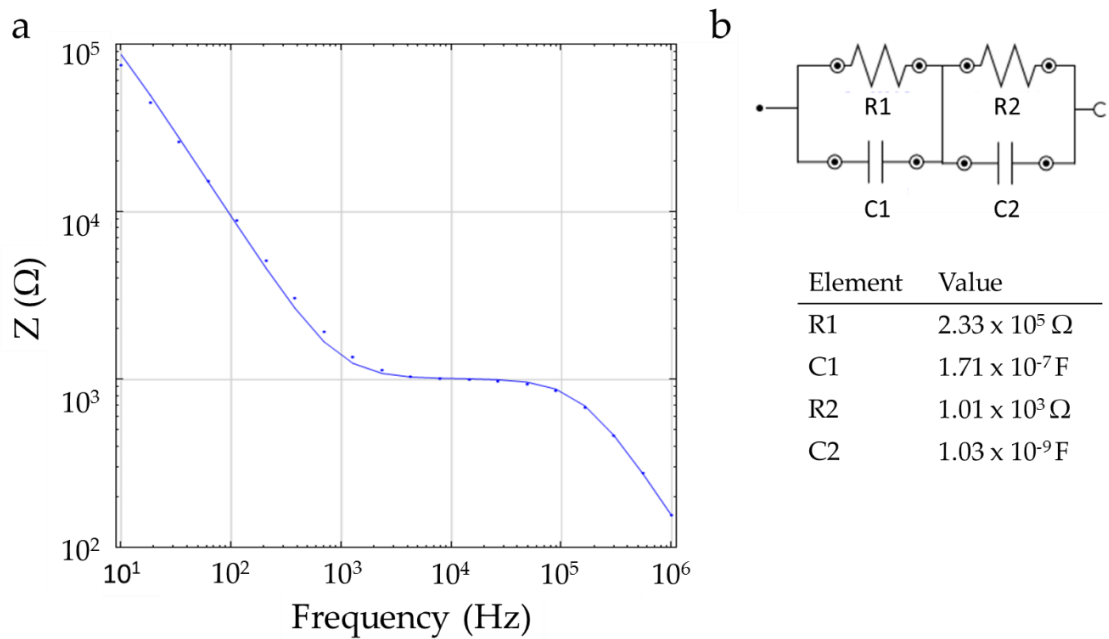
Fig. 3.3.15: Fitting of the impedance measurement using the analysis tool from Nova 1.11. **(a)** Fitting of the equivalent circuit simulation result (solid line) to the measurement results (dotted line). **(b)** Equivalent circuit and calculated values of corresponding elements.

3.3.3.8 Anodic Oxidation as Future Passivation Strategy

Although a high percentage of assembled ECLUs showed sufficient passivation characteristics verified by a capacitive current behavior, incomplete ohmic decoupling was observed when the electrode surface area was increased.

Thermal oxidation of titanium generates rough surfaces due to crystallization kinetics[130,131] and the occurrence of surface defects can frequently be observed[132]. Hence, in order to produce a flow through device with higher volume capacity to process more sample per time, a better quality of the electrode passivation layer has to be guaranteed. A promising alternative for a highly controllable generation of passivation layers is anodic oxidation. Densely packed oxides with smoother surfaces compared to thermal oxidation can be generated which allows to utilize thinner oxide layers.

The group of Prof. Achim Walter Hassel from the Institute for Chemical Technology of Inorganic Materials at the Johannes Kepler University Linz kindly provided anodized grade 2 titanium for a first feasibility study.
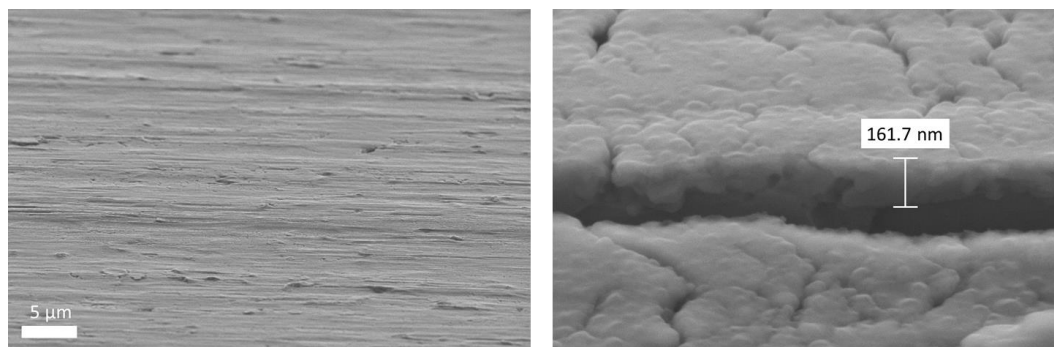
Fig. 3.3.16: SEM micrographs of anodic oxidized titanium electrodes. Left: Image of the electrode surface. Right: The oxide layer thickness was made visible by fracturing the electrode.

The provided anodized titanium foils were covered by an oxide layer of 100-200 nm thickness (Fig. 3.3.16). An ECLU was constructed (Fig. 3.3.17 a) and whole blood lysis was performed with a 50 Hz sqAC signal of 8 V. Application of the voltage again resulted in capacitive current characteristics (Fig. 3.3.17 b). The reduction in cell number by 60% with only 8 V applied (~1 kV/cm), as shown in Fig. 3.3.17 c, indicates higher efficiency of electric field coupling compared to ECLUs constructed with thermally oxidized titanium electrodes, where lysis could only be observed above 10 V applied.
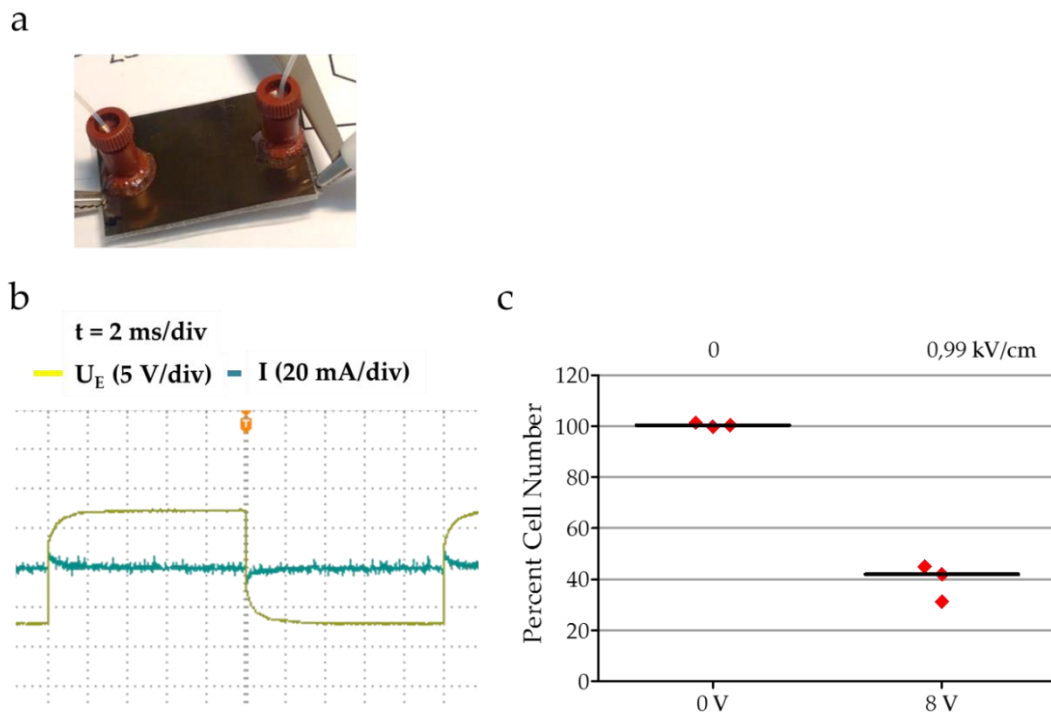
Fig. 3.3.17: Whole blood cell lysis using an ECLU comprising anodic oxidized titanium electrodes. **(a)** Photograph of the assembled ECLU. **(b)** I/V plot during application of 8 V 50 Hz square wave. **(c)** Lysis efficiency of whole blood cells when applying 8 V, 50 Hz square wave with 100 µl/min to 1 1:100 whole blood dilution.

As the anodic oxide was formed at 8 V, larger voltages could not be applied as those lead to a reversible dielectric breakdown of the passivation layer. Nevertheless, the observable lysis effect at such a low voltage indicates the optimization potential regarding the high-k passivation. Thus, a research proposal has been submitted to further investigate the possibility to use and optimize anodic oxidation to produce passivated electrodes for biotechnological applications using different high-k materials.

Chapter 4

Conclusion

This thesis started with the investigation of the status quo for molecular diagnosis of pathogens causing BSI and the current stage of developments into fully automated POC/μTAS devices. After thorough literature research and an evaluation of the state-of-the-art, the most essential challenge for pathogen detection in blood was identified. Although sensing and detection technologies have seen impressive improvements over the last decades, the low signal-to-noise ratio which is caused by the vast amount of human material in blood is still the biggest hurdle when transferring such assays to clinically relevant samples. Thus, focus has also to be set on the upstream process of sample preparation, especially in the view of the stringent requirements for POC/μTAS applications. However, current sample preparation methods are time consuming, involve the use of multiple pieces of equipment such as centrifuges, require reagents that must be stored in a fridge and are not fully integrable in fully automated POC systems. On the contrary, for the use at the point of care, devices need to be small, fully automatable, optimally stable at room temperature and provide quick results. Thus, the missing link of pathogen purification and concentration is addressed in this thesis by the development a new technology for efficient purification of sepsis-causing pathogens from human blood in a fast, cost effective and fully automated manner. The exploitation of the physical distinctions of human blood cells from pathogenic cells by using electric fields to enable efficient and specific blood cell lysis was chosen as a promising strategy.

As discussed in *3.1 Direct Electrode Contact Leads to Unspecific Cell Lysis*, first electric field cell lysis experiments with human fibroblast cells and human leukocytes were performed using published designs and parameters in a microfluidic manner. Although cell lysis was recorded when electrical potentials were applied to the electrodes, decomposition and color-change of the electrodes were also observed. Additionally, spike-in experiments using *E. coli* indicated effects leading to unspecific cell lysis. It was hypothesized that the loss of specificity of the electric field was due to the occurrence of significant indirect electric field effects due to direct electrode contact of the sample or the cells. Indeed, when the electrodes were coated with a PTFE layer, cell specific lysis of human leukocytes was achieved. Due to the high variance of the Teflon-covered electrode functionality however, several other electrode coating strategies were tested. As a loss in the field effect on cells

was observed, focus was set on the electrical considerations when an electrode coating is introduced.

As discussed in chapter *3.2 Capacitive Coupled High Frequency Electric Fields Lead to Specific Cell Lysis*, the role of the electrical passivation was elaborated and tested in batch cell lysis experiments. Using a 1 μm thick polymer electrode coating, only minor cell lysis was observed at elevated voltages. To gain efficient electric field coupling from the electrode to the sample, the strategy of using thin-film passivation layers in order to minimize the layer's capacitive reactance was investigated. Heavily p-doped silicon wafers with a 50 nm SiO_2 coating resulted in whole blood cell lysis at lower applied voltages compared to a 1 μm polymer passivation. In addition, with confirmed capacitive current characteristics, repeated blood cell specific lysis was shown via spike-in experiments performed with *E. coli*.

As a further successful development of the envisioned automated sample preparation technology had to lead to a disposable low-cost device, the strategy of using silicon wafers had to be replaced by a more cost effective alternative. The use of metal foils covered with a high dielectric oxide film was conceived as such an alternative. The implementation of high-k passivation layers was investigated in *3.3 High-k Dielectric Electrode Passivation Enables Reproducible and Cell Specific Lysis at Low Frequencies, Low Voltage and at Low Cost in a Microfluidic Flow-Through Device*. Using thermally oxidized titanium electrodes and a microfluidic flow-through approach, optimized lysis efficiency and highly reproducible cell specific lysis was achieved, which was shown by over 99.8% human blood cell lysis without affecting Gram positive or Gram negative bacterial spike-in viability. Besides efficient cell lysis at low applied voltages (40 V) enabled by the microfluidic design, the liberation from electrochemical superimposing effects lead to high reproducibility and exact controllability of electric field effects, two major aspects when aiming at commercialization.

Hence, the work discussed in this thesis resulted in a substantial proof-of-principle for a novel sample preparation strategy, feasible for automated point of care (POC) devices, for

the purification of blood borne pathogens to speed up systemic infection diagnosis, allowing early pathogen characterization and resistance identification.

The use of electric fields offers full automation, no need for chemical or enzymatic additives and easy integration into already existing workflows. As the bacteria remain viable after blood cell lysis, nucleic acid based tests offered by Roche or Cepheid or phenotypic characterization using MALDI-TOF are possible. Thus, the result of this thesis is the basis of an ongoing development that targets to bridge the gap between the complex sample blood and modern analysis technologies struggling to gain gold standard status (see Fig. 4.1). Further improvements of this concept will address the processing time which is also affected by the limitation of reducing sample conductivity via dilution. Due to the fast dynamics of electric field induced lysis however, more sample volume per time can be processed by increasing the chamber volume. Owing to the scalability of the design, by increasing the electrode area and thus the ECLU volume, efficient processing could be achieved.
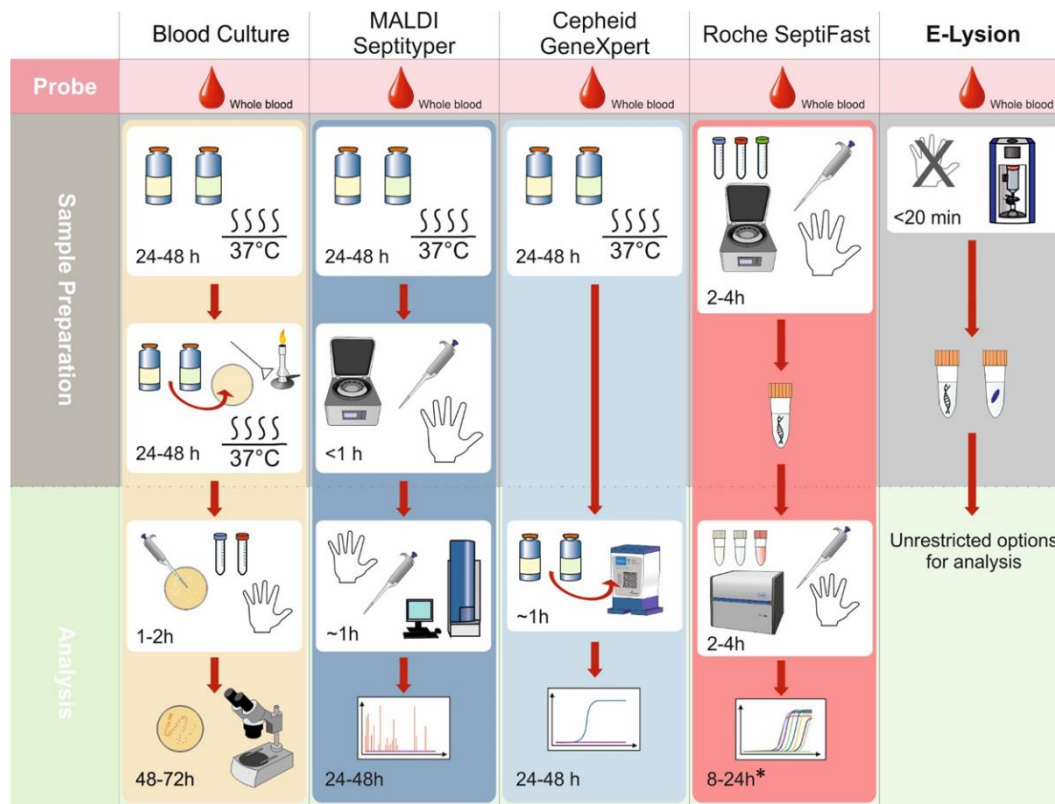
Fig. 4.1: Illustration of the current clinical BSI diognostic procedures and the potential of the developed concept "E-Lysion" to bridge the gap between sampling and analyis.

*Due to the elaborate workflow, multiple samples are first collected in everyday clinical practice before they are processed together.

In addition to the use as novel sample preparation strategy, the investigation of the solid to liquid interface between the electrode and the biological surface and the concept of high-k electrode passivation presented in this thesis could start an important development in the area of electric field applications in biology in general.

Although first patents for biotechnological applications of electric fields were already filed in the 1960's by Doevenspeck in the area of sterilization and food processing[68], the electrode design has not changed significantly ever since.[133] In the majority of devices found on the market and in literature still the "classical approach" design for applying high electric fields to biological samples consists of two metallic electrodes (e.g. aluminum, platinum, gold) in direct ohmic contact to the electrolyte. The use of such a design, however, results in massive charge transfer between the metallic electrode and the

biological sample when high electric potentials are applied, triggering electrochemical reactions followed by bubble formation, pH changes, electrode decomposition and fouling as well as joule heating.[91,117,118,134] This multitude of effects might also be one reason for the inconsistent study conclusions, the contradicting parameter dependencies and the still unclear action of electric fields on cells.

Surprisingly, the very fundamental aspect of electrode passivation has thus far been majorly neglected. The shown reproducible and efficient cell type specific lysis by electric fields due to the introduction of a high-k dielectric electrode passivation hence shows a novel approach in comparison to conventional biological electric field applications. To the best of my knowledge, only one report exists thus far regarding cell-type specific lysis using electric fields.[135] Eppich *et al.* investigated the depletion of tumor cells in a mixture with PBMCs (peripheral blood mononuclear cells). However, due to the "classical approach" of using non-passivated electrodes separated in the mm range, voltages above 600 V had to be applied making water assisted cooling necessary to minimize effects through heating. In addition, the high variance of the results, indicates the low controllability and reproducibility of electric field effects. In this regard, the presented work represents the first report to show continuous flow cell-specific lysis in such an efficient and reproducible manner by inhibiting electrochemical and thermal superimposition due to the strategy of using high-k dielectric electrode passivation.

Besides the potential to open up a wide range of biotechnological applications, the ability for new microfluidic designs by drastically reducing superimposing faradaic current based effects could also be of importance for fundamental electric field research.

It has to be noted that, as the effect of the electric field is inversely proportional to the solution conductivity, the role of displacement current on the action of electric fields on biological matter needs thorough consideration in the future. For this, the investigations performed in Chapter *3.3.3.7 Electrical Characterization of the Electric Cell Lysis Unit* can only be considered as a first starting point. As the thermally oxidized titanium electrodes clearly show diode characteristics, several questions of how the electric field is coupled into the liquid in detail are raised. It can be speculated that as such, only

one side of the electrode passivation acts as insulator and the other side as low-ohmic resistor. Thus, the equivalent circuit built from the impedance data has to be taken with precaution at this point.

Future investigations will focus on developing a more detailed model of the ECLU to allow electrodynamic simulations of electric field propagations through the passivation layer and the fluid to the cell. In parallel, the gained specificity and controllability of electric field settings will be used to investigate the response of other cell types *in-vitro*.

References

1. European Commission's Directorate for Health Research. Challenges and Solutions in the Development of New Diagnostic Tests to Combat Antimicrobial Resistance. Report on the Joint EU-US Workshop. *Report on the Joint EU-US Workshop* **2011** (2011).

2. National Action Plan for Combating Antibiotic-Resistant Bacteria. *The White House* **2015**.

3. Federal Ministry of Health. Combating Antimicrobial Resistance. *G7 Summit Germany 2015* (2015).

4. Brunkhorst, F. M. *et al.* 25th International Symposium on Intensive Care and Emergency Medicine. *Crit Care* **9,** P196 (2005).

5. Dark, P. M., Dean, P. & Warhurst, G. Bench-to-bedside review: the promise of rapid infection diagnosis during sepsis using polymerase chain reaction-based pathogen detection. *Crit Care* **13,** 217 (2009).

6. Seifert, H. The clinical importance of microbiological findings in the diagnosis and management of bloodstream infections. *Clinical infectious diseases : an official publication of the Infectious Diseases Society of America* **48 Suppl 4,** S238-45 (2009).

7. Lehmann, L. E. *et al.* Improved detection of blood stream pathogens by real-time PCR in severe sepsis. *Intensive care medicine* **36,** 49–56 (2010).

8. G. D. Hammer & S. J. MacPhee (eds.). *Pathophysiology of disease. An introduction to clinical medicine* (Lange Med. Books; McGraw-Hill, New York, 2014).

9. Wikipedia. Sepsis - Wikipedia. Available at https://en.wikipedia.org/w/index.php?oldid=780711335 (2017).

10. Bone, R. C. *et al.* Definitions for sepsis and organ failure and guidelines for the use of innovative therapies in sepsis. The ACCP/SCCM Consensus Conference Committee. American College of Chest Physicians/Society of Critical Care Medicine. *Chest* **101,** 1644–1655 (1992).

11. Wheeler, A. P. & Bernard, G. R. Treating patients with severe sepsis. *The New England journal of medicine* **340,** 207–214 (1999).

12. Sugita, H., Kinoshita, Y. & Baba, H. The duration of SIRS before organ failure is a significant prognostic factor of sepsis. *International journal of emergency medicine* **5,** 44 (2012).

13. Markiewski, M. M., DeAngelis, R. A. & Lambris, J. D. Complexity of complement activation in sepsis. *Journal of Cellular and Molecular Medicine* **12,** 2245–2254 (2008).

14. Mwaigwisya, S., Assiri, R. A. M. & O'Grady, J. Emerging commercial molecular tests for the diagnosis of bloodstream infection. *Expert Review of Molecular Diagnostics* **15,** 681–692 (2015).

15. Fleischmann, C. *et al.* EPIDEMIOLOGY OF SEPSIS IN GERMANY. INCIDENCE, MORTALITY AND ASSOCIATED COSTS OF CARE 2007-2013. *Intensive Care Med Exp* **3,** A50 (2015).

16. Kumar, A. *et al.* Duration of hypotension before initiation of effective antimicrobial therapy is the critical determinant of survival in human septic shock*. *Critical Care Medicine* **34,** 1589–1596 (2006).

17. Reinhart, K., Bauer, M., Riedemann, N. C. & Hartog, C. S. New approaches to sepsis: molecular diagnostics and biomarkers. *Clinical microbiology reviews* **25,** 609–634 (2012).

18. Rello, J. *et al.* De-escalation therapy in ventilator-associated pneumonia. *Critical Care Medicine* **32,** 2183–2190 (2004).

19. Florio, W., Morici, P. & Rizzato, C. Diagnosis of Bloodstream Infections by Mass Spectrometry. Present and Future. *Mass Spectrom Purif Tech* **01** (2015).

20. Liesenfeld, O., Lehman, L., Hunfeld, K.-P. & Kost, G. Molecular diagnosis of sepsis: New aspects and recent developments. *European journal of microbiology & immunology* **4,** 1–25 (2014).

21. Vincent, J.-L. *et al.* Sepsis in European intensive care units. Results of the SOAP study*. *Critical Care Medicine* **34,** 344–353 (2006).

22. Rivers Emanuel *et al.* Early Goal-Directed Therapy in the Treatment of Severe Sepsis and Septic Shock.

23. Afshari, A., Schrenzel, J., Ieven, M. & Harbarth, S. Bench-to-bedside review: Rapid molecular diagnostics for bloodstream infection--a new frontier? *Critical care (London, England)* **16,** 222 (2012).

24. Fenselau, C. & Demirev, P. A. Characterization of intact microorganisms by MALDI mass spectrometry. *Mass spectrometry reviews* **20,** 157–171 (2001).

25. Lay, J. O., JR. MALDI-TOF mass spectrometry of bacteria. *Mass spectrometry reviews* **20,** 172–194 (2001).

26. Clark, A. E., Kaleta, E. J., Arora, A. & Wolk, D. M. Matrix-assisted laser desorption ionization-time of flight mass spectrometry: a fundamental shift in the routine practice of clinical microbiology. *Clinical microbiology reviews* **26,** 547–603 (2013).

27. Wunschel, S. C. *et al.* Bacterial analysis by MALDI-TOF mass spectrometry: an inter-laboratory comparison. *Journal of the American Society for Mass Spectrometry* **16,** 456–462 (2005).

28. Venkatesh, M., Flores, A., Luna, R. A. & Versalovic, J. Molecular microbiological methods in the diagnosis of neonatal sepsis. *Expert review of anti-infective therapy* **8,** 1037–1048 (2010).

29. Saiki, R. K. *et al.* Enzymatic amplification of beta-globin genomic sequences and restriction site analysis for diagnosis of sickle cell anemia. *Science (New York, N.Y.)* **230,** 1350–1354 (1985).

30. Liu, B. & Pop, M. ARDB--Antibiotic Resistance Genes Database. *Nucleic acids research* **37,** D443-7 (2009).

31. Mwaigwisya, S., Assiri, R. A. M. & O'Grady, J. Emerging commercial molecular tests for the diagnosis of bloodstream infection. *Expert Review of Molecular Diagnostics* **15,** 681–692 (2015).

32. Fournier, P.-E. *et al.* Modern clinical microbiology: new challenges and solutions. *Nature reviews. Microbiology* **11,** 574–585 (2013).

33. Ulrich, M. P. *et al.* Evaluation of the Cepheid GeneXpert system for detecting Bacillus anthracis. *J. Appl. Microbiol.* **100,** 1011–1016 (2006).

34. Rossney, A. S., Herra, C. M., Brennan, G. I., Morgan, P. M. & O'Connell, B. Evaluation of the Xpert methicillin-resistant Staphylococcus aureus (MRSA) assay using the GeneXpert real-time PCR platform for rapid detection of MRSA from screening specimens. *Journal of clinical microbiology* **46,** 3285–3290 (2008).

35. Elizabeth M. Marlowe & Donna M. Wolk. GeneXpert Testing: Applications for Clinical Microbiology, Part II. *Clin. Microbiol. Newsletter* (2008).

36. Liao, J. C. *et al.* Use of electrochemical DNA biosensors for rapid molecular identification of uropathogens in clinical urine specimens. *J. Clin. Microbiol.* **44,** 561–570 (2006).

37. Elsholz, B. *et al.* Automated detection and quantitation of bacterial RNA by using electrical microarrays. *Anal. Chem.* **78,** 4794–4802 (2006).

38. Liu, R. H., Yang, J., Lenigk, R., Bonanno, J. & Grodzinski, P. Self-contained, fully integrated biochip for sample preparation, polymerase chain reaction amplification, and DNA microarray detection. *Anal. Chem.* **76,** 1824–1831 (2004).

39. Cheong, K. H. *et al.* Gold nanoparticles for one step DNA extraction and real-time PCR of pathogens in a single chamber. *Lab Chip* **8,** 810–813 (2008).

40. Lee, J.-G. *et al.* Microchip-based one step DNA extraction and real-time PCR in one chamber for rapid pathogen identification. *Lab Chip* **6,** 886–895 (2006).

41. Guillén, Gustavo, Adolfo, Zelada. ULTRASENSITIVE DETECTION OF PATHOGENS IN REAL-TIME. POTENTIOMETRIC BIOSENSORS BASED ON SINGLE-WALLED CARBON NANOTUBES AND APTAMERS. *Thesis* (2011).

42. Zelada-Guillén, G. A., Bhosale, S. V., Riu, J. & Rius, F. X. Real-time potentiometric detection of bacteria in complex samples. *Anal. Chem.* **82,** 9254–9260 (2010).

43. Mujika, M. *et al.* Magnetoresistive immunosensor for the detection of Escherichia coli O157:H7 including a microfluidic network. *Biosens Bioelectron* **24,** 1253–1258 (2009).

44. Yeung, S.-W., Lee, T. M.-H., Cai, H. & Hsing, I.-M. A DNA biochip for on-the-spot multiplexed pathogen identification. *Nucleic Acids Res.* **34,** e118 (2006).

45. Easley, C. J. *et al.* A fully integrated microfluidic genetic analysis system with sample-in-answer-out capability. *Proc. Natl. Acad. Sci. U.S.A.* **103,** 19272–19277 (2006).

46. Mahalanabis, M., Al-Muayad, H., Kulinski, M. D., Altman, D. & Klapperich, C. M. Cell lysis and DNA extraction of gram-positive and gram-negative bacteria from whole blood in a disposable microfluidic chip. *Lab Chip* **9,** 2811–2817 (2009).

47. Mairhofer, J., Roppert, K. & Ertl, P. Microfluidic systems for pathogen sensing: a review. *Sensors (Basel)* **9,** 4804–4823 (2009).

48. Shramik, S., Jason, G. & Hsueh-Chia, C. Microfluidic Diagnostic Systems for the Rapid Detection and Quantification of Pathogens. *Microfluidics for Biological Applications,* 271–322 (2009).

49. Foudeh, A. M., Fatanat Didar, T., Veres, T. & Tabrizian, M. Microfluidic designs and techniques using lab-on-a-chip devices for pathogen detection for point-of-care diagnostics. *Lab Chip* **12,** 3249–3266 (2012).

50. McCann, C. D. & Jordan, J. A. Evaluation of MolYsis Complete5 DNA extraction method for detecting Staphylococcus aureus DNA from whole blood in a sepsis model using PCR/pyrosequencing. *Journal of Microbiological Methods* **99,** 1–7 (2014).

51. Hansen, W. L. J., Bruggeman, C. A. & Wolffs, P. F. G. Evaluation of new preanalysis sample treatment tools and DNA isolation protocols to improve bacterial pathogen detection in whole blood. *J. Clin. Microbiol.* **47,** 2629–2631 (2009).

52. Loonen, A. J. M. *et al.* Comparison of Pathogen DNA Isolation Methods from Large Volumes of Whole Blood to Improve Molecular Diagnosis of Bloodstream Infections. *PLoS ONE* **8,** e72349 (2013).

53. Hou, H. W. *et al.* Microfluidic Devices for Blood Fractionation. *Micromachines* **2,** 319–343 (2011).

54. Zhu, L. *et al.* Filter-based microfluidic device as a platform for immunofluorescent assay of microbial cells. *Lab Chip* **4,** 337–341 (2004).

55. Lay, C. *et al.* Enhanced microfiltration devices configured with hydrodynamic trapping and a rain drop bypass filtering architecture for microbial cells detection. *Lab Chip* **8,** 830–833 (2008).

56. Yobas, L. *et al.* Microfluidic Chips for Viral RNA Extraction & amp; Detection. 30 October - 3 November 2005, Irvine, CA. *Sensors,* 49–52 (2005).

57. Laurell, T., Petersson, F. & Nilsson, A. Chip integrated strategies for acoustic separation and manipulation of cells and particles. *Chem Soc Rev* **36,** 492–506 (2007).

58. Petersson, F., Aberg, L., Swärd-Nilsson, A.-M. & Laurell, T. Free flow acoustophoresis: microfluidic-based mode of particle and cell separation. *Anal. Chem.* **79,** 5117–5123 (2007).

59. Park, S., Zhang, Y., Wang, T.-H. & Yang, S. Continuous dielectrophoretic bacterial separation and concentration from physiological media of high conductivity. *Lab Chip* **11,** 2893–2900 (2011).

60. Cho, Y.-K., Kim, T.-h. & Lee, J.-G. On-chip concentration of bacteria using a 3D dielectrophoretic chip and subsequent laser-based DNA extraction in the same chip. *J. Micromech. Microeng.* **20,** 65010 (2010).

61. Del Moral-Zamora, B. *et al.* Combined dielectrophoretic and impedance system for on-chip controlled bacteria concentration: Application to Escherichia coli. *Electrophoresis* **36,** 1130–1141 (2015).

62. Iliescu, C., Tresset, G. & Xu, G. Dielectrophoretic field-flow method for separating particle populations in a chip with asymmetric electrodes. *Biomicrofluidics* **3,** 44104 (2009).

63. Ma, W. *et al.* High-throughput dielectrophoretic manipulation of bioparticles within fluids through biocompatible three-dimensional microelectrode array. *Electrophoresis* **32,** 494–505 (2011).

64. ABQ startup acquired by London biotech firm. Available at http://www.spv.com/abq-startup-acquired-by-london-biotech-firm/.

65. Zhou, L. & Pollard, A. J. A novel method of selective removal of human DNA improves PCR sensitivity for detection of Salmonella Typhi in blood samples. *BMC Infect Dis* **12,** 164 (2012).

66. Horz, H.-P., Scheer, S., Huenger, F., Vianna, M. E. & Conrads, G. Selective isolation of bacterial DNA from human clinical specimens. *Journal of Microbiological Methods* **72,** 98–102 (2008).

67. Horz, H.-P., Scheer, S., Vianna, M. E. & Conrads, G. New methods for selective isolation of bacterial DNA from human clinical specimens. *Anaerobe* **16,** 47–53 (2010).

68. Doevenspeck, H. *Verfahren und Vorrichtung zur Gewinnung der einzelnen Phasen aus dispersen Systemen / Process and apparatus for changing the charge of particles* ,

69. Sale, A. J. & Hamilton, W. A. Effects of high electric fields on micro-organisms. 3. Lysis of erythrocytes and protoplasts. *Biochimica et biophysica acta* **163,** 37–43 (1968).

70. Maxwell, J. C. *A Treatise on Electricity and Magnetism* (Clarendon Press, 1873).

71. Weaver, J. C., Powell, K. T., Mintzer, R. A., Ling, H. & Sloan, S. R. The electrical capacitance of bilayer membranes. *Bioelectrochemistry and Bioenergetics* **12,** 393–404 (1984).

72. Weaver, J. C. & Chizmadzhev, Y. Theory of electroporation. A review. *Bioelectrochemistry and Bioenergetics* **41,** 135–160 (1996).

73. Ho, S. Y. & Mittal, G. S. Electroporation of cell membranes: a review. *Critical reviews in biotechnology* **16,** 349–362 (1996).

74. Kirsch, S. A. & Bockmann, R. A. Membrane pore formation in atomistic and coarse-grained simulations. *Biochimica et biophysica acta* **1858,** 2266–2277 (2016).

75. Lee, D. W. & Cho, Y.-H. A continuous electrical cell lysis device using a low dc voltage for a cell transport and rupture. *Sensors and Actuators B: Chemical* **124,** 84–89 (2007).

76. Bao, N. & Lu, C. A microfluidic device for physical trapping and electrical lysis of bacterial cells. *Appl. Phys. Lett.* **92,** 214103 (2008).

77. Schoenbach, K. H., Joshi, R. P., Stark, R. H., Dobbs, F. C. & Beebe, S. J. Bacterial decontamination of liquids with pulsed electric fields. *IEEE Trans. Dielect. Electr. Insul.* **7,** 637–645 (2000).

78. Church, C., Zhu, J., Huang, G., Tzeng, T.-R. & Xuan, X. Integrated electrical concentration and lysis of cells in a microfluidic chip. *Biomicrofluidics* **4,** 44101 (2010).

79. Fox, M. B. *et al.* Electroporation of cells in microfluidic devices: a review. *Anal Bioanal Chem* **385,** 474–485 (2006).

80. Wang, S. & Lee, L. J. Micro-/nanofluidics based cell electroporation. *Biomicrofluidics* **7,** 11301 (2013).

81. Morshed, B., Shams, M. & Mussivand, T. Electrical Lysis. Dynamics Revisited and Advances in On-chip Operation. *Crit Rev Biomed Eng* **41,** 37–50 (2013).

82. Wang, H.-Y. & Lu, C. Electroporation of mammalian cells in a microfluidic channel with geometric variation. *Analytical chemistry* **78,** 5158–5164 (2006).

83. Munce, N. R., Li, J., Herman, P. R. & Lilge, L. Microfabricated system for parallel single-cell capillary electrophoresis. *Analytical chemistry* **76,** 4983–4989 (2004).

84. Okumura, Y. & Oana, S. Effect of counter electrode in electroformation of giant vesicles. *Membranes* **1,** 345–353 (2011).

85. Yasukawa, T., Hatanaka, H. & Mizutani, F. Simple detection of surface antigens on living cells by applying distinct cell positioning with negative dielectrophoresis. *Analytical chemistry* **84,** 8830–8836 (2012).

86. Lu, H., Schmidt, M. A. & Jensen, K. F. A microfluidic electroporation device for cell lysis. *Lab Chip* **5,** 23–29 (2005).

87. Grosse, C. & Schwan, H. P. Cellular membrane potentials induced by alternating fields. *Biophysical Journal* **63,** 1632–1642 (1992).

88. Schoenbach, K. H., Peterkin, F. E., Alden, R. W. & Beebe, S. J. The effect of pulsed electric fields on biological cells. Experiments and applications. *IEEE Trans. Plasma Sci.* **25,** 284–292 (1997).

89. Aronsson, K., Lindgren, M., Johansson, B. R. & Rönner, U. Inactivation of microorganisms using pulsed electric fields. The influence of process parameters on Escherichia coli, Listeria innocua, Leuconostoc mesenteroides and Saccharomyces cerevisiae. *Innovative Food Science & Emerging Technologies* **2,** 41–54 (2001).

90. Kinosita, K. & Tsong, T. Y. Formation and resealing of pores of controlled sizes in human erythrocyte membrane. *Nature* **268,** 438–441 (1977).

91. Kim, J. A. *et al.* A novel electroporation method using a capillary and wire-type electrode. *Biosens Bioelectron* **23,** 1353–1360 (2008).

92. Kinosita, K. & Tsong, T. T. Hemolysis of human erythrocytes by transient electric field. *Proceedings of the National Academy of Sciences of the United States of America* **74,** 1923–1927 (1977).

93. Bao, N., Le, T. T., Cheng, J.-X. & Lu, C. Microfluidic electroporation of tumor and blood cells: observation of nucleus expansion and implications on selective analysis and purging of circulating tumor cells. *Integr Biol (Camb)* **2,** 113–120 (2010).

94. Shah, D., Steffen, M. & Lilge, L. Controlled electroporation of the plasma membrane in microfluidic devices for single cell analysis. *Biomicrofluidics* **6,** 14111–1411110 (2012).

95. Wassermann, K., Peham, J. R., Wiesinger-Mayr, H. & Noehammer, C. *WO 2015044191A1 I* (2014).

96. Yin, Y. G., Jin, Z. X., Wang, C. L. & An, W. Z. The effect of pulsed electric field on DNA extraction from bovine spleens. *Separation and Purification Technology* **56,** 127–132 (2007).

97. Geng, T., Bao, N., Sriranganathanw, N., Li, L. & Lu, C. Genomic DNA extraction from cells by electroporation on an integrated microfluidic platform. *Analytical chemistry* **84,** 9632–9639 (2012).

98. Geng, T. & Lu, C. Microfluidic electroporation for cellular analysis and delivery. *Lab Chip* **13,** 3803–3821 (2013).

99. Moschallski, M. *et al. in World Congress on Medical Physics and Biomedical Engineering,* edited by O. Dössel (Springer, [Berlin, Heidelberg, New York, NY], 2009), pp. 157–160.

100. Tomov, T. C., Tsoneva, I. C. & Doncheva, J. C. Electrical stability of erythrocytes in the presence of divalent cations. *Biosci Rep* **8,** 421–426 (1988).

101. Lee, S.-W. & Tai, Y.-C. A micro cell lysis device. *Sensors and Actuators A: Physical* **73,** 74–79 (1999).

102. Mernier, G., Martinez-Duarte, R., Lehal, R., Radtke, F. & Renaud, P. Very High Throughput Electrical Cell Lysis and Extraction of Intracellular Compounds Using 3D Carbon Electrodes in Lab-on-a-Chip Devices. *Micromachines* **3,** 574–581 (2012).

103. Ramadan, Q. *et al.* Simultaneous cell lysis and bead trapping in a continuous flow microfluidic device. *Sensors and Actuators B: Chemical* **113,** 944–955 (2006).

104. Wang, H.-Y., Bhunia, A. K. & Lu, C. A microfluidic flow-through device for high throughput electrical lysis of bacterial cells based on continuous dc voltage. *Biosens Bioelectron* **22,** 582–588 (2006).

105. Pucihar, G., Kotnik, T., Kandušer, M. & Miklavčič, D. The influence of medium conductivity on electropermeabilization and survival of cells in vitro. *Bioelectrochemistry* **54,** 107–115 (2001).

106. Vulto, P. *et al.* A microfluidic approach for high efficiency extraction of low molecular weight RNA. *Lab Chip* **10,** 610–616 (2010).

107. Edd, J. F. & Davalos, R. V. Mathematical Modeling of Irreversible Electroporation for Treatment Planning. *Technology in Cancer Research & Treatment* **6,** 275–286 (2007).

108. Albritton, N., Guann-Pyng, L., Bachmann, M., Sims, C. E. & Futian, H. *Fast electrical lysis of cells and rapid collection of the contents thereof using capillary electrophoresis ,* WO 2003093791 A3

109. Jensen, G., Thomsen, L. & Veltman, O. *Method, chip, device and system for extraction of biological materials ,* WO 2005083078 A1

110. Kotnik, T., Pucihar, G., Reberšek, M., Miklavčič, D. & Mir, L. M. Role of pulse shape in cell membrane electropermeabilization. *Biochimica et Biophysica Acta (BBA) - Biomembranes* **1614,** 193–200 (2003).

111. Lu, C., Wang, H.-Y. & Wang, J. *Fluidic device ,* US 20120276635 A1

112. Cheng, J. *et al. Integrated portable biological detection system,* WO 2000037163 A1

113. Iliescu, C., Xu, G. & Tay, F. *Biochip for sorting and lysing biological samples,* WO 2006004558 A1

114. Tai, Y.-C. & Lee, S.-W. *Cell lysis device,* US 6534295 B2

115. Takinoue, M., Onoe, H., Kiriya, D. & Takeuchi, S. in *MEMS 2011 Cancun Mexico* (IEEE, [Piscataway, N.J.], 2011), pp. 1177–1180.

116. Mathews, S., Hans, M., Mücklich, F. & Solioz, M. Contact killing of bacteria on copper is suppressed if bacterial-metal contact is prevented and is induced on iron by copper ions. *Appl. Environ. Microbiol.* **79,** 2605–2611 (2013).

117. Saulis, G., Lapė, R., Pranevičiūtė, R. & Mickevičius, D. Changes of the solution pH due to exposure by high-voltage electric pulses. *Bioelectrochemistry* **67,** 101–108 (2005).

118. Pakhomova, O. N. *et al.* Oxidative effects of nanosecond pulsed electric field exposure in cells and cell-free media. *Archives of Biochemistry and Biophysics* **527,** 55–64 (2012).

119. An, R., Massa, K., Wipf, D. O. & Minerick, A. R. Solution pH change in non-uniform alternating current electric fields at frequencies above the electrode charging frequency. *Biomicrofluidics* **8,** 64126 (2014).

120. Schneider, C. A., Rasband, W. S. & Eliceiri, K. W. NIH Image to ImageJ. 25 years of image analysis. *Nat Meth* **9,** 671–675 (2012).

121. Bao, N. *et al.* Single-cell electrical lysis of erythrocytes detects deficiencies in the cytoskeletal protein network. *Lab on a chip* **11,** 3053–3056 (2011).

122. Schäuble, K. Silica passivation layer on aluminium brazing sheets. *Thesis* (2010).

123. Diebold, U. The surface science of titanium dioxide. *Surface Science Reports* **48,** 53–229 (2003).

124. Velten, D. *et al.* Preparation of TiO(2) layers on cp-Ti and Ti6Al4V by thermal and anodic oxidation and by sol-gel coating techniques and their characterization. *J. Biomed. Mater. Res.* **59,** 18–28 (2002).

125. Donachie, M. J. *Titanium. A technical guide.* 2nd ed. (2000).

126. Tebbe, D. Funktionalisierung von Titan(dioxid)oberflächen mit kovalent gebundenem und in Depots eingebrachtem Wirkstoff für den Blutkontakt. *Thesis* (2007).

127. Al-Mobarak, N. A. & Al-Swayih, A. A. Development of Titanium Surgery Implants for Improving Osseointegration Through Formation of a Titanium Nanotube Layer. *Int. J. Electrochem. Sci.* **9** (2014).

128. Uemura, K. & Isobe, S. Developing a new apparatus for inactivating Escherichia coli in saline water with high electric field AC. *Journal of Food Engineering* **53,** 203–207 (2002).

129. Eveke, D. J. G. & Brunkhorst, C. Inactivation of in Apple Juice by Radio Frequency Electric Fields. *Journal of Food Science* **69,** FEP134-FEP0138 (2004).

130. Park, Y.-J., Song, H.-J., Kim, I. & Yang, H.-S. Surface characteristics and bioactivity of oxide film on titanium metal formed by thermal oxidation. *J Mater Sci Mater Med* **18,** 565–575 (2007).

131. Kumar, S., Narayanan, T. S., Raman, S. G. S. & Seshadri, S. K. Thermal oxidation of CP Ti — An electrochemical and structural characterization. *Materials Characterization* **61,** 589–597 (2010).

132. Stringer, J. The oxidation of titanium in oxygen at high temperatures. *Acta Metallurgica* **8,** 758–766 (1960).

133. Pavlin, M. *et al.* Effect of cell electroporation on the conductivity of a cell suspension. *Biophys. J.* **88,** 4378–4390 (2005).

134. Morshed, B., Shams, M. & Mussivand, T. Analysis of Electric Fields inside Microchannels and Single Cell Electrical Lysis with a Microfluidic Device. *Micromachines* **4,** 243–256 (2013).

135. Eppich, H. M. *et al.* Pulsed electric fields for selection of hematopoietic cells and depletion of tumor cell contaminants. *Nat. Biotechnol.* **18,** 882–887 (2000).

Curriculum Vitae

Name   Klemens Johannes Wasserman, Mag.

Date of birth May 5th 1984

Affiliation   AIT Austrian Institute of Technology GmbH

Center for Health & Bioresources

Molecular Diagnostics

Muthgasse 11 | 1190 Vienna | Austria

+43 664 882 560 17

Klemens.wassermann@ait.ac.at

Position   Scientist, Group Leader

Children   2 Children (11 & 3 years)

Career

Since July 2015: Scientist (Group leader) at the Austrian Institute of Technology (AIT), Health & Environment Department, Molecular Diagnostics (Vienna, Austria)

Since July 2012: PhD Thesis: "Lab-on-a-chip for pathogen detection from blood" at the Austrian Institute of Technology (AIT), Health & Environment Department, Molecular Diagnostics (Vienna, Austria)

2012: Co-operation with JW-IDEE and Knorr-Bremse to develop a novel emergency-brake system for modern cabel cars

2010-2012: Research freelancer "miRNAs in osteogenic differentiation and as clinical markers for osteoporosis" at the Institute of Applied Microbiology, University of Natural Resources and Life Sciences (Vienna, Austria) in cooperation with Trauma Care Consult/ Ludwig Boltzmann Institute for Experimental and Clinical Traumatology

2007/08: Diploma Thesis "The Molecular Biology of HIV - Cloning and

Characterization of SHIV-1157ipEL: A New Tool for Vaccine Studies" at Dana Farber Cancer Institute/Harvard Medical School (Boston, MA)

2006-2007/2008-2010: Employee at the Trauma Care Consult/ Ludwig Boltzmann Institute for Experimental and Clinical Traumatology

Scholarships and Prices

Young Investigator Award, 1st World Congress on Electroporation and Pulsed Electric Fields in Biology, Medicine and Food & Environmental Techniques 2015

1st Place Jury Award Winner & Audience Award Winner Falling Walls Lab 2013

A.T. Kearney Scholarship for the Falling Walls Conference 2013

Publications

Siddappa NB, Watkins JD, Wassermann KJ, Song R, Wang W, Kramer VG, Lakhashe S, Santosuosso M, Poznansky MC, Novembre FJ, Villinger F, Else JG, Montefiori DC, Rasmussen RA, Ruprecht RM. R5 clade C SHIV strains with tier 1 or 2 neutralization sensitivity: tools to dissect env evolution and to develop AIDS vaccines in primate models. PLoS One. 2010

Adamskaya N, Dungel P, Mittermayr R, Hartinger J, Feichtinger G, Wassermann K, Redl H, van Griensven M. Light therapy by blue LED improves wound healing in an excision model in rats. Injury. 2010

Feichtinger GA, Hacobian A, Hofmann AT, Wassermann K, Zimmermann A, van Griensven M, Redl H. Constitutive and inducible co-expression systems for non-viral osteoinductive gene therapy. Eur Cell Mater. 2014

Wassermann K.J., Maier T., Keplinger F. and Peham J.R. A Novel Sample Preparation Concept for Sepsis Diagnostics using High Frequency Electric Fields. IFMBE Proceedings Issue 1st World Congress on Electroporation and Pulsed Electric Fields 2015

Schraml E., Weilner S., Wieser M., Messner P., Schneider K., Wassermann K., Micutkova L., Fortschegger K., Maier A.B., Westendorp R., Resch H., Wolbank S., Redl H., Jansen-Dürr P., Pietschmann P., Grillari-Voglauer R. and Grillari J. Secreted microvesicular miR-31 inhibits osteogenic differentiation of mesenchymal stem cells ACE-14-0169.R2. Aging Cell. 2016

Wassermann K.J., Barth S., Keplinger F., Noehammer C. and Peham J.R. High-k Dielectric Passivation: Novel Considerations Enabling Cell Specific Lysis Induced by Electric Fields. ACS Appl. Mater. Interfaces. 2016

Patents and Patent Application

European Patent Application 13185831.8 "Method for pathogen diagnosis", Wassermann Klemens, Peham Johannes, Christa Nöhammer, Herbert Wiesinger-Mayr, filed September 2013

Austrian Patent Application A 50390/2012 "Komfort-Auflage", Wassermann Klemens, filed September 2012

Poster Presentations & Oral Talks

Non-viral sonoporation gene therapy for orthotopic bone regeneration. Feichtinger G, Schuetzenberger S, Hofmann A, Slezak P, Kaipel M, Schwartz E, Pfeifer S, Wassermann K, van Griensven M, Nau T, McHale A, Redl H. Termis World Congress 2012. Poster Presentation

MicroRNA-31 – a novel therapeutic target for bone regeneration and osteoporosis. Schraml E, Weilner S, Wassermann K, Wieser M, Messner P, Maier AB, Redl H, Pietschmann P, Grillari-Voglauer RG, Grillari JG. Genau Meeting 2012. Poster Presentation

MicroRNA-31 as novel biomarker of aging? Secretion by senescent endothelial cells and inhibition of osteogenic differentiation of mesenchymal stem cells. Wassermann K, Schraml L, Weilner S, Redl H, Grillari J. Resolve Meeting 2011 - Tissue Remodeling in Ageing and Disease. Poster Presentation

A New Sample Preparation Strategy for Point-of-Care Sepsis Diagnostics from Whole Blood. Klemens Wassermann, Peham Johannes, Christa Nöhammer, Herbert Wiesinger-Mayr. Austrian Institute of Technology Poster Award. Poster Presentation.

Breaking the Wall of Infection Diagnostics. Klemens Wassermann. Falling Walls Lab 2013. Oral Presentation

Breaking the Wall of Infection Diagnostics. Klemens Wassermann. Falling Walls Conference 2013. Oral Presentation

A Novel Sample Preparation Concept for Sepsis Diagnostics: Efficient Cell Type-Specific Lysis by Electric Fields using High-K Dielectric Electrode Passivation. K.J. Wassermann, T. Maier, F. Keplinger, C. Nöhammer and J.R. Peham. Bioelectrochemistry and more…2015. Poster Presentation

A Novel Sample Preparation Concept for Sepsis Diagnostics using High Frequency Electric Fields. K.J. Wassermann, T. Maier, F. Keplinger and J.R. Peham. 1st World Congress on Electroporation and Pulsed Electric Fields 2015. Poster Presentation

A Novel Sample Preparation Concept for Sepsis Diagnostics: Efficient Cell Type-Specific Lysis by Electric Fields using High-K Dielectric Electrode Passivation. K.J. Wassermann, T. Maier, F. Keplinger and J.R. Peham. Austrian Biomarker Symposium 2016. Oral Presentation